REVEALING HEMODYNAMIC RESPONSE AND DYNAMIC CHANGES IN FUNCTIONAL CORTICAL NETWORKS USING FUNCTIONAL NEAR-INFRARED SPECTROSCOPY (FNIRS)

by

JIANWEI CAO

Presented to the Faculty of the Graduate School of

The University of Texas at Arlington in Partial Fulfillment

of the Requirements

for the Degree of

DOCTOR OF PHILOSOPHY

THE UNIVERSITY OF TEXAS AT ARLINGTON

NOV 2017

Acknowledgements

First and foremost I would like to thank my supervising professor Dr. George Alexandrakis for all his contributions of time, guidance and funding to make my journey rewarding. I appreciate his support on my first full time job. The enthusiasm he has for his research sets an excellent example for me on my career. I would also like to thank my dissertation committee of Dr. Hanli Liu, Dr. Shouyi Wang and Dr. Yuze Sun for their support and valuable suggestions on my dissertation.

I would like to thank the members of the Alexandrakis group for their help, support and friendship. Dr. Bilal Khan trained me on the equipment and assisted me with algorithms development. Nathan Hervey and Pallavi Natekar gave me valuable feedback on my research. I would also like to thank Dr. Xinlong Wang for his suggestion on my project, Dr. Bingbing Cheng for his help whenever I need a subject, and Dr. Yuan Liu for her encouragement during my tough time.

Last but not least, I would like to express my special gratitude to my family members. I would not make it so far if without them. I would like to thank my parents Guoxing Cao and Dongmei Zang for their unconditional love, advice and support. I would like to thank my dear husband, Hongjun Yang for his love and humor, to make my life more colorful. I would also like to thank my lovely son, Lucas, who makes our life a new start!

November 10, 2017.

Abstract

REVEALING HEMODYNAMIC RESPONSE AND DYNAMIC CHANGES IN FUNCTIONAL CORTICAL NETWORKS USING FUNCTIONAL NEAR-INFRARED SPECTROSCOPY (FNIRS)

Jianwei Cao, PhD

The University of Texas at Arlington, 2017

Supervising Professor: George Alexandrakis

Therapeutic interventions, such as physical therapy and non-invasive brain electrical stimulation can enhance the physical performance of persons with brain disorders. One often-used form of physical therapy named constraint-induced movement therapy (CIMT) improves motor control skills of children with cerebral palsy (CP) through forced intensive use of the affected extremity. A complementary method to physical rehabilitation methods for overcoming a deficit is to facilitate use of the affected brain areas by non-invasive brain electrical stimulation. One currently popular form of brain stimulation is transcranial direct current stimulation (tDCS), which has been shown to enhance both motor and language performance in adult stroke patients. Though many studies have researched how those interventions affect performance, few studies have systematically investigated the underlying mechanisms of how the interventions affect cortical plasticity, which drive the externally observed performance improvements.

To address this knowledge gap, my dissertation work has focused on objective measures of altered hemodynamic response and functional connectivity patterns induced by therapeutic interventions (CIMT and tDCS) on the human brain. Functional changes in the brain were mapped by use of functional near infrared spectroscopy (fNIRS) technology, the design of novel

experimental protocols, and the implementation of data analysis algorithms to these studies. My dissertation achieved those goals through implementation of the three following steps:

1) In Chapter 2, my research focused on evaluating cortical plasticity of the sensorimotor cortex in children with CP undergoing CIMT by fNIRS. Brain activation patterns indicated by hemodynamic activity metrics, namely the laterality index, time-to-peak/duration of activation ratio, and resting-state functional connectivity changes were mapped by fNIRS before, immediately after and six months post-CIMT. The fNIRS imaging metrics, acquired concurrently with changes in motor performance, provided insightful information to help explain why some children had better performance after the CIMT intervention and why that performance declined six months later.

2) In Chapter 3, I investigated the altered resting-state functional connectivity patterns of language areas when tDCS was applied over the Broca's area, which is central to language processing. Transient cortical reorganization patterns in steady-state functional connectivity (seed-based and graph theory analysis) and temporal functional connectivity (sliding window correlation analysis) were recorded before, during and after High Current tDCS (1mA, 10mins). The findings of this work demonstrated that tDCS induced significantly ($p < 0.05$) increased functional connectivity between Broca's area and its neighboring cortical regions, enhanced the small-world features of the cortical network globally, and caused significant ($p<0.05$) increases to the functional connectivity variability (FCV) of remote cortical regions related to language processing. In addition, Low Current tDCS (0.5mA, 2 min 40 s) was found to qualitative predict the increase in clustering coefficient (Cp) and FCV at higher stimulation currents, but not the enhancement of local connectivity.

3) In Chapter 4, my research further explored the direction of information flow by Phase Transfer Entropy (PTE) before tDCS, during Low Current tDCS, during High Current tDCS and after High Current tDCS. The results demonstrated that tDCS induced alterations in information flow from the stimulated Broca's area and its homologous area in the right brain

hemisphere to other language-related cortical regions. In addition, the direction of information flow was examined in three fNIRS frequency bands: endothelial, neurogenic and myogenic. An increase in outgoing information flow was seen consistently for the stimulated Broca's area for the endothelial frequency band, and the patterns of information flow during Low Current tDCS were similar with those seen after High Current tDCS. Interestingly, a different pattern was seen in the neurogenic frequency band, where the outgoing information flow during High Current tDCS was similar with low patterns seen after the High Current tDCS session. In the myogenic frequency band, there is no significant change in key language areas (Broca's area and Wernicke's area), but global patterns were seen that were interpreted as Mayer waves.

Table of Contents

List of Figures

List of Tables

Chapter 1 Introduction

Over one million Americans are diagnosed annually with brain disorders in the United States[1-4]. Brain disorders could cause impairment in activities of daily living that could have debilitating effects in one's quality of life. Therapeutic interventions, such as physical therapy[5, 6], pharmacological interventions[7, 8], electrical stimulation[9, 10] or combinations of them with the aim of improving rehabilitation outcomes. For example, constraint induced motion therapy (CIMT) improved the motor control skills of children with cerebral palsy (CP) by restraining the unaffected extremity and forcing intensive use of the affected extremity[11]. Non-invasive brain stimulation techniques, such as transcranial direct current stimulation (tDCS), which delivers weak currents through a pair of anode-cathode electrodes, has shown to be effective in improving naming accuracy or speed in stroke patients with brain lesion over speech recognition and production areas[9, 12, 13]. In addition, combined tDCS and CIMT has shown promise in improving motor control skills in stroke patients[14, 15].

The behavioral effects of these therapeutic interventions were observed in many studies as described above. However, the mechanisms of how these interventions could affect cortical plasticity are still unclear. It is highly desirable to image the brain activation patterns and relevant brain networks before and after an intervention to better evaluate brain disorders and guide therapeutic interventions. Functional magnetic resonance imaging (fMRI) is the gold standard for neuroimaging employed in a few recent studies to evaluate the effects of therapeutic interventions. Laterality index of sensorimotor activation between the two cerebral hemispheres[16, 17] was proposed as a measure of CIMT response on children with CP. Meinzer et al.[18] used resting-state fMRI to assess the impact of anodal tDCS on the functional connectivity networks of healthy subjects. Their results showed an increase of functional connectivity strength in language-associated regions, such as dorsolateral and medial prefrontal regions, pre-Supplementary Motor Area (pre-SMA) and SMA, but a decrease in more posterior and occipital regions. Marangolo et al.[19] revealed that increased connectivity strength was most pronounced in the left hemispheric

structures related to planning, maintenance and execution of speech. However, studies on how the interventions affect cortical activity and functional connectivity reorganization were not detailed, especially on functional connectivity reorganization. Also, previous studies mainly focused on steady-state functional connectivity, and dynamic fluctuations in functional connectivity have not yet been explored even though the study of these fluctuations has been shown to elucidate fundamental properties of brain networks[20-23]. In another aspect, little is known about the directionality of functional connectivity after theraputic interventions. It is challenging to estimate directionality of connectivity between functional regions from fMRI due to its limited temporal resolution. On the other hand, functional near-infrared spectroscopy (fNIRS), which detects changes in the concentration of oxyhemoglobin (ΔHbO) and deoxyhemoglobin (ΔHb) resulting from neurovascular coupling[24], has been increasingly shown to be a viable alternative neuroimaging modality to fMRI despite its lower spatial resolution and ability to only map cortical activation[25, 26]. fNIRS provides higher temporal resolution relative to fMRI, which is valuable for investigating time-varying functional connectivity and directionality of functional connectivity in the brain[27]. Furthermore, fNRIS is more relative robustness to motion artifacts[28-30] and compatible with electrical stimulation such as tDCS[31].

Overall, this dissertation focuses on (1) the establishment of the methodology on cortical activity and resting-state functional connectivity to evaluate by fNIRS cortical plasticity in children with CP undergoing CIMT; (2) Measuring and understanding altered steady-state functional connectivity and time-variant functional connectivity from anodal tDCS over the human Broca's area; (3) Evaluating the altered directionality of functional connectivity in three fNIRS frequency bands (endothelial, neurogenic and myogenic) from anodal tDCS over the human Broca's area.

As shown in Figure 1-1, this dissertation has 5 chapters, which consists of one peer-reviewed publication (Chapter 2), one submitted manuscript (Chapter 3) and one manuscript that is ready to submit (Chapter 4). Chapter 1 is a brief introduction of therapeutic interventions for brain disorders and the current problems in assessing the mechamisms and effects of the

interventions. In Chapter 2, spatial and temporal metrics of crotical activation, and resting-state functional connectivity were proposed as measures for evaluating cortical plasticitiy of children with CP before, immediately after and six months after CIMT. In Chapter 3, steady-state functional connectivity (seed-based and graphy theory analysis) and temporal functional connectivity (sliding window correlation analysis) were measured before, during and after High Current tDCS (1 mA, 8 mins) to reveal the effects of anodal tDCS over the Broca's area for right hand dominant adults. Low Current tDCS (0.5 mA, 2 min 40 s) was also applied to test whether the transient effects of lower stimulation current could qualitatively predict cortical connectiivity alterations induced by higher current. In Chapter 4, directionality of functional connectivity between cortical regions in three fNIRS frequency bands (endothelial, neurogenic and myogenic) by Phase Transfer Entrophy (PTE) was evaluated and imaged before tDCS, during Low Current tDCS, during High Current tDCS and after High Current tDCS. Finally, Chapter 5 concludes the dissertation and provides some directions for future work.

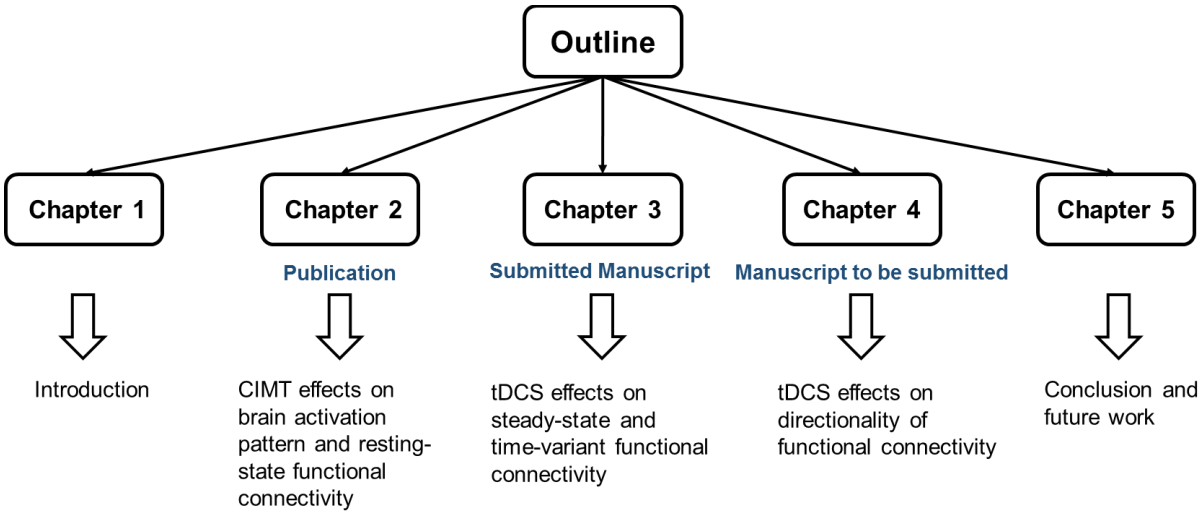

Figure 1-1 Outline of the dissertation organization

In summary, Chapter 2, 3 and 4 demonstrate my major PhD research work from August 2013 to November 2017.

Chapter 2 Evaluation of Cortical Plasticity in Children with Cerebral Palsy undergoing Constraint-Induced Movement Therapy based on Functional Near-Infrared Spectroscopy

This chapter is a publication at the journal of Biomedical Optics on April 2015 (Journal of biomedical optics 20.4 (2015): 046009-046009.)

Authorship: *Jianwei Cao, Bilal Khan, Nathan Hervey, Fenghua Tian, Mauricio R. Delgado, Nancy J. Clegg, Linsley Smith, Heather Roberts, Kirsten Tulchin-Francis, Angela Shierk, Laura Shagman, Duncan MacFarlane, Hanli Liu, George Alexandrakis*

2.1 Introduction

Cerebral palsy (CP) describes a group of permanent neurodevelopmental disorders, the core feature of which is abnormal gross and fine motor function caused by a non-progressive lesion to the brain that occurred in the developing fetal or infant brain[32-34]. Hemiplegic cerebral palsy is one of the most prevalent types of CP, characterized by unilateral motor and/or sensory impairments in the upper and lower limb. Patients with hemiplegic CP often help their affected limb while performing daily tasks by compensatory use of their unaffected limb[35, 36]. Even though CP cannot be cured, motor control skills in these children can be improved through repetitive task-specific treatments targeting an increased involvement of the affected limb[11]. Constraint-induced movement therapy (CIMT) is one such common treatment for children with upper limb hemiplegia[5]. The aim of CIMT is to restrain the unaffected extremity and thus force intensive use of the affected extremity[37].

Upper limb motor severity in patients with CP can be classified using the Manual Ability Classification System (MACS)[38]. Several upper extremity functional outcome measures have been developed and validated in this population[39, 40]. The Melbourne Assessment[41] measures unilateral upper limb function, while Assisting Hand Assessment (AHA) [42] measures bimanual function. Although very useful, clinical assessments do not yield insights about how

improved motor performance relates to therapy-induced plastic changes in the brain, for which functional imaging methods are needed[43, 44].

Functional magnetic resonance imaging (fMRI) is the gold standard for neuroimaging employed in a few recent studies to evaluate the effects of CIMT on children with CP[16, 17, 45]. In these studies the laterality index of sensorimotor activation between the two cerebral hemispheres[16, 17] was proposed as a measure of treatment response. However, fMRI requires subjects to remain steady for long periods of time in a restricted space, which limits the success rate of functional imaging studies in healthy children[46]. This may be even more relevant in children with CP. Changes in gray matter volume in the sensorimotor cortex of the lesioned hemisphere measured by anatomical MRI were also proposed as a treatment response metric[45] though this approach does not offer measures of change in brain function. In addition, changes in motor-evoked potentials (MEPs) of the affected hand were quantified by transcranial magnetic stimulation (TMS) as an alternate treatment response metric[47].

In recent years functional near-infrared spectroscopy (fNIRS) has been increasingly shown as a viable alternative neuroimaging modality to fMRI for monitoring brain activation.[25, 26] FNIRS detects changes in near-infrared light absorption caused by changes in the concentration of oxyhemoglobin (ΔHbO) and deoxyhemoglobin (ΔHb) resulting from neuronal activity, known as neurovascular coupling.[24] As light penetration in the brain is limited due to multiple scattering, fNIRS can only image cortical regions with limited spatial resolution[48, 49]. However, the portability and relative robustness of this technology to motion artifacts[28-30] make it advantageous for monitoring brain activity in children with motor deficits, as is the case for CP. Several studies utilized fNIRS to investigate cortical activation in response to motor skills in individuals with CP[50-52]. We have previously demonstrated that fNIRS can be used to image sensorimotor cortex activity in children with CP and derived a variety of related activation metrics[52]. However, no fNIRS studies have been performed to date that use activation metrics

for assessing plasticity in children with CP after CIMT and any related information reported in fMRI studies so far remains very limited[16, 17, 45].

In this work, we demonstrate how analysis of sensorimotor cortex activation patterns obtained by fNIRS during finger tapping enables quantification of spatial and temporal activation metrics for assessing plastic changes immediately after and six months after CIMT. Changes in resting-state functional connectivity patterns between sensorimotor centers are also explored as an additional metric for assessing treatment effects. Furthermore, changes in manual performance were quantified using the Melbourne and AHA clinical scales at the same time points as fNIRS measurements. The observed differences in trends between fNIRS-based metrics relative to clinical metrics provide insights into how cortical plasticity can affect manual performance. The findings of this work are a first step towards exploring in the future the intriguing possibility of using fNIRS-based metrics as long term predictors of CIMT outcomes.

2.2 Methods

2.2.1 Subjects and CIMT

Six subjects with hemiplegic CP (two female and four male, 10.2 ± 2.1 years old) were included in this study. Two subjects (Subject 4 and Subject 8) were right hemiparetic and the other four subjects were left hemiparetic. Two subjects (Subject 1 and Subject 4) were classified as MACS 1 and another four subjects (Subject 3, 6, 7 and 8) as MACS 2. Subjects with light impairment of their affected hand that was often hardly noticeable were classified as MACS 1. Subjects classified as MACS 2 had impaired use of their affected hand, but could perform life daily activities adequately through compensatory use of their unaffected hand. Five healthy children (two female and three male, 9.8 ± 1.3 years old) were also included as controls. All the controls were right handed. All children with CP included in this study had a successful MRI scan that identified a single subcortical/cortical lesion affecting their motor area in one of the two cerebral hemispheres. In addition, Subject 3 had undergone a right functional peri-insular

hemispherectomy due to intractable epileptic seizures and had a physical shift of 1.3 cm to the right of the brain midline separating the two hemispheres, as verified by the anatomical MRI. The children with CP participated in a two-week, pirate themed, CIMT camp that took place five days a week, six hours a day, at the Texas Scottish Rite Hospital for Children in Dallas. During CIMT camp, the children took part in group and individual activities such as ball games and painting, focused on improving gross and fine motor skills and increasing independence with activities of daily living under the supervision of occupational therapists. The unaffected arm of each child was immobilized by a removable splint during camp hours, which forced the use of their affected arm during play activities. FNIRS measurements, MACS[38] classification and clinical assessments using the Melbourne assessment of upper limb function[41] and AHA[42] of bimanual limb function were performed on each child with CP before, immediately after and six months after therapy. Only Subject 4 missed one fNIRS measurement at six months after therapy. The occupational therapists inquired about the children's affected arm activity levels after therapy and although these varied between subjects no additional therapies or intensive manual training were performed by any subject in the six months after CIMT. Control subjects were also measured by fNIRS at the same time points, but no clinical assessments were performed on them. The study was approved by the University of Texas Southwestern Medical Center at Dallas (UTSW) Institutional Review Board protocol (IRB No. : 042007-064).

2.2.2 Experimental Set-up and Protocol

A continuous wave fNIRS brain imager (CW-6, Techen Inc., Milford, Massachusetts) was used to map the ΔHbO and ΔHb induced by sensorimotor cortical activation during a finger tapping task. As ΔHb dynamics are highly correlated with those of ΔHbO[53] and have significantly lower amplitudes than the latter, making them susceptible to cross-talk from ΔHbO[54] and to interference from physiological artifacts, we have focused on the analysis of ΔHbO dynamics only. The source-detector probe geometry of fNIRS is shown in Fig. 2-1. There were

16 source and 32 detector fiber bundles to cover most of the sensorimotor cortex. The rows of sources and detectors were centered around the Cz position of the EEG International 10/20 system[55] and attached onto the subjects' heads by perforated Velcro straps. Near-infrared light at wavelengths of 690 nm and 830 nm was delivered from the source fiber bundles simultaneously at each source location as the CW-6 system enables all laser sources to be on at the same time with distinct modulation frequencies (6.4 to 12.6 kHz, with an increment of 200 Hz). The back-reflected light was sampled at the frequency of 25 Hz. Each source had up to six detectors with 3 cm separation, and each detector received light from up to three sources, which resulted in a total of 84 source-detector pairs for each wavelength. This setup enabled monitoring cortical activation over an 11 cm × 20 cm field of view. Additionally, eight short-distance (1.5 cm) source-detector pairs, indicated by yellow lines in Fig. 2-1, were used as references to subsequently filter out superficial background hemodynamics unrelated to activation (details in Sec. 2.2.3 below).

EEG International 10/20 system Cz, C3, C4, F3, and F4 anatomical measurements[55] were used as reference points to ensure the optical probe setup was placed over the sensorimotor cortex. The optical probe setup was centered on the Cz reference point and covered a large area of sensorimotor cortex such that the probe set extended a fixed distance of 5 cm anterior to the C3 and C4 positions to map the primary motor/sensory area (M1/S1) and was 0.21 ± 0.13 cm posterior of the measured F3 and F4 positions covering the supplementary motor area (SMA) and pre-motor cortex (PMC) of both hemispheres, as indicated in Fig. 2-1. Anatomical measurements were performed on the head of each subject at all three visits and the standard deviations of the distances between Cz and any one of C3, C4, F3, and F4, across all visits, did not exceed ~ ±1.5 mm.

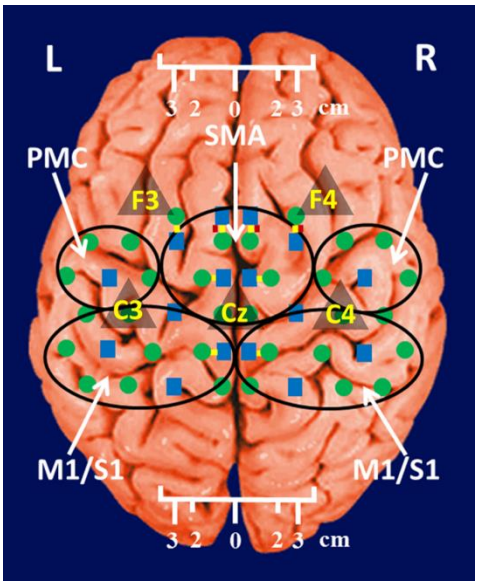

Figure 2-1 The fNIRS measurement geometry (sources: blue squares; detectors: green circles) spanned a field of view covering the PMC (pre-motor cortex), SMA (supplementary motor area) and M1/S1 (primary motor/sensory cortex) areas indicated by black ovals. Yellow lines connect the short distance source-detector pairs sampling the scalp hemodynamics. Dark gray triangles indicate the EEG International 10/20 system Cz, C3, C4, F3, and F4 locations.

After subjects were set up for fNIRS measurements they were asked to perform a finger tapping task, once with their left hand and once with their right hand. Subjects were instructed to tap with four fingers in unison (excluding the thumb) and keep their wrists on the table, while the other hand was to remain at rest as much as possible. An animation made on Adobe flash (Adobe Systems Incorporated, San Jose, CA) guided the subjects to tap at a frequency of 1 Hz. The experimental protocol for finger tapping by each hand started with a 3-min rest period, followed by eight 40-s blocks that started with 15 s of tapping followed by 25 s of rest.

2.2.3 Signal Processing and Image Analysis

In addition to detecting hemodynamic changes due to evoked cortical activation, fNIRS is also sensitive to cerebral hemodynamic fluctuations of systemic origin, which can be caused by

cardiac pulsation (0.8-2.0 Hz), respiration (0.1-0.33 Hz) and Mayer waves (0.1 Hz or lower)[56, 57]. The cortical hemodynamic response to the motion activation protocol can be found in the frequency range of 0.01-0.4 Hz, so a band-pass filter could only effectively remove cardiac pulsation, but not the respiration or Mayer waves that overlap in frequency with the activation induced hemodynamic fluctuations. In order to filter out these physiological interferences, recent studies have used component analyses[58, 59], state space estimation[56, 60], adaptive filtering[61], linear regression[62] or some combination of these[63, 64].

This study used a combination of band-pass filtering, adaptive filtering, and principal component analysis to filter the fNIRS signals as we have previously reported[52]. Briefly, the first step was to use a 0.01-0.4 Hz band-pass filter to remove cardiac pulsation signals. Subsequently, global fluctuations due to respiration and Mayer waves were removed by a combination of an adaptive least mean square (LMS) filter[61] and principal component analysis (PCA)[58]. One short source-detector pair of the eight available was used as the adaptive filter noise reference for the removal of global hemodynamic fluctuations from the fNIRS signals[61]. The reference channel chosen had the least amount of motion artifacts of the eight, which translated to having either zero or one motion-generated spikes in the time-series reference data. The spike in the reference channel time-series data was removed manually and the missing data were interpolated by the *spline* cubic spline function in MATLAB (Mathworks, Natick, Massachusetts). Moreover, any block of data with obvious motion artifacts in any tapping/rest period was manually excluded from further analysis.

Reconstruction and visualization of fNIRS images from the acquired reflectance data was performed by the open-source HomER software implemented in MATLAB[65]. In this software, activation images were reconstructed by the Tikhonov perturbation solution to the photon diffusion equation, which employs a regularized Moore–Penrose inversion scheme.[66, 67] The resulting ΔHbO maps were reconstructed 20 × 21 pixel images (0.55 cm × 0.95 cm for each pixel) for every 0.04 s time interval.

The determination of image pixels with activation was based on a two-step process. Firstly, the image pixels with temporal hemodynamic patterns that correlated significantly with evoked cortical activation were identified by a general linear model (GLM) similar to previous fMRI studies.[68-70] A value of $p < 0.0001$ based on Bonferroni's correction was used as the threshold to identify pixels with activation. Secondly, a k-means clustering algorithm[71] was used to calculate the signal to noise ratio (SNR) per image pixel. This was done to exclude any pixels with low SNR that the GLM still found to correlate significantly with the model-based hemodynamic response function[72] calculated for the finger tapping protocol being used in this study. The algorithm considered the entire temporal responses for each pixel after GLM and divided the pixel values into three clusters: activation, baseline, or deactivation[52]. The pixel values in the baseline cluster were regarded as noise. The SNR of activation for each pixel was then calculated as the mean signal amplitude of the activation cluster over the standard deviation of the hemodynamic fluctuation amplitudes of the noise cluster in that pixel. Pixels with SNR ≥2 were considered to be part of regions of activation when the ΔHbO amplitude equaled or exceeded two standard deviations of the amplitude of background hemodynamic fluctuations. The selected SNR threshold corresponded to a probability of 95%, or more, for the fluctuation amplitudes of these pixels to be different from those due to background hemodynamics.

The sequence of post-processing steps described above is shown in Fig. 2-2. More details can be found in a prior publication from our group[52].

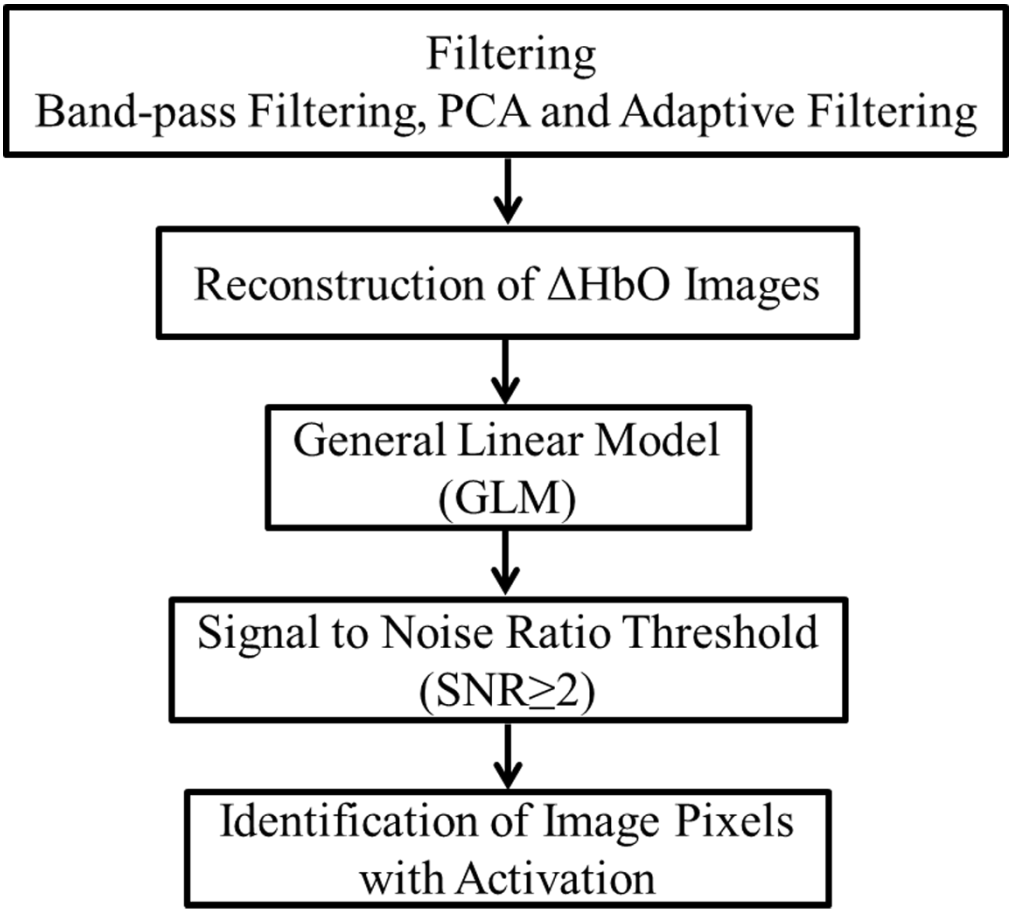

Figure 2-2 Flowchart of post-processing steps.

2.2.4 FNIRS Based Metrics Derived from Activation Images and Detector Level Resting-State Data

The laterality index and time-to-peak/duration metrics were derived from the analysis of activation images. The time series data from each subject were first analyzed to find all image pixels with significant activation, as described in Sec. 2.2.3 above. Subsequently, the laterality index metric was calculated using Eq. (1) and the time-to-peak metric was computed for each pixel with activation and was then averaged across pixels. Resting-state functional connectivity between sensorimotor regions was computed from source-detector channel data that were first averaged within each region indicated in Fig. 2-1.

2.2.4.1 Laterality index

Laterality of activation, representing the dominance of one side of the brain in controlling motor functions, was quantified by the laterality index[73]:

$$L = \frac{N_{contral} - N_{ipsi}}{N_{contral} + N_{ipsi}}, \quad (1)$$

where $N_{contral}$ was the number of activation pixels in the contralateral hemisphere and N_{ipsi} was the number of activation pixels in the ipsilateral hemisphere. Equation (1) indicates that an L value of '+1' corresponds to complete contralateral activation, an L value of '-1' represents complete ipsilateral activation and an L of '0' reflects bilateral activation. The midline separating the two hemispheres for calculating laterality index was shifted for Subject 3, as described in Sec. 2.2.1. Laterality index was averaged across subjects for each visit time point before comparing data between visits.

2.2.4.2 Resting-state functional connectivity

Resting-state functional connectivity represents the regional interactions between cortical centers that occur when a subject is not performing an explicit task[74]. Source-detector channels were assigned to the M1/S1, PMC or SMA, as identified by the EEG International 10/20 system Cz, C3, C4, F3, and F4 anatomical measurements[55]. The signal of the 3-minute rest period at the beginning of the protocol from the fNIRS detector fiber bundles found within each of these three regions was averaged separately for each hemisphere. Due to Subject 3's anatomical midline shift, as described in Sec. 2.2.1, only those source and detectors that were at least 2 cm to the right of the measured Cz position were considered part of the right hemisphere. The resting-state functional connectivity between these sensorimotor areas was subsequently computed using a synchronization likelihood (SL) metric[31]. Cortical regions were considered as functionally connected for SL ≥ 0.6[75]. This threshold was lower than what is typically used in

studies on adults[76, 77], as correlation strength is known to be weaker in children[78]. The connection frequency between pairs of sensorimotor regions was calculated for each visit time point as the percentage of subjects having this connection according to the SL metric used.

2.2.4.3 Activation time-to-peak/duration

Temporal aspects of cortical activation patterns in fNIRS images were quantified by the time-to-peak/duration metric. The rationale behind this metric was that in children with CP performing finger tapping the time-to-peak tends to be shorter and the activation duration longer compared to controls[52]. Thus an increase in this ratio would reflect treatment induced normalization of activation patterns. The duration of activation in each pixel was defined as the total time for which the hemodynamic fluctuation amplitude in that pixel exceeded a threshold, which was defined as the maximum value of the baseline cluster identified by the k-means algorithm (Sec. 2.2.3). The activation duration metric was then computed as the average of all image pixels within the activation area. The time difference between the beginning of the tapping interval and the time point of maximum ΔHbO, averaged over all pixels with activation in the image, was defined as the time-to-peak metric. Time-to-peak/duration was averaged across subjects for each visit before comparing data between visits.

2.2.4.4 Statistical analysis

Two-sampled t-tests were performed using SAS 9.2 (SAS Institute Inc. Cary, North Carolina) to see if there was a significant difference ($p < 0.05$) of metric means between control subjects and subjects with CP. Paired t-tests were also performed to determine if there was a significant difference ($p < 0.05$) of metric means between visits of subjects with CP. In cases where dataset was found to be non-normally distributed ($p<0.05$), Wilcoxon rank sum test and Wilcoxon signed-rank test were performed instead, respectively. A post hoc power analysis was performed

to validate the statistical power (1- β) of the t-test for the cases where there was a statistically significant difference between the two metric categories being compared[79].

2.3 Results

It was found that when children with CP tapped with their unaffected hand there were no statistically significant changes for any of the fNIRS activation metrics between measurement time points. In this work the activation metrics obtained from children with CP tapping with their affected hand were compared to those obtained from controls tapping with their dominant hand at the same measurement time points.

2.3.1 Laterality Index

Activation in M1/S1 cortical regions only was used for the laterality index metric calculations following previously reported fMRI and fNIRS studies[16, 17, 80]. Figure 2-3 shows the mean and standard deviation of the laterality index for controls and children with CP. The three visits for the controls were averaged into a single group of values as the laterality index was not found to change significantly over time for these subjects ($p = 0.84$). As shown in Fig. 2-3, controls had preferential activation in the contralateral sensorimotor cortex during finger tapping. In contrast, children with CP showed bilateral activation on average before therapy. At the second visit immediately after therapy, the laterality index for children with CP increased and was closer to that of controls. At six months after therapy only one child with CP retained a high laterality index while all others relapsed. As result the mean laterality index relapsed close to the values before treatment.

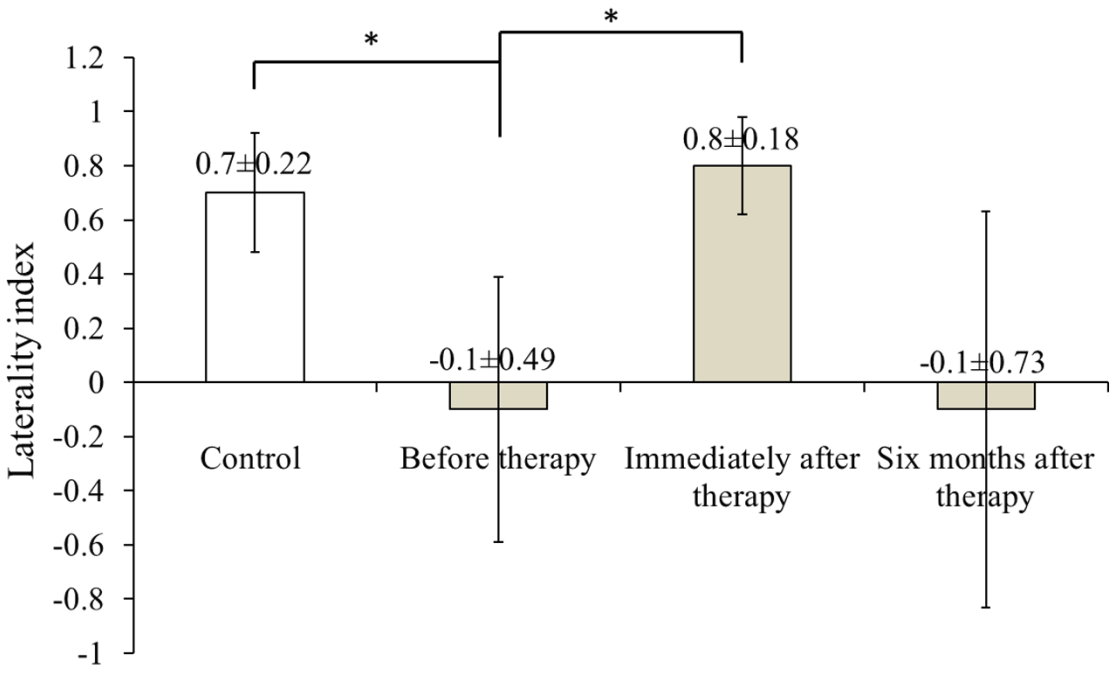

Figure 2-3 Laterality index for controls tapping with their dominant hand and children with CP tapping with their affected hand across the three visits (White: Controls, Grey: Children with CP). Error bars indicate +/- one standard deviation. Asterisks indicate statistically significant differences in laterality index ($p < 0.01$).

A high statistical significance was found ($p = 0.007$, power $(1-\beta) = 0.91$) for the mean value difference in laterality index between controls and children with CP before therapy. Moreover, the laterality index of children with CP immediately after therapy was significantly different ($p = 0.006$, power $(1-\beta) = 0.98$) from that of before therapy. No significant difference was observed between six months after therapy and prior visits due to the larger standard deviation of the group's laterality index six months after therapy.

2.3.2 Resting-State Functional Connectivity

Changes in the resting-state functional connectivity between five cortical regions (Fig. 2-1) were explored as a metric of response to CIMT. Based on the aforementioned SL ≥ 0.6 criterion

the two MACS 1 subjects showed significant pair-wise connectivity between all sensorimotor regions that did not change between the three visits. The four children with CP that did show connectivity changes, all MACS 2, were compared to the average connectivity pattern from five controls in this part of the study. The thickness of lines in Fig. 2-4 connecting any two sensorimotor regions represents the percentage of MACS 2 subjects for whom a given pair of activation regions was connected.

The frequency of connections between any two regions for controls was no more than 60%. In contrast, the frequency of pair-wise connection between regions for children with CP before therapy was much higher, even reaching 100% for some connections between the SMA and other cortical regions. Interestingly, immediately after therapy children with CP on average had weaker connectivity frequencies, especially between the SMA and other cortical regions, which was similar to what was observed in controls. Therefore these results imply a certain level of sensorimotor network normalization occurring immediately after CIMT. However, at the six months after therapy time point, the connectivity frequencies between almost all cortical regions reversed back towards values found before therapy.

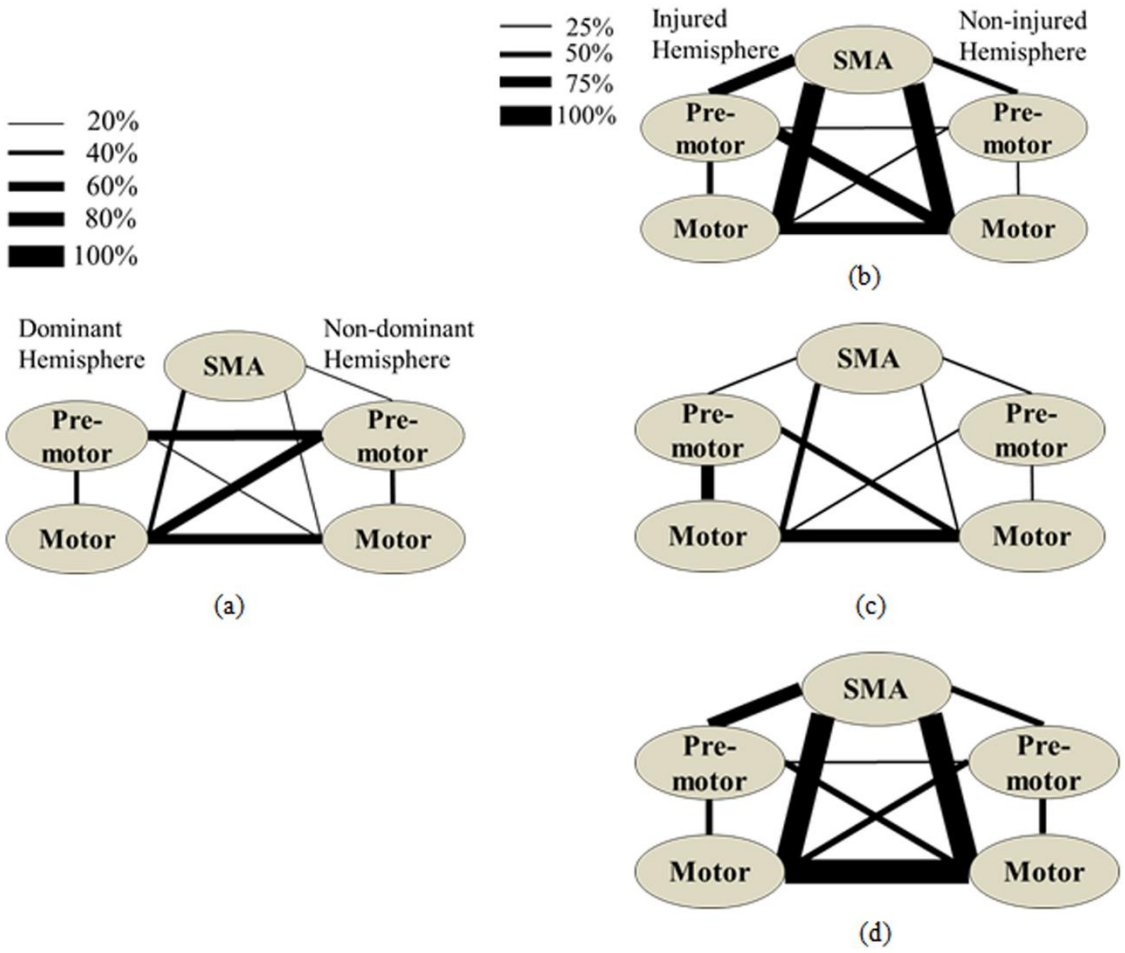

Figure 2-4 Group-wise resting-state functional connectivity in controls (a) and children with CP at the three assessment time points: (b) before therapy, (c) immediately after therapy, (d) six months later after therapy. Black line thickness represents the percentage of subjects with significant connectivity between a given pair of sensorimotor centers.

2.3.3 Activation Time-to-Peak/Duration

Figure 2-5 shows the mean and standard deviation of the time-to-peak/duration metric for controls and the three visits of children with CP. No significant difference was observed for controls between the three visits ($p = 0.69$) and they were averaged into a single group. A significant difference was found in time-to-peak/duration between controls and children with CP before therapy ($p = 0.001$, power $(1-\beta) = 0.97$). Most subjects with CP had a smaller time-to-

peak/duration metric before therapy, which increased significantly immediately after therapy ($p = 0.03$, power $(1-\beta) = 0.99$) and persisted at significantly higher values ($p = 0.006$, power $(1-\beta) = 0.97$) six months after therapy. The change of time-to-peak/duration towards higher values indicates a normalization of temporal activation patterns in all five sensorimotor regions after CIMT that persisted even six months later.

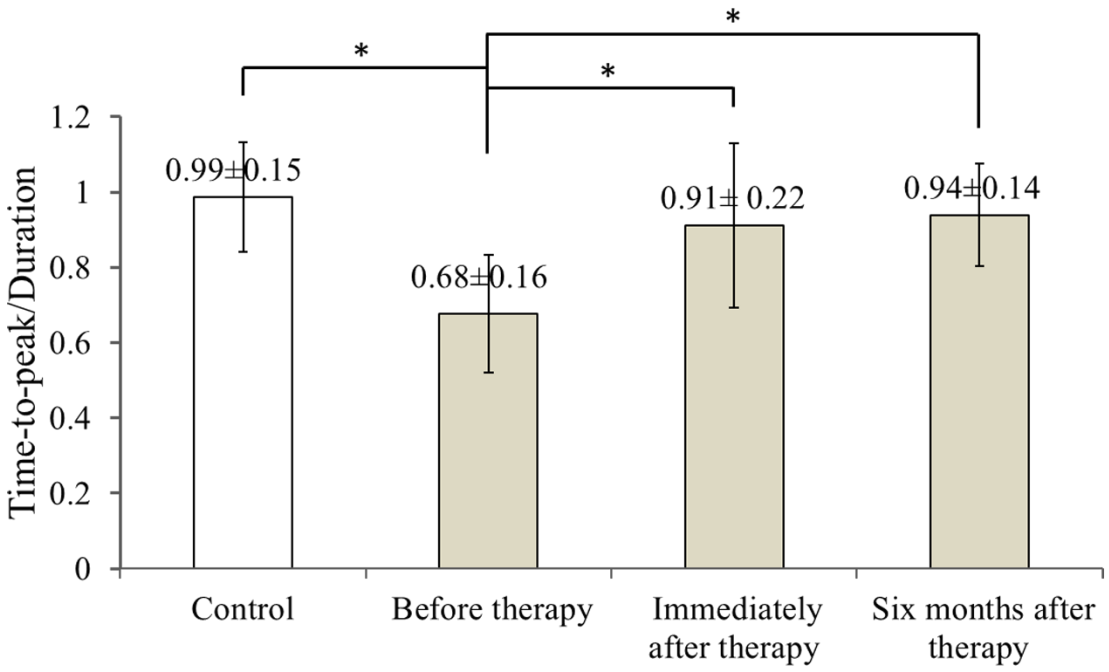

Figure 2-5 Time-to-peak/duration of activation for controls tapping with their dominant hand and children with CP tapping with their affected hand across the three visits (White: Controls, Gray: Children with CP). Error bars indicate +/- one standard deviation. Asterisks indicate statistically significant differences in time-to-peak/duration ($p < 0.05$).

2.3.4 Comparisons with Clinical Assessment Scores

2.3.4.1 Changes in Melbourne and AHA scores between visits

The Melbourne and AHA scales were employed to evaluate the unimanual and bimanual performance, respectively, of children with CP before, immediately and six months after therapy. Figure 2-6 illustrates changes in Melbourne scores versus changes in AHA scores for children

with CP between visits. The thresholds for clinically significant improvements in Melbourne and AHA scores were 14 and 5, respectively.[41, 42] These threshold values are depicted in Fig. 2-6 as dashed lines.

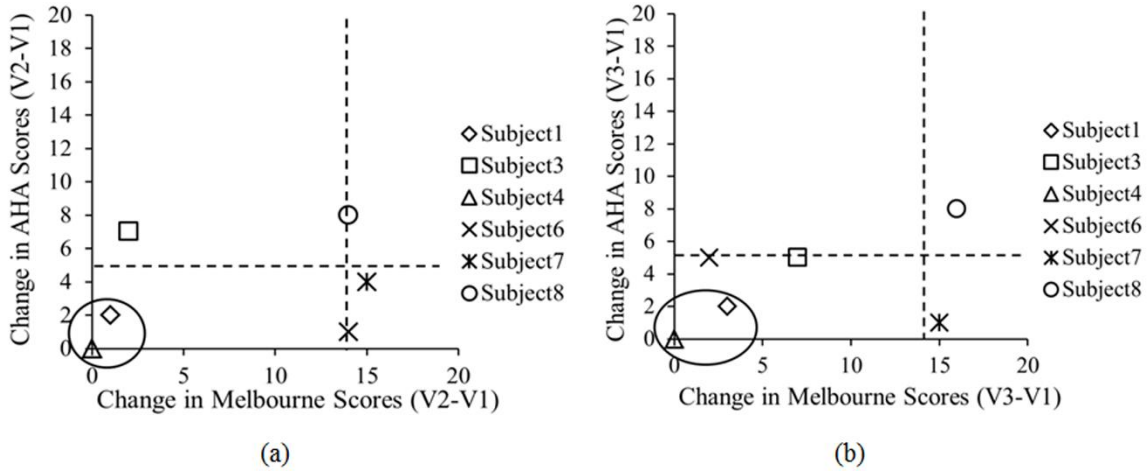

Figure 2-6 Change in clinical scores for six subjects with CP between visits (V1: before therapy, V2: immediately after therapy, V3: six months after therapy). (a) Change in scores between before and immediately after therapy (V2-V1). (b) Change in scores between before and six months after therapy (V3-V1). Thresholds for clinically significant improvements in Melbourne and AHA scores were 14 (vertical dashed lines) and 5 (horizontal dashed lines), respectively. Data for MACS1 subjects are inside ovals.

Changes in clinical scale scores varied greatly between immediately after therapy [Fig. 2-6(a)] and six months after therapy [Fig. 2-6(b)]. Nevertheless, all four MACS2 subjects improved significantly on Melbourne or AHA scores, or both, immediately after therapy and six months after therapy. On the contrary, the two MACS 1 subjects included in this study, Subjects 1 and 4 [circled with black ovals in Figs. 2-6(a) and 2-6(b)], did not show significant improvements on either assessment scale. As a result, the discussion below on the comparisons between clinical scale scores and fNIRS metrics focuses on the four MACS 2 subjects, who had significant changes in motor function after CIMT.

2.3.4.2 Changes in Melbourne and AHA scores versus changes in laterality index

Figures 2-7(a) and 2-7(b) illustrate the comparison between the change in Melbourne scores and the change in laterality index between visits for the four MACS 2 subjects. It is seen that for all subjects expect for Subject 3, an increase in laterality index representing a shift of cortical activation from the ipsilateral to the contralateral hemisphere was accompanied significant improvements in unimanual ability immediately after therapy, as reflected by the increased Melbourne scores [Fig. 2-7(a)]. The fact that Subject 3 appears to be an outlier is not surprising given that he had previously had brain surgery due to intractable epileptic seizures (see Sec. 2.2.1). The laterality index change of 2 for this subject indicates a complete switch of activation between hemispheres towards a more normal laterality pattern that however did not result in significant motor gains [Fig. 2-7(a)]. At six months after CIMT [Fig. 2-7(b)] Subject 6 had relapsed but all other subjects maintained and even slightly improved unimanual ability compared to before therapy. Even though there are not enough subjects to perform formal statistical analyses one can see a positive trend between laterality index and Melbourne score changes in Fig. 2-7(b).

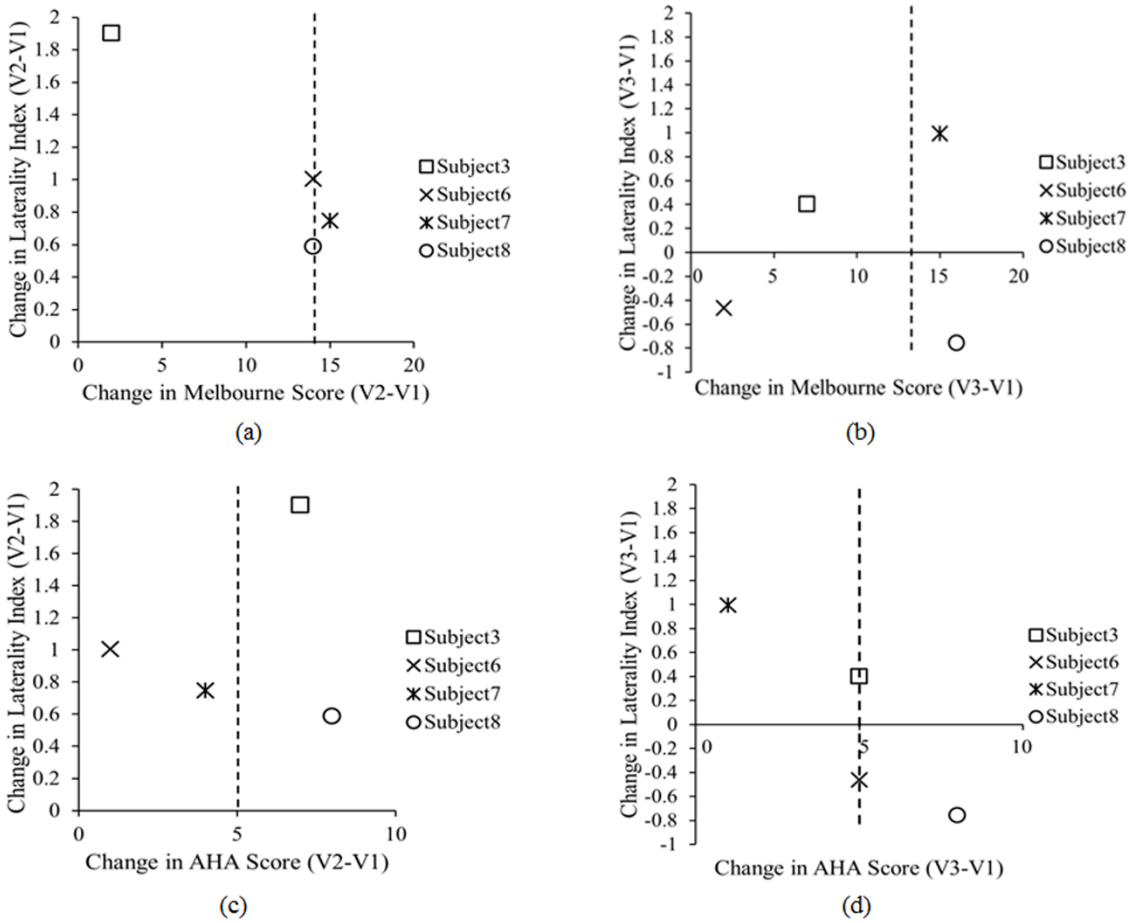

Figure 2-7 Change in clinical scores versus change in laterality index for MACS 2 subjects between visits (V1: before therapy, V2: immediately after therapy, V3: six month later after therapy). Change in Melbourne scores versus change in laterality index immediately after therapy (a) and (b) six months after therapy. Corresponding changes in AHA scores immediately after therapy (c) and (d) six months after therapy.

In contrast to Melbourne score changes, an overall negative trend between laterality index and AHA score changes could be discerned both immediately after therapy [Fig. 2-7(c)] and six months after therapy [Fig. 2-7(d)]. An exception to this trend was Subject 8 who had improvements in both Melbourne and AHA scores that were maintained six months later, but at the cost of a significant relapse in laterality index six months after therapy that was even more abnormal than the values before therapy.

Another noteworthy observation was that Subject 7 was the only one in the MACS 2 group who retained significant improvements in unilateral motor function, as assessed by the Melbourne scale, while also maintaining a normalized laterality index [Fig. 2-7(b)]. Interestingly, Subject 7 also had the highest average connectivity strength between sensorimotor centers (0.70) compared to the MACS2 group average (0.64). Nevertheless the connectivity pattern for Subject 7 was not different from that of the group average shown in Fig. 2-4(d).

Overall, the above results showed that each child had a unique way of responding to CIMT and attain some motor function improvements by increasing the involvement of the ipsilateral sensorimotor cortex (Subject 8), increasing the connectivity strength between sensorimotor centers (Subject 7), or by some combination thereof (Subjects 3 and 6). A positive trend between increases in Melbourne scores and increases in time-to-peak/duration, as well as a negative trend between increases in AHA scores and increases in time-to-peak/duration were also noticed (all results are compiled in Table 2-1).

Table 2-1 Clinical scores and fNIRS metrics of subjects with CP before, immediately after and six months after therapy (V1: before therapy, V2: immediately after therapy, V3: six months after therapy).

	Clinical scores						fNIRS metrics					
	Melbourne			AHA			Laterality index			Time-to-peak/duration		
Subject	V1	V2	V3	V1	V2	V3	V1	V2	V3	V1	V2	V3
S1	110	111	113	60	62	62	0.5	1	0.4	0.92	1.15	1.13
S3	74	76	81	34	41	39	-1	0.9	-0.6	0.62	0.81	0.86
S4	117	117	117	84	84	84	0	1	-	0.80	1.22	-
S6	45	59	47	47	48	52	0.1	0.9	-0.6	0.62	0.85	0.81
S7	54	69	69	64	68	65	-0.1	0.6	0.9	0.52	0.73	0.86
S8	58	72	74	44	52	52	0	0.6	-0.8	0.56	0.71	1.04
Controls (Averaged)	-	-	-	-	-	-	0.69	0.71	0.69	0.97	0.99	1.00

2.4 Discussion

For unilateral brain lesions causing hemiplegia there is a natural tendency for the affected sensorimotor control areas to recruit corresponding areas from the contralateral unaffected cerebral hemisphere. The increased connectivity between hemispheres is presumed to be a compensatory reaction to the loss of connections with white matter after brain injury[81]. CIMT has been used to enforce increased use of the affected hand and reduce over-reliance on the unaffected hemisphere[37], which is accompanied by partial normalization of brain activation patterns[16, 17].

In this work fNIRS was used to map the plastic changes that occurred in the sensorimotor cortex of six children with CP immediately after and six months after two weeks of CIMT. Changes in the unimanual and bimanual ability of these children were assessed by the Melbourne and AHA functional scales respectively at the same time points as fNIRS measurements. Subsequent data analysis and comparisons yielded some interesting insights:

Firstly, though larger numbers of subjects would need to be tested in the future, the clinical results of this work suggest that subjects with a higher (MACS 2) level of motor impairment could benefit more from CIMT, which is consistent with findings from a prior clinical report.[82] The two less impaired MACS 1 subjects did not benefit as much, as proven by the non-significant changes in their clinical scores after CIMT (Fig. 2-6). These subjects had high manual ability scores to begin with. As this was an initial exploratory study, only children with CP with lower level motor impairment classified as MACS 1 or MACS 2 were included to avoid possible issues with more impaired subjects who may have had difficulty following the fNIRS finger tapping protocol.

Secondly, there were no children with CP in this study that significantly improved both their unimanual and bimanual abilities after CIMT while also normalizing their sensorimotor activation patterns, as measured by fNIRS. Normalization in this context meant that the laterality index and time-to-peak/duration metric values became closer to corresponding values seen in the group of healthy children that were closer to unity for both metrics. From Fig. 2-6(a) and Fig. 2-

6(b), it was interesting to see that for three of the four MACS 2 subjects (Subjects 3, 6 and 7) there was significant improvement in either the Melbourne or AHA scores, but not both, at any one assessment time point. Since Melbourne scores reflected unimanual ability and AHA scores reflected bimanual ability, it is possible that a trade-off existed between using unilateral or compensatory bilateral limb movements to perform manual tasks. This trade-off was also observed by the positive trend between laterality index and Melbourne score changes in Fig. 2-7(b) and an overall negative trend between laterality index and AHA score changes both immediately after therapy [Fig. 2-7(c)] and six months after therapy [Fig. 2-7(d)]. This observation suggests that normalization of the laterality index, while improving unimanual ability [Fig. 2-7(b)], results in the trade-off of reduced bimanual ability [Fig. 2-7(d)] for these children. However, one MACS 2 subject, Subject 8, had significant improvements immediately after therapy that persisted six months after therapy for both clinical assessment scales. This subject not only improved the use of the affected arm, but also the cooperation between arms. However, the negative change in laterality index for this subject at six months after CIMT [Fig. 2-7(b)] suggests that the improvement in Melbourne score (unimanual ability) occurred at the expense of abnormally high compensatory use of the uninjured brain hemisphere.

Thirdly, an interesting difference was observed between how the time-to-peak/duration changed with time post-therapy compared to the laterality index and resting-state connectivity metrics studied here: Time-to-peak/duration, a local measure of hemodynamic response, sustained the improvements seen immediately after CIMT out to six months after therapy. In contrast, laterality index and resting-state connectivity, which are global measures of hemodynamic response, normalized immediately after CIMT but relapsed six months after therapy towards the values before therapy. These observations suggest that global metrics of hemodynamic pattern change may be more useful than local metrics for assessing longer term treatment response.

The results of this work are consistent with results from the few fMRI studies that that exist to date on the topic of CP and CIMT[16, 17]. Specifically, in a case report on a child with CP with MACS2 the laterality index changed from -0.25 before three weeks of CIMT to 0.43 immediately afterwards.[16] In another study including four children with CP (MACS1 and MACS2), two maintained a high laterality index between before (0.80 ± 0.08) and immediately after CIMT (0.72 ± 0.07) while the other two showed a positive shift in laterality index from -0.14 ± 0.16 before to 0.34 ± 0.13 after CIMT[17]. In all, in these prior studies subjects with a low pre-CIMT laterality index showed an increase immediately after therapy. These studies also reported concurrent improvements in manual ability metrics after CIMT, but the limited number of subjects studied and the variability of manual ability assessment methods used between studies precludes any further comparisons. Finally, an fMRI resting-connectivity study on children with CP showed similarly bilateral patterns as reported in this work,[83] but the effects of CIMT on resting-connectivity patterns have not been reported previously.

2.5 Conclusion

This work demonstrated the utility of portable fNIRS technology as a means of mapping sensorimotor cortex plasticity in children with CP to help explain changes seen in manual ability after a therapeutic intervention. The fNIRS results provided insights that would not be accessible by looking at changes in clinical scores alone. Larger numbers of subjects would need to be followed in future studies for longer periods of time to assess whether fNIRS metrics could be used as predictors of CIMT outcomes.

Chapter 3 Modulating the resting-state functional connectivity patterns of language processing areas in the human brain with anodal transcranial direct current stimulation (tDCS) applied over the Broca's area

This Chapter is a manuscript submitted to Neurophotonics.

Authorship: *Jianwei Cao, Hanli Liu, George Alexandrakis*

3.1 Introduction

Transcranial direct current stimulation (tDCS), is a noninvasive brain stimulation technique that has been applied to modulate cognitive function so as to enhance performance in healthy subjects[84-86] and facilitate neurorehabilitation during stroke recovery[87]. Typically, tDCS is used with the intention to alter cortical excitability by delivering weak currents (1-2 mA) through a pair of anode-cathode electrods for 8-20 min[88]. The primary mechanisms of the excitability shifts are depolarization of resting membrane potential by anodal stimulation and hyperpolarization of resting membrane potential by cathodal stimulation, as has been illustrated in animal studies.[89, 90] In the context of human subject studies on areas of the brain controlling language processing, which is the focus of this work, it has been suggested that anodal tDCS over either Broca's area or Wernicke's area can improve naming accuracy or speed both in stroke-induced aphasia patients[9, 12, 13] and in healthy subjects[86, 91, 92].

Despite the above-described growing number of studies investigating how tDCS affects language performance through stimulation of language processing areas there has been relatively little study of how tDCS affects cortical functional connectivity reorganization during those interventions. Meinzer et al.[18] used resting-state functional Magnetic Resonance Imaging (fMRI) to assess the impact of anodal tDCS on the functional connectivity networks of healthy subjects. Their results showed an increase of functional connectivity strength in language-associated regions, such as dorsolateral and medial prefrontal regions, pre-Supplementary Motor Area (pre-

SMA) and SMA, but a decrease in more posterior and occipital regions. Marangolo et al.[19] revealed that increased connectivity strengh was most pronounced in the left hemispheric structures related to planing, maintenance and execution of speech. They used resting-state fMRI to study the effects of bilateral tDCS on aphasia patients, with the anodal patch applied over the Broca's area of the lesion-containing left brain hemisphere and the cathodal patch applied over the homologous contralateral brain region. Also, the presently few studies of tDCS-mediated changes on connectivity have focused on steady-state rather than the temporal aspects of those changes. The fact that tDCS could affect dynamic fluctuations in functional connectivity has not yet been explored even though the study of these fluctuations has been shown to elucidate fundamental properties of brain networks[20-23].

One additional aspect of tDCS studies that remains underexplored to date is the effect of electrode placement on language performance. For example, Monti et al.[93] found out that anodal tDCS over the left Broca's area did not improve naming accuracy in chronic non-fluent aphasic patients, while Baker et al.[9] reported improved naming performance for stimulation over the same area. It is conceivable that due to heterogeneity of lesion effects in aphasic patients an optimal tDCS electrode placement for language enhancement and recovery would differ between subjects. In an ideal scenario, investigators would be able to try different tDCS electrode placements rapidly to find the one that could maximize performance improvements in each patient. However, the current intensities used in tDCS interventions produce long-lasting effects on cortical activity with durations from hours to days,[94] which makes the rapid testing of multiple electrode placements impossible. One potential way to reduce testing time could be to use lower tDCS currents, which reduce the duration of tDCS effects on the brain hemodynamics to a few minutes. We have previously shown that use of lower tDCS currents allows multiple tDCS placements to be tested within one single session[95]. However, the potential utility of this lower current tDCS depends on whether it could predict what the connectivity changes would be like during the High Current tDCS condition.

This work is a first step towards addressing the aformentioned knowledge gaps in tDCS studies, namely (1) to study the effect of stimulation current on the stady-state and temporal connectivity changes in brain networks related to language processing, and (2) study whether lower current tDCS patterns could predict connectivity changes occuring during and after the application of larger tDCS currents. Here, we have studied the effect of tDCS current intensity on the cortical connectivity maps of healthy adults by use of functional near-infrared spectroscopy (fNIRS). FNIRS can detect changes in the concentration of oxyhemoglobin (ΔHbO) and deoxyhemoglobin (ΔHb) resulting from neurovascular coupling[24], and has been increasingly shown to be a viable alternative neuroimaging modality to fMRI despite its lower spatial resolution and ability to only map cortical activation[25, 26]. Also, the compatibility of fNIRS with tDCS makes it advatangeous for studying brain reorganization induced during tDCS[31]. Furthermore, fNIRS provides higher temporal resolution relative to fMRI, which is valuable for investigating time-varying functional connectivity in the brain[27].

To our knowledge, no fNIRS studies to date have reported how tDCS affects the reorganization of language area networks. Specifically, in this work we wanted to assess the alterations of functional connectivity due to anodal tDCS over the left Broca's area and whether a low tDCS current (0.5 mA) could qualitatively predict cortical connectivity patterns occuring after a high tDCS current (1 mA), which is a standrad intervention current choice in the literature. Cortical connectivity patterns were computed using seed-based functional connectivity with the seed located on the anodally stimulated left Broca's area and on its homologous area on the right hemisphere. Furthermore, we compuetd changes in time-variant functional connectivity with the same seeds and also employed graph theory analysis to assess global pattern changes with tDCS current intensity. Cortical reorgnization patterns of functional networks created in response to Low Current tDCS were compared to those during and after High Current tDCS. The findings of this work are discussed in light of their potential future utility for helping guide therapeutic interventions.

3.2 Method and Materials

3.2.1 Subjects

Thirteen right-hand subjects (2 Females, 11 Males, mean ± SD age = 35.4 ± 8.4) were recruited in this study. Subject handedness was determined by the Edinburgh Handedness Inventory [96]. All subjects were healthy and did not have a history of neurological disorders. Written informed consent was obtained from each participant before the experiments. The studies were carried out under the approval of the University of Texas at Arlington Institutional Review Board protocol (UTA #2015-0819).

3.2.2 FNIRS Imaging Setup Combined with tDCS

Fig. 3-1(a) illustrates the overall instrumentation setup. A continuous-wave fNIRS imaging system (LABNIRS, Shimadzu, Japan) was used, which utilized near-infrared light diode sources (at wavelengths of 780nm, 805nm, and 830nm) and photomultiplier detectors. A schematic of the fNIRS source-detector geometry is shown in Fig. 3-1(b). The setup geometry consisted of 26 sources and 28 detectors with a separation of 3 cm, resulting in 83 source-detector channels, that were inserted into the optode holder on the subject's head. This probe geometry covered cortical areas known to be part of the language network, including the Broca and Wernicke's areas of the left hemisphere and their homologous locations in the right hemisphere, as well as some prefrontal cortical regions including the frontopolar, dorsolateral prefrontal cortex and premotor areas. FNIRS signals were sampled at a frequency of 12.35 Hz.

A co-registration procedure was performed based on cranial landmark measurements on all the subjects[25] to estimate the cortical regions covered by the fNIRS source-detector geometry. A motion tracking system (Fastrak, POLHEMUS) was used to measure five reference cranial landmarks (nasion, inion, left and right preauricular points and vertex), as well as the location of all source and detector optodes. The Montreal Neurological Institute (MNI) coordinates were calculated from the real-world stereotaxic coordinates of the optodes with the five cranial

landmarks as reference positions[97]. NIRS-SPM[98] was used to register the optodes on the standard MRI brain template and identify the Brodmann areas of each source-detector channel. Fig. 3-2 shows the spatially registered channels (averaged over all thirteen subjects) on the standard human brain atlas.

TDCS current was applied by a battery-driven electrical stimulator (Phoresor II, IOMED Inc., Salt Lake City, UT) connected by a pair of saline-soaked gauze covered gel electrodes (5 × 5 cm; IOMED Inc., Salt Lake City, Utah). The tDCS patches were placed on the head using the EEG International 10/20 system[55] as a reference. The anodal patch was placed over the FC5 position to stimulate left Broca's area, which is centered at Channel 27 in our setup, and a cathodal patch was centered over the Fp2 position[92] as control (dashed square in Figs. 3-2(a) – (d)). Two 0.5 cm-diameter holes were punctured on each patch to fit through optical fiber bundles that overlapped spatially with the patches.

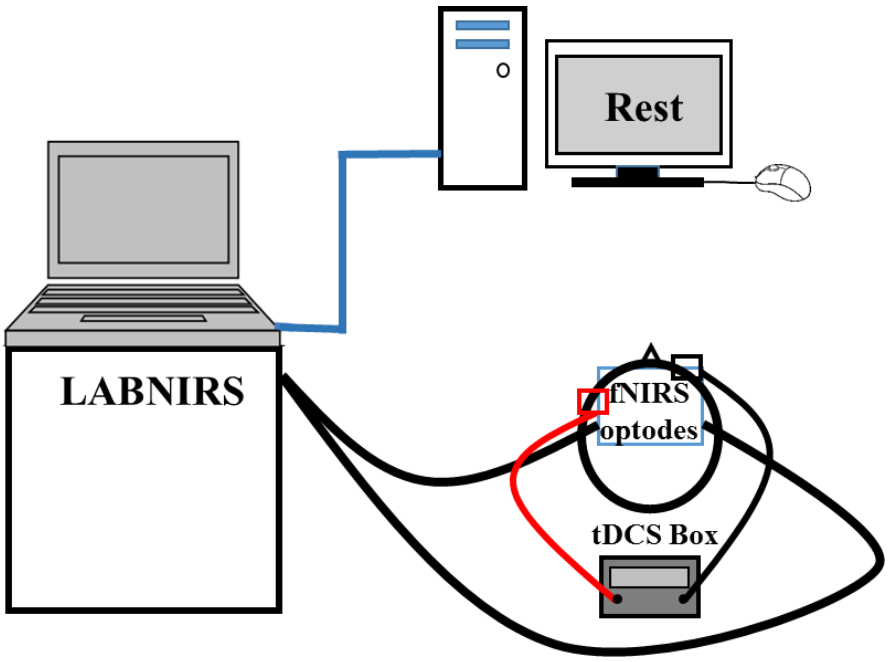

(a)

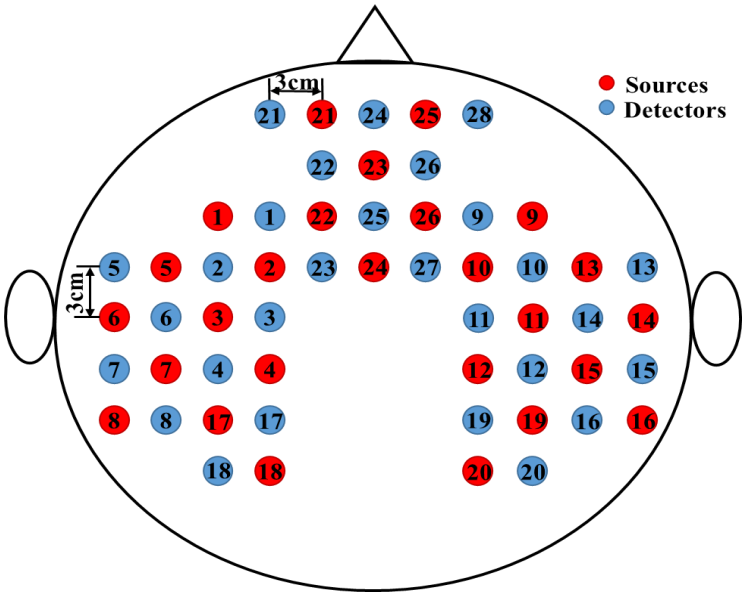

(b)

Figure 3-1 (a) A schematic representation of the overall instrumentation setup. The protocol only with "Rest" is shown on the screen. FNIRS optodes and tDCS electrodes were placed on the subject's head as described in Sec 2.2. (b) Schematic of the fNIRS probe geometry with 26 sources and 28 detectors placed over a subject's head. The separation of all source and detectors is 3 cm. (Red dots: sources, blue dots: detectors)

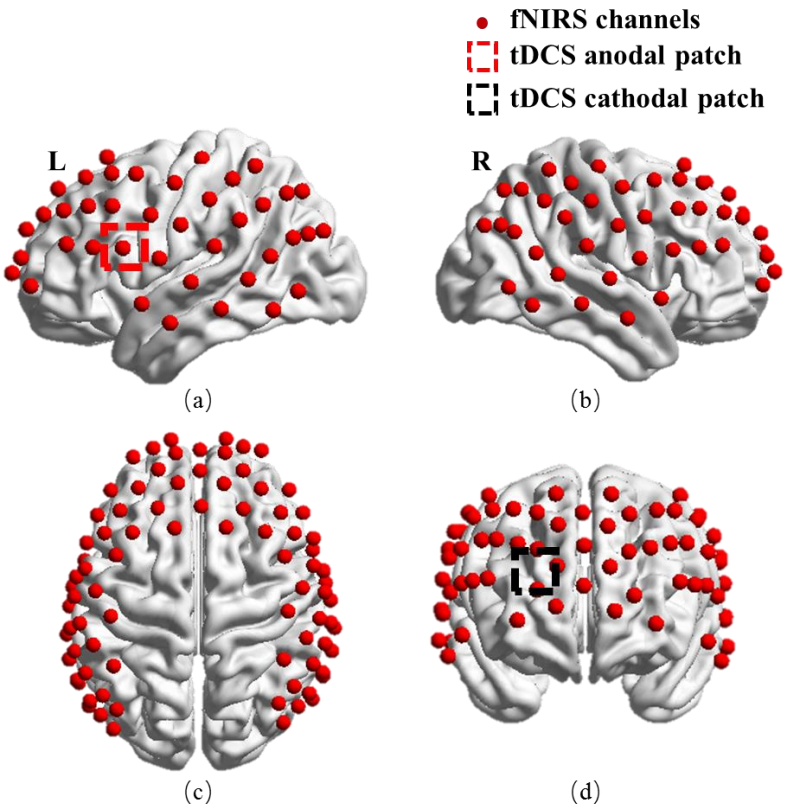

Figure 3-2 Co-registration of fNIRS source-detector channels (mid-way points between source and detector pairs) on a standard human brain atlas: (a) Sagittal view (Left), (b) Sagittal view (Right), (c) Top view and (d) Coronal view. TDCS anodal patch (red dashed square) and cathodal patch (black dashed square) are placed on the left FC5 position (a) and right Fp2 position (d).

3.2.3 Protocol Design

Subjects were asked to rest for 32 minutes with eyes closed but awake, while fNIRS measurements were performed. The first 6 minutes before tDCS were used as baseline, and then 0.5 mA current tDCS, henceforth referred to as Low Current tDCS, was applied for 2 min 40 s. Subsequently, subjects were asked to continue to rest for 5 min and 20 s, which was ample time for any hemodynamic signatures of the Low Current tDCS to disappear.[88, 95, 99] After that, a higher current of 1mA, henceforth referred to as High Current tDCS, was applied for 8 min. The fNIRS imaging session concluded with 10 min of acquiring data while subjects rested so as to

record changes in the hemodynamics immediately after the end of the 1mA tDCS. A schematic of the timeline of the protocol is shown in Fig. 3-3. All subsequent fNIRS data analyses were performed separately for each one of the four stimulation conditions: No tDCS (0-6 min), Low Current tDCS (6-14 min), High Current tDCS (14-22 min), After High Current tDCS (22-32 min). Subjects were not told when tDCS was applied.

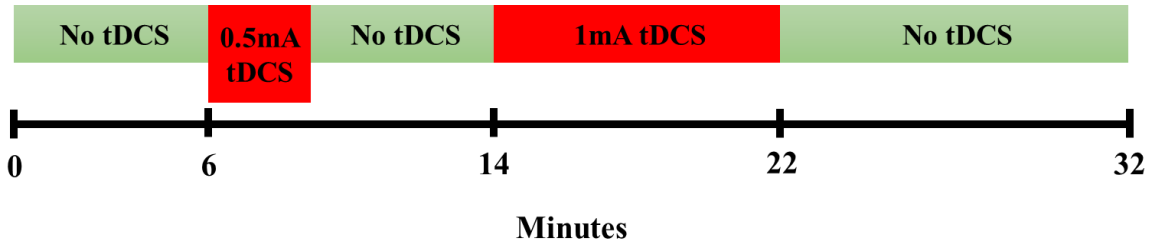

Figure 3-3 *The tDCS protocol timeline*

3.2.4 Data Preprocessing

This study used a publically available toolbox named Homer[65] to process the time-series fNIRS data. Firstly, the data from each channel was band-pass filtered (0.009 - 0.1Hz) to reduce low-frequency drift and high-frequency neurophysiological noise.[100, 101] Subsequently, changes in hemoglobin concentration relative to the baseline (ΔHbO) were quantified by a modified Beer-Lambert Law[101]. Correlation-based signal improvement (CBSI)[102] was adopted to remove motion artifacts based on negative correlation between oxygenated and deoxygenated hemoglobin dynamics.

3.2.5 Data Analysis

3.2.5.1 Seed-based functional connectivity

Channel 27 and 34 were chosen as seeds. Channel 27 was located over the stimulated left Broca's area, which is the dominant language area for right-handed subjects. Channel 34 was

located over the contralateral Broca's area, which is known to endow verbal communication with additional meaning by contributing to the analysis of emotional and tonal context in language.[103] Pearson's correlation coefficients were calculated between the seed channel and all the other channels and a Fisher's z-transformation was employed to transform the correlation coefficients to z-values[104] for each subject. For each stimulation session z-values between all the other channels and the seed channel were averaged across subjects. Significant seed-based functional connectivity changes between stimulation sessions were identified based on the following criteria[105]: 1) Using a paired t-test, for each z-value between sessions (i.e. Session 1 vs. Session 2) at a threshold of uncorrected $p < 0.05$ and 2) z-values were significantly different from zero at a $p < 0.05$ significance using a one-sample t-test in at least one session. The significant changes in functional connectivity were mapped by BrainNet Viewer software[106].

3.2.5.2 Time-variant functional connectivity

Time-variant functional connectivity was also calculated for the same seed locations. For each individual subject, sliding-window correlation (SWC) analysis[20, 107] was performed on each one of the four session data. In our SWC analysis, a 60-s time window was selected and then shifted by an increment of 1 s along the time course of each session.[20] Then the functional connectivity within each sliding-time window was calculated between the seed channel and all other channels using the Pearson correlation method. For each stimulation session, functional connectivity variability (FCV) was calculated as the standard deviation of the correlation coefficient along time[108]. For group analyses, the FCV of each correlation coefficient for each channel was averaged across subjects for each session. Paired t-tests were used to compare the FCV of each correlation coefficient between sessions, i.e. Session 1 vs. Session 2, to determine whether the FCV between the seed channel and other channels in each stimulation session were significantly different ($p < 0.05$). The channels with significant changes in FCV of the correlation

coefficients with respect to the seed channels were plotted using the BrainNet Viewer software[106].

3.2.5.3 Graph theory analysis

Graph theory analysis was applied to investigate the changes in topographical patterns of functional networks across the entire cortical regions mapped by fNIRS. In our study, for each subject, we defined each fNIRS channel as a node, resulting in a total of 83 nodes. The edges e_{ij} in the network were determined by setting a threshold, T, to the 83×83 Pearson's correlation matrix values r_{ij} by the following formula [109]:

$$e_{ij} = \begin{cases} 1, if\ |r_{ij}| > T \\ 0, otherwise \end{cases}$$

A certain range of $[T_{min}\ T_{max}]$ for T was chosen so that T_{min} excluded weak and potentially non-significant connections, while selecting the Pearson's correlation coefficients that were significant and corresponded to $p < 0.05$ in the channel-level correlation matrix.[110] T_{max} was set based on the condition that the mean node degree $\bar{k} \geq 2\log(\#\text{ of channels})$, which was equal to 8.8 for our setup[110, 111]. This value for T_{max} can be interpreted as the node being tested having connections with no less than 8.8 other nodes on average. Furthermore, this threshold value meant that the total number of edges in the network was no less than 365 (=83×8.8/2), equivalent to around 10% of the maximum number of edges possible (83×82/2=3,403) in a network of 83 nodes[112, 113]. Once the statistically significant nodes and edges were identified, graph theory based metrics were calculated by the Gretna software for each session[109]: Small-world properties (clustering coefficient C_p and characteristic path length L_p) and efficiency parameters (global efficiency E_{glob} and local efficiency E_{loc}) were calculated by setting the threshold from T_{min} to T_{max} with a step size of 0.01[110, 111, 114]. Then the area under the curve (AUC) for each metric and stimulation session was computed. For group analyses,

paired t-tests were used to compare the AUC for each metric and any significant changes ($p < 0.05$) between stimulation sessions were identified.

3.3 Results

3.3.1 Functional Connectivity Analysis Using the Stimulated Cortical Region and Contralateral Cortical Region as the Seed

3.3.1.1 Using the stimulated left Broca's area as the seed

Fig. 3-4 shows the detector locations over cortical areas with significant changes in connectivity strength, as deduced from paired t-tests between the No tDCS condition versus each one of the other stimulation conditions (Low Current tDCS, High Current tDCS and After High Current tDCS). Figs. 3-4(a) – (c) show lateral left views and Figs. 3-4(d) – (f) show top views for each stimulation condition comparison. Figs. 3-4(a) and 3-4(d) indicate that functional connectivity strength decreased significantly for longer distance connections with respect to the seed location at the left Broca's area during the Low Current tDCS condition. Furthermore, Figs. 3-4(b) and 3-4(e) show that High Current tDCS not only decreased significantly the connectivity strength with longer distance brain regions, but also significantly increased the connectivity strength with nearby regions. This near-neighbor effect persisted during the After High Current tDCS condition as shown in Figs. 3-4(c) and 3-4(f), but the change in connectivity strength compared to the No tDCS condition was smaller compared to the High Current tDCS condition. The increased connectivity strength between regions indicated by green and yellow ovals in Figs. 3-4(b) and 3-4(c) was most pronounced in the left dorsolateral prefrontal [green oval in Fig. 3-4(b)], premotor and SMA areas [yellow oval in Fig. 3-4(b) and 3-4(c)], which regulate the planning, maintenance and execution of speech[115-118].

3.3.1.2 Using the contralateral right Broca's area as the seed

Fig. 3-5 shows detector locations over cortical areas with significant changes in connectivity strength using the contralateral Broca's area as the seed. These connectivity changes were deduced from paired t-tests between the No tDCS condition versus each one of the other stimulation conditions. Several qualitative similarities were observed in the connectivity strength changes when comparing to the left Broca's area stimulation conditions: (1) Low Current tDCS induced significant decreases in connectivity strength for long-distance brain regions [Figs. 3-5(a) and 3-5(d)]; (2) High Current tDCS brought in significant increases in connectivity strength for the nearby right dorsolateral prefrontal [green oval in Fig. 3-5(b)] and premotor and SMA areas [yellow ovals in Figs. 3-5(b) and 3-5(c)]; (3) Similar distance-dependent effects were seen for the After High Current tDCS condition [Figs. 3-5(c) and 3-5(f)]. However, in contrast to the case of the left Broca's area was the seed, High Current tDCS also brought about a significant increase in connectivity strength with right Broca's area for detector location over another language-related cortical area, the superior temporal gyrus[119] [purple oval in Fig. 3-5(b)]. This cortical region is part of Wernicke's area and is related with prosody comprehension[103]. In addition, we attribute the larger number of channels observed with significant connectivity changes compared to the case of stimulating left Broca's area to the brain's known asymmetry with more connections stemming from the right hemisphere of right-handed adults[120].

In addition, Tables 3-1 and 3-2 list Brodmann areas with significantly decreased functional connectivity for the three stimulation sessions compared to the No tDCS condition when the seed was on Channel 27 and Channel 34, respectively.

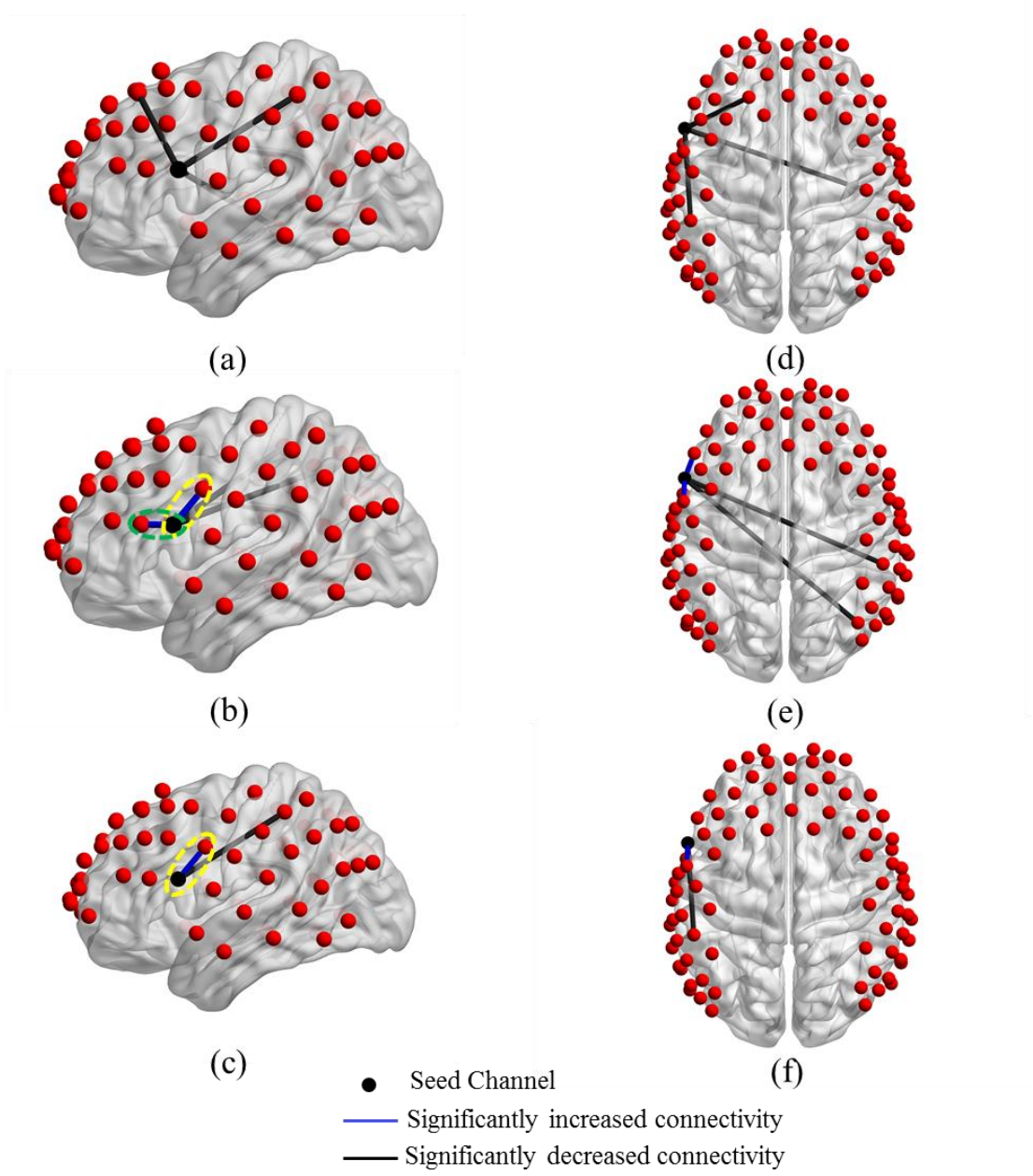

Figure 3-4 Changes in functional connectivity strength between the left Broca's area (seed) and other cortical regions induced by different tDCS stimulation conditions. Group-level significant differences ($p < 0.05$) in connectivity strength between pairs of detector locations for the No tDCS condition versus Low Current tDCS [(a) and (d)], versus High Current tDCS [(b) and (e)] and versus After High Current tDCS [(c) and (f)] stimulation conditions. Green ovals: Detector pair locations showing significantly increased connectivity with the dorsolateral prefrontal area. Yellow ovals: Detector pair locations showing significantly increased connectivity with the premotor and SMA areas.

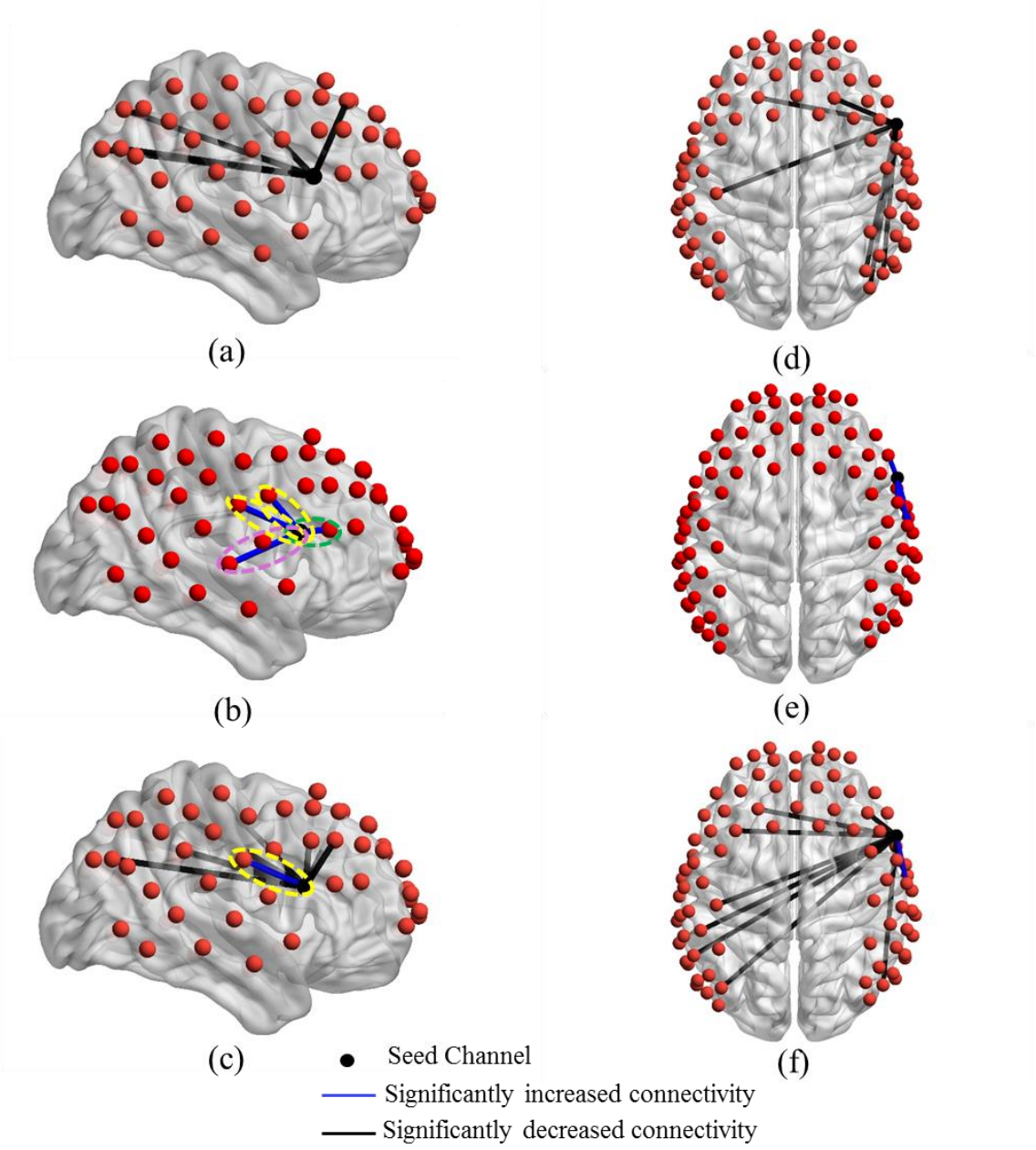

Figure 3-5 Changes in functional connectivity strength between the right Broca's area (seed) and other cortical regions induced by different tDCS stimulation conditions. Group-level significant differences ($p < 0.05$) in connectivity strength between pairs of detector locations for the No tDCS condition versus Low Current tDCS [(a) and (d)], versus High Current tDCS [(b) and (e)] and versus After High Current tDCS [(c) and (f)] stimulation conditions. Green ovals: Detector pair locations showing significantly increased connectivity with the dorsolateral prefrontal area. Yellow ovals: Detector pair locations showing

significantly increased connectivity with premotor and SMA areas. Purple oval: Detector pair locations showing significantly increased connectivity with the superior temporal gyrus.

Table 3-1 Brodmann areas with significantly decreased steady-state functional connectivity when the seed was on Channel 27 (left Broca's area).

Seed: Channel 27	Low Current tDCS	High Current tDCS	After High Current tDCS
Ipsilateral Hemisphere			
Brodmann Area 5	Yes		Yes
Brodmann Area 8	Yes		
Contralateral Hemisphere			
Brodmann Area 5		Yes	
Brodmann Area 7		Yes	
Brodmann Area 21	Yes		

Table 3-2 Brodmann areas with significant decreased steady-state functional connectivity when the seed was on Channel 34 (right Broca's area).

Seed: Channel 34	Low Current tDCS	High Current tDCS	After High Current tDCS
Ipsilateral Hemisphere			
Brodmann Area 7	Yes		Yes
Brodmann Area 8	Yes		Yes
Brodmann Area 19	Yes		
Contralateral Hemisphere			
Brodmann Area 3	Yes		Yes
Brodmann Area 5			Yes
Brodmann Area 7			Yes
Brodmann Area 8	Yes		Yes

3.3.2 Time-Variant Functional Connectivity using the Stimulated Left Broca's Area as Seed

Figs. 3-6(a) – (c) illustrate the detector locations over cortical regions (blue dots) with significantly increased FCV of the time-variant functional connectivity when the left Broca's area was the stimulated cortical region (red dots). Each row in that figure corresponds to a distinct stimulation condition, namely Low Current tDCS, High Current tDCS and After High Current tDCS. The cortical regions with increased FCV were similar for all three tDCS conditions: left Wernicke's area, right Wernicke's area and right Frontopolar area. Similar results were also found when using the contralateral Broca's area as the seed. The left and right Wernicke's areas and the left Frontopolar area also showed significantly increased FCV for all three tDCS sessions. Due to their similarity to the findings for the seed over the left Broca's area we do not show these results for brevity. These cortical regions belong to higher order brain regions (including language processing areas and frontopolar prefrontal cortex)[121, 122] and are remote to the seed regions. These FCV findings are in contrast to the above steady-state connectivity strength findings that mostly highlighted local connectivity strength increases.

Tables 3-3 and 3-4 list Brodmann areas with significantly increased FCV for the three stimulation sessions compared with No tDCS condition when seed was on Channel 27 and Channel 34, respectively.

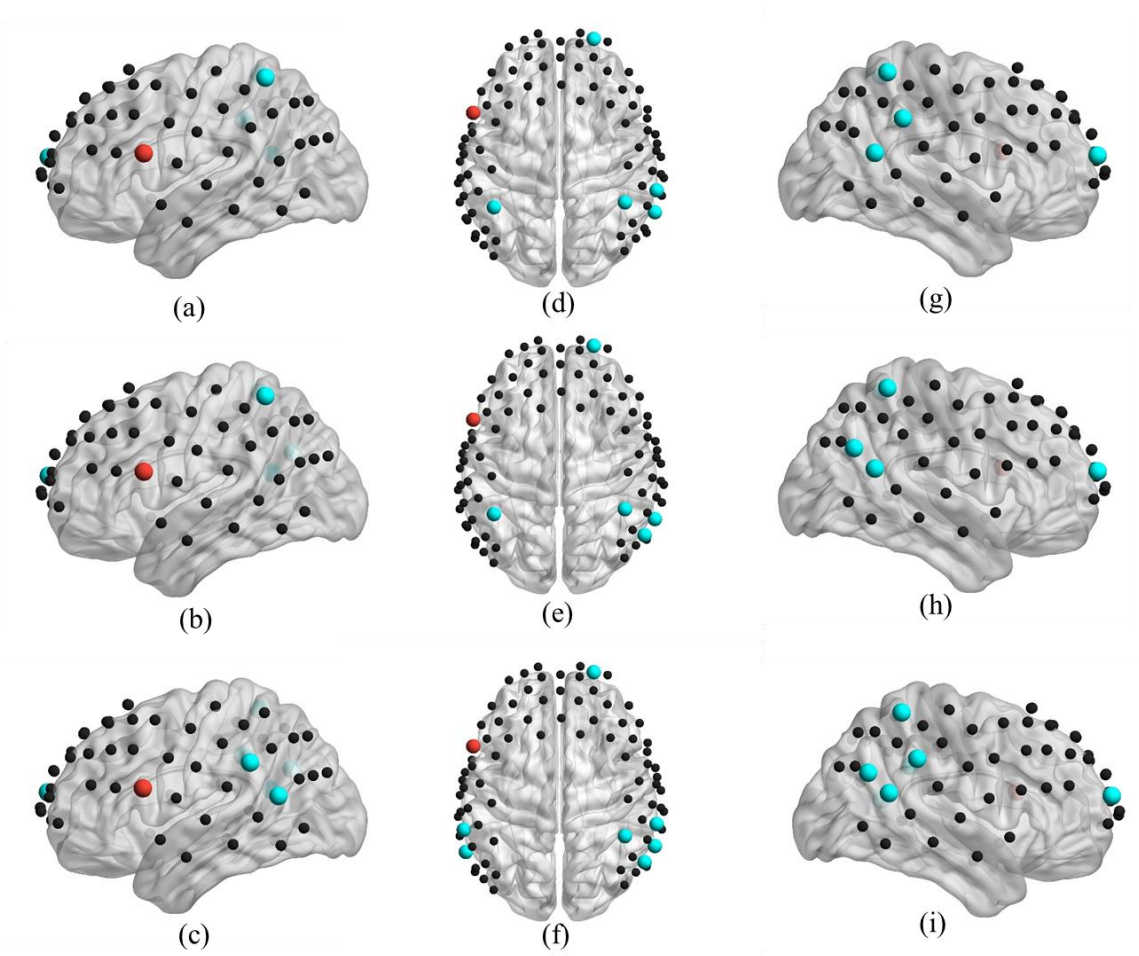

Figure 3-6 Brain cortical regions of significant increased FCV (Blue dots, functional connectivity variability, $p < 0.05$) with stimulated cortical region (Red dots) induced by different tDCS stimulation conditions: (a), (d), (g) No tDCS versus Low Current tDCS. (b), (e), (h) No tDCS versus High Current tDCS. (c), (f), (i) No tDCS versus After High Current tDCS.

Table 3-3 Brodmann areas with significant increased FCV when the seed was on Channel 27 (left Broca's area).

Seed: Channel 27	Low Current tDCS	High Current tDCS	After High Current tDCS
Ipsilateral Hemisphere			
Brodmann Area 22			Yes
Brodmann Area 40	Yes	Yes	Yes
Contralateral Hemisphere			
Brodmann Area 10	Yes	Yes	Yes
Brodmann Area 22	Yes	Yes	Yes
Brodmann Area 39		Yes	Yes
Brodmann Area 40	Yes	Yes	Yes

Table 3-4 Brodmann areas with significantly increased FCV when the seed was on Channel 34 (right Broca's area).

Seed: Channel 34	Low Current tDCS	High Current tDCS	After High Current tDCS
Ipsilateral Hemisphere			
Brodmann Area 39	Yes	Yes	Yes
Brodmann Area 40			Yes
Contralateral Hemisphere			
Brodmann Area 10	Yes	Yes	Yes
Brodmann Area 39	Yes	Yes	
Brodmann Area 40			Yes

3.3.3 Graph Theory Analysis

As described in Section 2.5.3, a certain range of functional connectivity thresholds, [0.3 0.59] with the step of 0.01, was chosen to perform graph theory analysis.

Figs. 3-7(a) and 3-7(b) illustrate the area under the curve (AUC) for the cortical network clustering coefficient (C_p) and local efficiency (E_{loc}), respectively, with the AUC being integrated as a function of threshold T[109] for the different stimulation conditions. It was found that the AUC for both C_p and E_{loc} had similar trends, showing an increase in going from the No tDCS to the After High Current tDCS condition. However, significant changes ($p < 0.05$) were found between the No tDCS condition and all other stimulation conditions for C_p, whereas for E_{loc} the only significant change was between the No tDCS and the After High Current tDCS conditions. The significant changes in the AUC of C_p for all stimulation conditions relative to baseline reflect an increase in the number of neighboring channel connections even for low stimulation currents and after the High Current tDCS was turned off. In addition, the significant change in the AUC for E_{loc} suggests that the After High Current tDCS condition enhanced the formation of network clusters, which is consistent with more efficient communication between nodes within the same immediate neighborhood[123, 124].

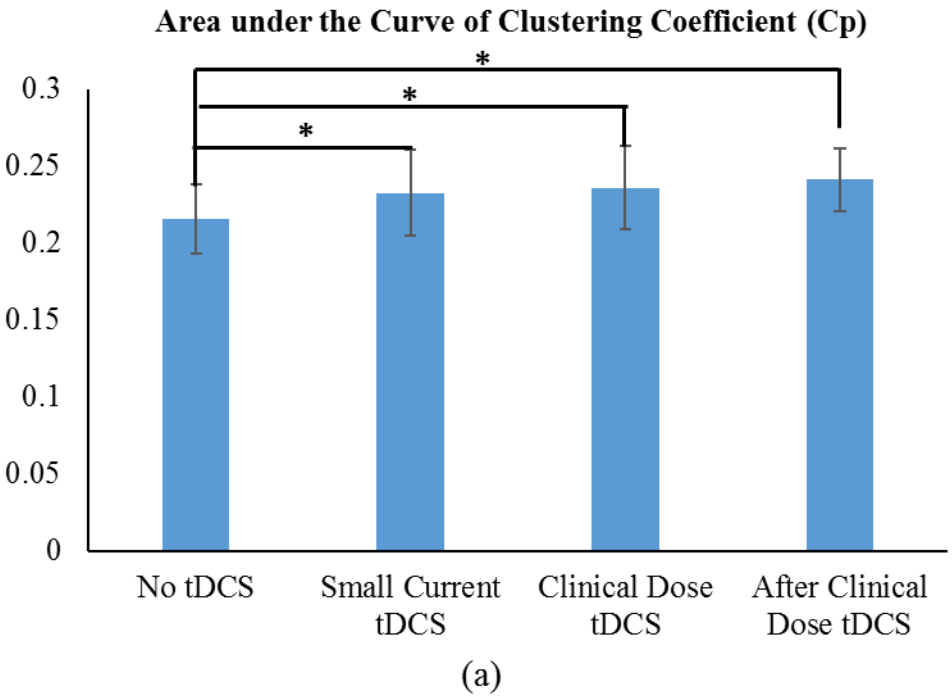

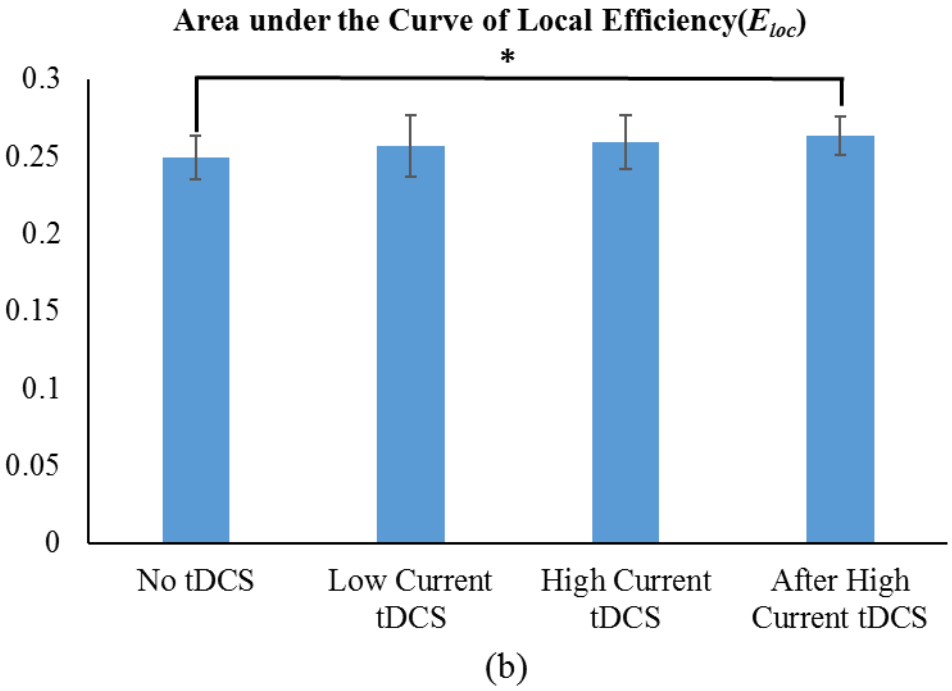

Figure 3-7 The differences of mean areas under the curve (AUC) for (a) clustering coefficient (C_p) and (b) local efficiency (E_{loc}) computed for the No tDCS, Low Current tDCS, High Current tDCS and After High

Current tDCS conditions. The asterisk indicates significant differences ($p < 0.05$). Error bars correspond to one standard deviation to the mean across subjects.

3.4 Discussion

This study systematically explored by use of resting state fNIRS the impact of two different anodal tDCS exposures applied over the left Broca's area, on functional connectivity reorganization. A lower tDCS current (Low Current tDCS) was applied to create transient hemodynamic changes, whereas a higher current (High Current tDCS) mimicked a current dose that is typical of tDCS interventions reported in the literatures[125, 126]. The purpose of this work was to test how tDCS modulated connectivity in the immediate neighborhood of the anodal stimulation location over left Broca's area versus the connectivity to distant cortical regions involved in language processing. A second goal was to explore whether lower currents could reproduce qualitatively the connectivity patterns seen for typical intervention currents, which would enable the lower currents to serve as predictors of connectivity responses to the higher currents.

3.4.1 TDCS Increased Steady-State Functional Connectivity in the Immediate Neighborhood of the Stimulation Location

Seed-based analysis revealed distinct differences in functional connectivity patterns between Low Current tDCS, High Current tDCS and within 10 minutes After High Current tDCS. Specifically, Low Current tDCS was more likely to suppress the connections with long distance brain regions, while High Current tDCS encouraged increased local connectivity. Interestingly, during the After High Current tDCS session a return to the suppression of long-distance connections was seen, combined with the short-distance increased connectivity seen during the immediately preceding High Current tDCS session. It is hypothesized that anodal tDCS induced subthreshold neuronal depolarization, resulting in the excitation of the stimulated cortical areas

near the anodal electrode.[89, 90] The local increase of spontaneous activity might also have decreased the synchronization with other remote brain regions,[105, 127] which could help explain the observed reduction in connectivity with those regions. Similar results with respect to changes in local versus long-distance connectivity were reported in prior work[127] for anodal tDCS, corresponding to High Current tDCS in this work, for stimulation over the left primary motor area. In this work, the brain regions with the most pronounced increases in functional connectivity strength were the dorsolateral prefrontal, premotor and SMA areas, known to be part of the language processing and production network[115-118]. These results were consistent with prior studies reporting on dual tDCS over the Broca's areas[18, 19], where it was illustrated that tDCS resulted in significantly increased functional connectivity with the premotor and SMA regions. High Current tDCS also brought about a significantly increased functional connectivity between the right Broca's area and the right superior temporal gyrus, which are known to be responsible for prosody comprehension function[103]. For the two channels with persistently increased connectivity strength during the After High Current tDCS sessions [Fig. 3-4(c) and Fig. 3-5(c)], the increase in connectivity strength during the High Current tDCS session was larger than other increased connections [Fig. 3-4(b) and Fig. 3-5(b)], with the latter going back to pre-stimulation levels during the After High Current tDCS session [Fig. 3-4(c) and Fig. 3-5(c)]. Our results suggest that anodal stimulation over the left Broca's area prepares the task-related language areas by enhancing functional connectivity with these cortical regions. These findings might be also helpful to explain the beneficial effects of anodal stimulation over the affected hemisphere in stroke aphasia patients[9, 128, 129]. In addition, Low Current tDCS could not predict the increased functional connectivity in the immediate neighborhood of the stimulation location induced by High Current tDCS. However, for the decreased functional connectivity in the remote regions of the stimulation location, seen Tables 3-1 and 3-2 as a whole, the Low Current tDCS had no predictive ability for the High Current tDCS, though it correctly predicted 5/7 Brodmann areas for After High Current tDCS condition.

3.4.2 TDCS Increased Functional Connectivity Variability with High-Order Cognitive Cortical Regions

In contrast to steady-state functional connectivity that focuses on connectivity strength, functional connectivity variability (FCV) focuses on the variation of the connectivity strength of transient states. It was observed (Fig. 3-6) that all of Low Current tDCS, High Current tDCS and After High Current tDCS sessions induced a significant increase in FCV between Wernicke's area and the right frontopolar areas after anodal stimulation of the left Broca's area. It is known that the left Wernicke's area is involved in comprehension or understanding of written and spoken language, while its homologous area has a role in the processing and resolution of subordinate meanings of ambiguous words[130]. Also, the right frontopolar area is associated with memory function[131] and both Wernicke's and frontopolar areas belong to high-order language and memory processing networks[121, 122]. Previous studies reported that higher-order brain networks show large variability in connection strength over time[107, 132]. Our results suggest that tDCS resulted in larger FCV in these regions, which we interpret as them having a higher degree of flexibility for performing higher-order language processing tasks after stimulation[107, 133]. The more variable functional connectivity in these connections potentially reflects tDCS facilitating the emergence of a large-scale network with flexible capability in functional coordination between language and memory systems. Besides, as shown in Tables 3-3 and 3-4, Low Current tDCS predicted 7/8 areas with increased FCV during High Current tDCS and 6/10 for the After High Current tDCS session. The majority of Brodmann areas missed (mainly Brodmann Area 40 when seed on channel 34) in the After High Current tDCS session were geographically nearby to the areas (Brodmann Area 39 when seed on channel 34) predicted correctly. Therefore, Low Current tDCS presented similar results with increased FCV in high-order cognitive cortical regions, thus offering the possibility to serve as a qualitative predictor of FCV changes induced by High Current tDCS and After High Current tDCS.

3.4.3 TDCS Enhanced the Small-World Features of the Cortical Network Globally

In contrast with seed-based functional connectivity, graph theory analysis quantified network connectivity changes induced by tDCS across the entire cortical area mapped by fNIRS. TDCS induced an increase in the density of local connections between detector channels across the entire cortical network that was quantified by the network's small-world features. These network features were the characteristic path length (Lp), the clustering coefficient (Cp), global efficiency (Egb) and the local efficiency (Eloc)[134-136]. Two of these small world properties were enhanced by tDCS: Cp became significantly higher for all stimulation sessions whereas Eloc became significantly higher only in the After High Current tDCS session. The enhancement of small-world features after tDCS are interpreted as the cortical networks becoming more segregated[134] and clustered with more locally efficient communication and higher fault tolerance[123]. The graph theory analysis findings were consistent with our seed-based functional connectivity results, where the seed areas were tightly connected with local cortical regions and desynchronized with more distant regions. In addition, changes in graph theory metrics induced by Low Current tDCS were qualitatively similar to the ones induced by High Current tDCS, which indicates that Low Current tDCS could be used as a tool for studying qualitatively the patterns brought about High Current tDCS**.**

3.5 Conclusion

Our work demonstrates the feasibility of using resting-state fNIRS to study cortical network reorganization induced by tDCS in the language processing cortical networks of healthy subjects. Seed-based functional connectivity, graph theory analysis, and time-variant functional connectivity were used to track changes in cortical functional connectivity for these networks. Seed-based connectivity and graph theory analyses revealed increased local and decreased remote functional connectivity induced by tDCS. At the same time, time-variant functional connectivity changes suggested that tDCS increased FCV of remote connections. In addition,

Low Current tDCS could predict qualitatively the increases in clustering coefficient and FCV, but not the increased local connectivity, created by High Current tDCS. The latter finding is not surprising though since the effect of local connectivity increase is known to only occur at higher currents that can create depolarization of the resting membrane potential and increasing neuronal firing rates[88]. Nevertheless, the qualitative capacity of Low Current tDCS to predict the regions remote to Broca's area showing suppressed connectivity After High Current tDCS, although not perfect, suggests the possibility of using Low Current tDCS in future work to test several different placements within one single session. Therefore, the findings of this work set the stage for future studies to explore how different tDCS electrode placements affect language networks with the aim of gaining insights for therapeutic intervention planning.

Chapter 4 Directional changes in information flow between human brain cortical regions after application of anodal transcranial direct current stimulation (tDCS) over Broca's area

This Chapter is a manuscript to be submitted soon.

4.1 Introduction

Transcranial direct current stimulation (tDCS) is a non-invasive brain stimulation technique used to modulate cortical activity in the human brain by delivering weak currents through a pair of anode-cathode electrodes (up to 2mA for up to 20 mins)[88, 137]. TDCS has been applied to enhance physical performance in healthy subjects[84-86] and facilitate neurorehabilitation during stroke recovery[87]. Several studies have suggested that anodal tDCS over either Broca's area or Wernicke's area could improve naming accuracy or speed both in stroke-induced aphasia patients[9, 12, 13] and in healthy subjects[86, 91, 92].

Recent resting-state functional magnetic resonance imaging (fMRI) studies[18, 19] explored the altered connectivity strength within large-scale functional networks related to tDCS stimulation over language cortical regions. However, little is known about the directionality of cortical interactions in functional language networks when tDCS is applied. To the best of our knowledge, only one study[138] to date has investigated the direction of information flow, which was done by use of Dynamic Causal Modelling (DCM) during a concurrent tDCS-fMRI study of overt picture naming. Nevertheless, DCM requires complicated *a priori* parameters and strong assumptions on the underlying neuronal interaction mechanisms[139, 140]. Here, we used Phase Transfer Entropy (PTE)[139, 141], which is a computationally efficient and data-driven method, to estimate changes in the direction of information flow affected by tDCS.

In this study we used functional near-infrared spectroscopy (fNIRS) to investigate directionality in cortical interactions involving the language processing areas. FNIRS can detect

changes in the concentration of oxyhemoglobin (ΔHbO) and deoxyhemoglobin (ΔHb) resulting from neurovascular coupling secondary to neuronal activation[24]. The higher temporal resolution of fNIRS and its easier implementation in a compatible setup with tDCS, relative to fMRI, makes it advantageous for studying alterations in functional connectivity induced during tDCS[27, 31]. Previous studies[142, 143] have shown that vasomotion-induced oscillations measured by fNIRS, which lead to improved perfusion[144] and local tissue oxygenation[145], could be divided into three frequency bands: an endothelial component (0.003-0.02Hz) related to microvascular activity[146], a neurogenic component (0.02-0.04Hz) linked to intrinsic neuronal activity[147] and a myogenic component (0.04-0.15Hz) attributed to the activity of smooth muscles of arterioles[146]. In this study, we explored how tDCS affected the directionality of information flow, encoded by changes in PTE, in these three fNIRS frequency bands.

One additional aspect we explored in this work was the effect of tDCS current intensity on the information flow patterns of language-processing networks. A subdivision of information flow analysis into endothelial, neurogenic and myogenic frequency band contributions to the information flow computed by the PTE method was performed with the aim of helping clarify the relative roles of neuronal verus vascular physiological responses to different tDCS currents. Furthermore, we wanted to evaluate whether alterations of information flow due to anodal tDCS over the left Broca's area for a low intesity tDCS current (0.5 mA) could qualitatively predict directionality patterns occuring after a high intesity tDCS current (1 mA), a standrad intervention current choice in the literature. The aim of this latter part of the work was to test whether a rapid way exists to predict by use of low tDCS currents the information flow directionality changes occuring at therapeutic level currents, which have long-lasting effects. The findings of this work are intended to contribute towards a better understanding of cortical plasiticy induced by tDCS during therapeutic interventions.

4.2 Method and Materials

4.2.1 Subjects

Thirteen healthy right-handed subjects (2 Females, 11 Males, mean ± SD age = 35.4 ± 8.4) participated in this study. Subject handedness was determined by the Edinburgh Handedness Inventory [96]. None of them had a history of neurological disorders. Written informed consent was obtained from each participant before the experiments. The studies were conducted under the approval of the University of Texas at Arlington Institutional Review Board protocol (UTA #2015-0819).

4.2.2 FNIRS Imaging Setup Combined with tDCS

Fig. 4-1(a) demonstrates the overall experimental setup. A continuous-wave fNIRS imaging system (LABNIRS, Shimadzu, Japan) was used to collect signals. Fig. 4-1(b) illustrates the fNIRS source-detector geometry, which consisted of 26 sources and 28 detectors with a separation of 3 cm, resulting in 83 source-detector channels. The optical fiber bundles of sources and detectors were inserted into the optode holder on the subject's head. Light was emitted at wavelengths of 780nm, 805nm, and 830nm simultaneously from each source. FNIRS signals were sampled at a frequency of 12.35 Hz. This probe geometry covered language-related cortical regions, including the Broca's and Wernicke's areas as well as some prefrontal cortical regions including the frontopolar, dorsolateral prefrontal cortex (DPFLC) and premotor areas, all for both hemispheres.

A co-registration procedure was applied to measure the covered cortical regions based on cranial landmark measurements on all the subjects[25]. Five reference cranial landmarks (nasion, inion, left and right preauricular points and vertex) and the locations of all source and detector optodes were measured by a motion tracking system (Fastrak, POLHEMUS). NIRS-SPM[98] was used to calculate the Montreal Neurological Institute (MNI) coordinates of the optodes[97] and register them on a standard MRI brain template to identify the Brodmann areas

imaged by each source-detector channel. The layout of spatially registered channels (averaged over all thirteen subjects) on the standard human brain atlas is shown in Fig. 4-2.

TDCS current was delivered by a battery-driven electrical stimulator (Phoresor II, IOMED Inc., Salt Lake City, UT) through a pair of saline-soaked gauze covered gel electrodes (5 × 5 cm; IOMED Inc., Salt Lake City, Utah). The placement of tDCS patches used the EEG International 10/20 system[148] as a reference, with the anodal patch placed over the FC5 position (centered at Channel 27 in our setup) to stimulate left Broca's area, and the cathodal patch centered over the Fp2 position[92] as a control location [dashed square in Figs. 4-2(a)-4-2(d)]. In order to accommodate optical fiber bundles overlapped spatially with the patches, two 0.5 cm-diameter holes were punctured on each patch.

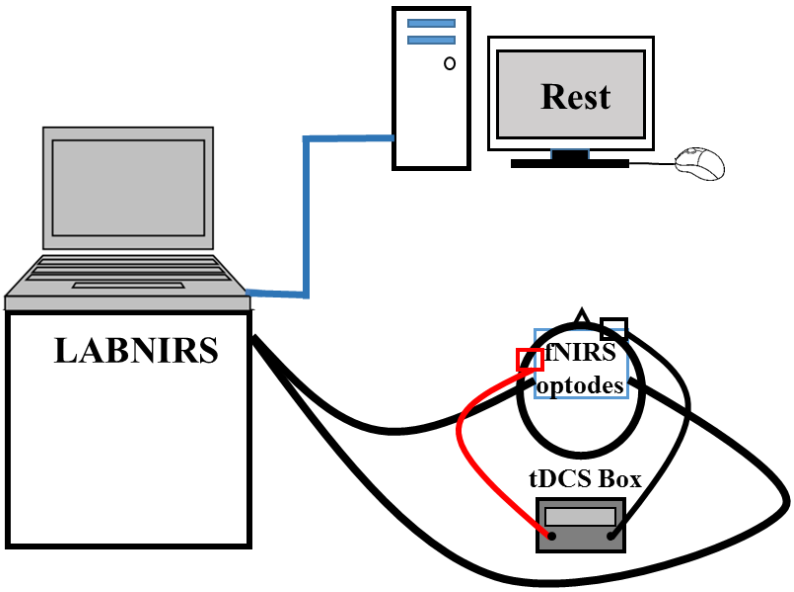

(a)

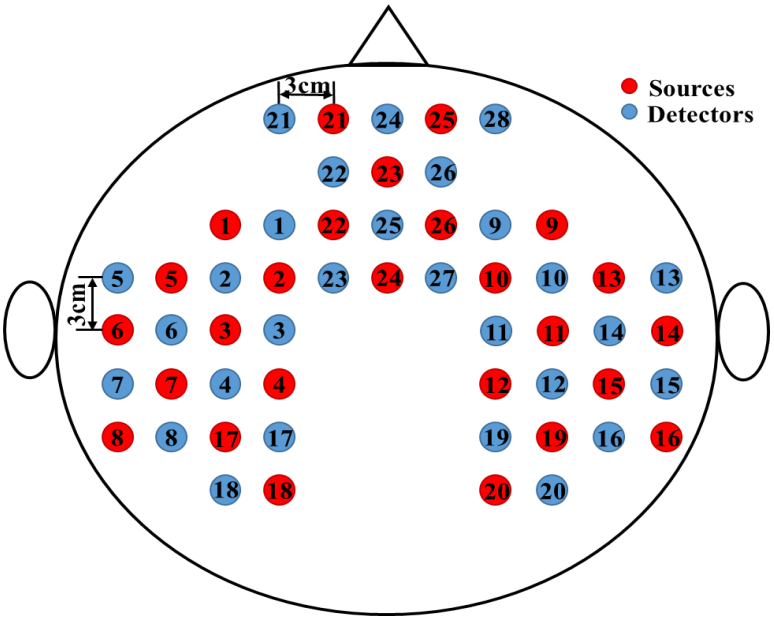

(b)

Figure 4-1 (a) Overall experimental setup. The computer screen only displays the word “Rest” during data acquisition. FNIRS optodes and tDCS electrodes were placed on the subject’s head as described in Section 2.2. (b) The fNIRS probe geometry with 26 sources and 28 detectors placed over a subject’s head. The separation of all source and detectors was 3 cm. (Red dots: sources, blue dots: detectors)

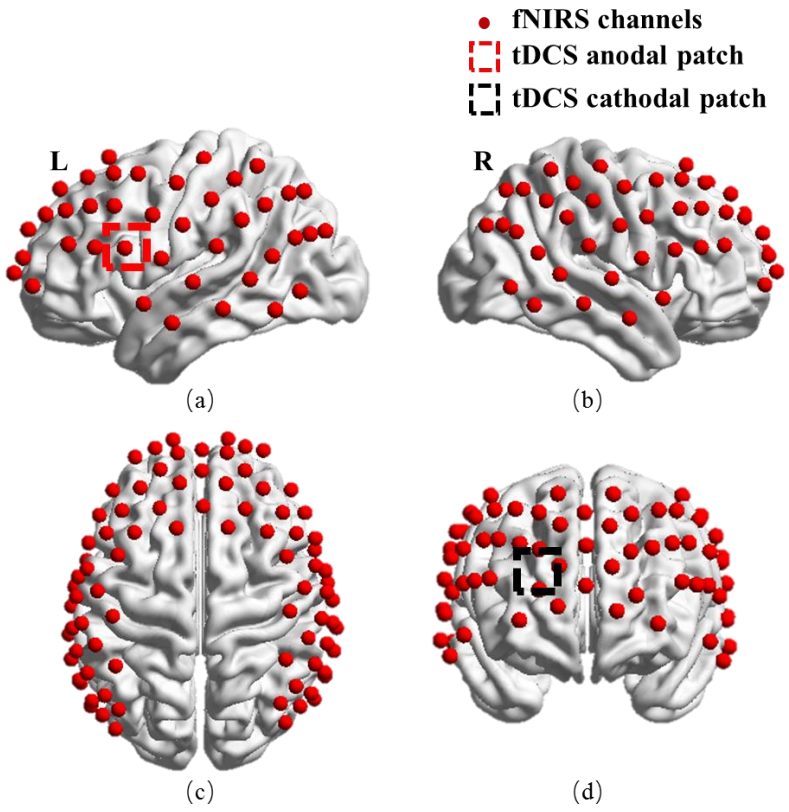

Figure 4-2 Co-registration of fNIRS source-detector channels (mid-way points between source and detector pairs) on a standard human brain atlas: (a) Sagittal view (Left), (b) Sagittal view (Right), (c) Top view and (d) Coronal view. The tDCS anodal (red dashed square) and cathodal (black dashed square) patches were placed on the left FC5 position (a) and right Fp2 position (d), respectively.

4.2.3 Protocol Design

During fNIRS measurements, subjects were asked to keep at rest with their eyes closed but staying awake for 32 minutes. Fig. 4-3 illustrates the timeline of the protocol. There were four stimulation sessions: (1) No tDCS (0-6 min) was the first 6 minutes without tDCS applied, which was regarded as the baseline measurement. (2) Low Current tDCS (6-14 min), which entailed 0.5 mA current tDCS being applied for 2 min 40 s, followed by a no-stimulation period of 5 min and 20 s to allow any hemodynamic changes incurred by Low Current tDCS to go back to baseline[88, 95, 99]. (3) High Current tDCS (14-22 min), which entailed a higher current of 1 mA being applied

for 8 min. (4) After High Current tDCS (22-32 min), which was the 10 min period immediately after High Current tDCS. Subjects were not told when tDCS was being applied.

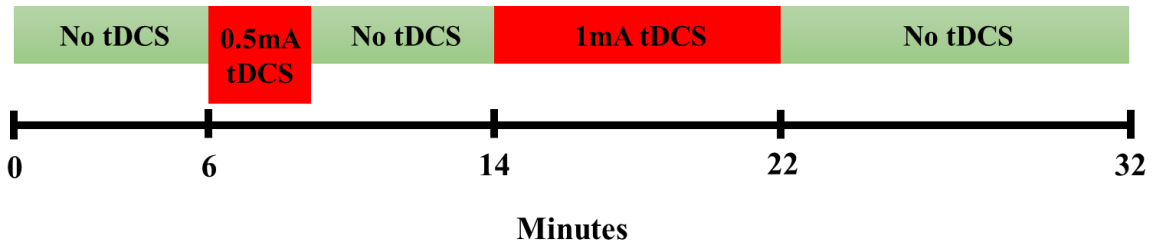

Figure 4-3 The tDCS protocol timeline.

4.2.4 Data Preprocessing

This study used the publically available Homer toolbox [65] to process the acquired time-series fNIRS data. Firstly, the data from each channel was band-pass filtered: 0.003-0.15Hz to isolate the entire range of physiologically relevant hemodynamic fluctuations, 0.003-0.02 Hz for endothelial origin fluctuations, 0.02-0.04 Hz for neurogenic origin fluctuations and 0.04-0.15 Hz for myogenic origin fluctuations[142, 143, 149]. Subsequently, global fluctuations that were detected across all channels were removed by principal component analysis (PCA)[150]. Then changes in hemoglobin concentration relative to the baseline (ΔHbO) were quantified by a modified Beer-Lambert Law[101]. Correlation-based signal improvement (CBSI)[102] was adopted to remove motion artifacts based on negative correlations between oxygenated and deoxygenated hemoglobin dynamics.

4.2.5 Data Analysis

4.2.5.1 Phase Transfer Entropy (PTE) Analysis

PTE estimates the information flow between regions of interest (ROIs) based on the same principle as Wiener-Granger Causality[139, 141]. It is calculated as the difference between the

uncertainty of the target signal Y conditioned only on its own past and the uncertainty of the target signal conditioned on both the past of its own and the source signal X[141]:

$$PTE_{xy} = H(Y_{t+\delta}|Y_t) - H(Y_{t+\delta}|Y_t, X_t).$$

where PTE_{xy} denotes the phase transfer entropy from X to Y, H represent the entropy, δ denotes the time delay. If PTE_{xy} is larger than zero, then the source signal X has a causal influence on the target signal Y. Since PTE_{XY} is lack of a meaningful upper bound, a normalization process is utilized to reduce biases[151, 152]:

$$dPTE_{xy} = \frac{PTE_{xy}}{PTE_{xy}+PTE_{yx}}.$$

If $0.5 < dPTE_{xy} \leq 1$, the information flow is preferentially from X to Y. If $0 \leq dPTE_{xy} < 0.5$, the information flow is preferentially from Y to X. If $dPTE_{xy} = 0.5$, there is no preferential information flow between X and Y.

4.2.5.2 Data Processing Steps for Directed PTE (dPTE) Analysis

DPTE analysis was applied to calculate information flow for the entire physiologically relevant range of hemodynamic fluctuation frequencies, and the individual endothelial, neurogenic and myogenic frequency bands for the four stimulation sessions described above (No tDCS, Low Current tDCS, High Current tDCS and After High Current tDCS). Specifically, for each subject, PTE was performed to determine the causality between every two channels among all 83 channels. Then PTE values were normalized into dPTE values. This generated a 83×83 dPTE matrix determining information flow between all channel pairs. The value at Xth row and Yth column determined the scale of information flow from Y to X. Then dPTE was averaged along rows to produce a 1×83 matrix, which was the mean dPTE of each one channel and all other channels. If the mean dPTE of one channel was larger than 0.5, then the average information flow between this channel and all the other channels was outgoing. If the mean dPTE of one channel was smaller than 0.5, then the average information flow between this channel and all the

other channels was incoming. The group-averaged mean dPTE was calculated by averaging the mean dPTE by subject. The above procedures were repeated for all hemodynamic frequency bands for each of the four stimulation sessions. Next, a set of paired t-tests among the 13 subjects was performed on dPTE between the four stimulation sessions for each frequency band. Significant enhancements of information flow ($p<0.05$) from selected seeds, i.e. the left stimulated Broca's area and the right contralateral Broca's area, were identified. Lastly, the group-averaged mean dPTE values for each channel were interpolated on a standard MRI brain template by EasyTop software[153], and significant enhancements of information flow from selected seeds were displayed topographically on the standard MRI brain template by BrainNet View software[106].

4.3 Results

4.3.1 Information Flow in the Entire fNIRS Frequency Band (0.003 – 0.15 Hz)

4.3.1.1 Averaged Direction of Information Flow

Fig. 4-4 shows the map of average information flow between each channel and all other channels over the cortical regions being mapped by fNIRS by use of dPTE analysis for the four stimulation sessions (No tDCS, Low Current tDCS, High Current tDCS and After High Current tDCS). The color-coded map illustrates a single estimate of preferred direction of information flow (outgoing or incoming) for each channel. Figs. 4-4(a)-(d) show top views, (e)-(h) lateral left views, (i)-(l) lateral right views and (m)-(p) frontal views. Figs. 4-4(f)-(h) show that, compared to the No tDCS session, the stimulated left Broca's area (BA44/45) indicated by black circles became an outgoing information flow hot spot during Low Current tDCS, High Current tDCS and After High Current tDCS. In addition, the left middle temporal gyrus (MTG, BA 21) indicated by a pink circle in Fig. 4-4(g) became an additional hot spot of outgoing information only during High Current tDCS. Figs. 4-4(j)-(l) illustrate the extended cortical areas contralateral to the stimulated hemisphere, including

right Broca's area (BA44/45), superior temporal gyrus (STG, BA22) and MTG (BA21) collectively circumscribed by blue ovals, that also became hot spots of outgoing information during Low Current tDCS, High Current tDCS and After High Current tDCS. Overall, tDCS stimulation induced an increase in outgoing information both from the stimulated area and the contralateral hemisphere region that was distant from the anodal stimulation patch. In addition, the areas with outgoing information flow became slightly more spatially extended during High Current tDCS compared to all other stimulation conditions. The cortical locations of fNIRS channels receiving the information emanating from individual seed fNIRS channels located near the center of the hot spots identified in this section was analyzed next.

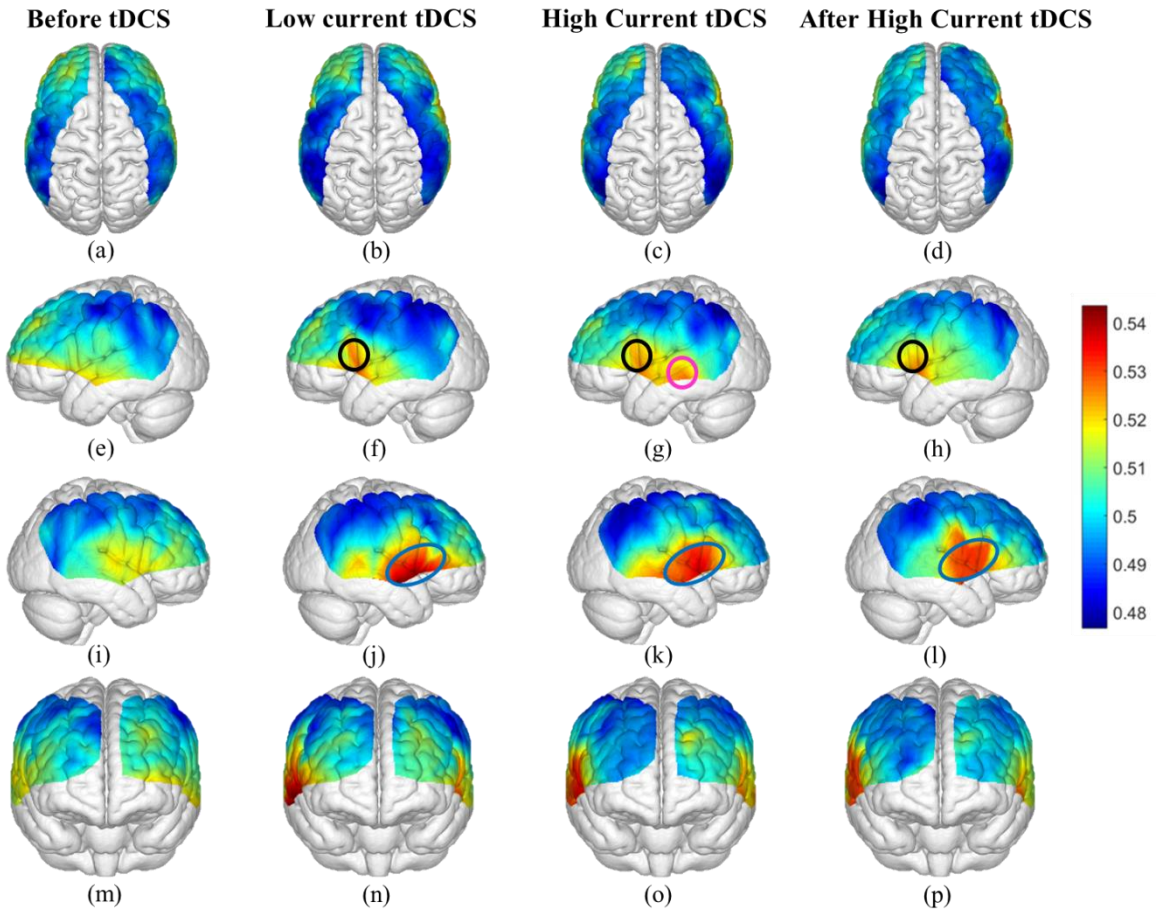

Figure 4-4 Mean dPTE for each channel displayed as a color-coded map viewed from top, left, right and front for the four stimulation sessions: No tDCS [(a), (e), (i) and (m)], Low Current tDCS [(b), (f), (j) and

(n)], High Current tDCS [(c), (g), (k) and (o)] and After High Current tDCS [(d), (h), (l) and (p)]. Hot (yellow – red) and cold (blue – green) colors indicate information outflow and inflow, respectively.

4.3.1.2 Using the Stimulated Left Broca's Area as the Seed

The channel near the center of the stimulated left Broca's area, indicated as by a black circle in Figs. 4-4(f)-(h), was chosen as the seed to compute the outgoing information patterns for all stimulation conditions. Fig. 4-5 shows the channel locations over cortical areas with significant changes in information flow direction between the No tDCS condition versus each one of the other three stimulation conditions (Low Current tDCS, High Current tDCS and After High Current tDCS), as deduced from paired t-tests. Figs. 4-5(a)-(c) show lateral left views and Figs. 4-5(d)-(f) show top views. Only enhanced efflux of information from the left Broca's area was observed for each comparison condition. The information out of the left Broca's area flowed towards a more spatially extended range of cortical regions during the High Current tDCS condition. Table 4-1 lists the Brodmann areas with significantly increased outgoing information emanating from the left Broca's area for the three stimulation conditions compared to No tDCS. It is noteworthy that High Current tDCS brought about a significant increase in information flowing into the left MTG (BA 21), as seen in Fig. 4-5(b), which was also a hot spot for outgoing information during High Current tDCS as indicated by the area in the pink circle in Fig. 4-4(g).

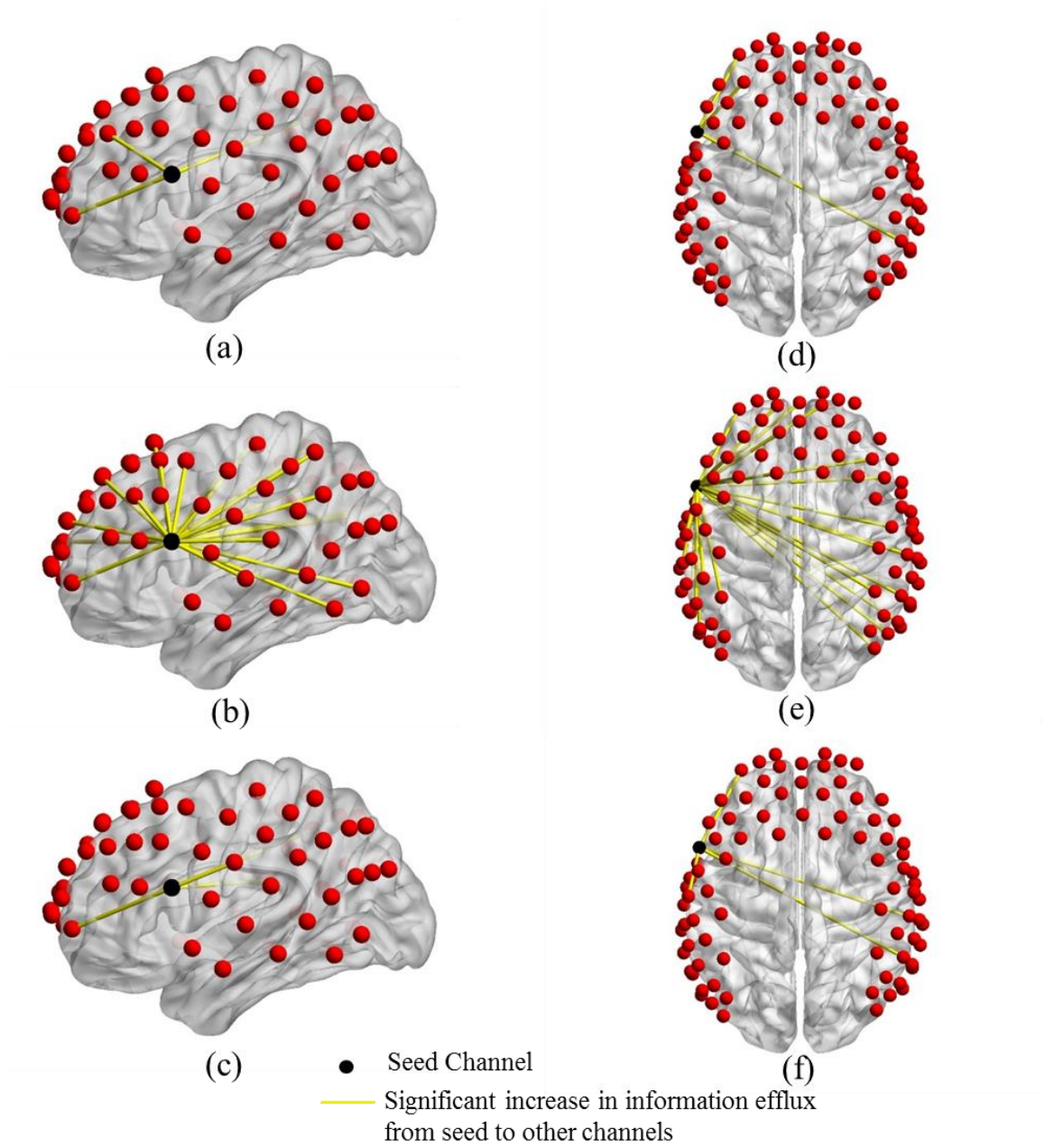

Figure 4-5 Changes in information flow direction between the left Broca's area (seed) and other cortical regions induced by different tDCS stimulation conditions. Group-level significant differences ($p<0.05$) in information flow direction between pairs of detector locations for the No tDCS condition versus Low Current tDCS [(a), (d)], versus High Current tDCS [(b), (e)], and versus After High Current tDCS [(c), (f)] stimulation conditions.

Table 4-1 Brodmann areas with significantly increased information influx originating from Channel 27 (left Broca's area)

Seed: Channel 27	Low Current tDCS	High Current tDCS	After High Current tDCS
Ipsilateral Hemisphere			
Brodmann Area 6	Yes	Yes	
Brodmann Area 9		Yes	Yes
Brodmann Area 10	Yes	Yes	Yes
Brodmann Area 21		Yes	
Brodmann Area 22/39/40		Yes	
Contralateral Hemisphere			
Brodmann Area 6		Yes	
Brodmann Area 9		Yes	
Brodmann Area 10		Yes	
Brodmann Area 22/39/40	Yes	Yes	Yes

BA 6: Premotor Area; BA 9: Dorsolateral Prefrontal Cortex; BA 10: Frontopolar Area; BA 21: Middle Temporal Gyrus (MTG); BA 22/39/40: Wernicke's area.

Also, the left MTG, which was an outgoing information flow hot spot for High Current tDCS, showed enhanced information flow into the frontopolar (BA 10), DLPFC (BA 9), premotor (BA 6) and Wernicke's (BA 22/39/40) areas for both hemispheres. Due to the similarity of these findings to the case where the left Broca's area was the seed, we do not show these results for brevity.

4.3.1.3 Using the Contralateral Right Broca's Area as the Seed

The right Broca's area contralateral to the stimulated region, included within the blue ovals in Figs. 4-4(j)-(l), was also studied for changes in information flow patterns as was done for the stimulated left Broca's area above. Fig. 4-6 shows channel locations over cortical areas with significant changes in information flow direction using the contralateral Broca's area as the seed. These information flow direction changes were deduced from paired t-tests between the No tDCS

condition versus each one of the other stimulation conditions. Several qualitative similarities were observed in the information flow direction changes when comparing to the corresponding left Broca's area stimulation conditions: (1) Only enhanced efflux of information from the right Broca's area was observed for each stimulation condition comparison, and (2) Information flowed into more spatially extended cortical regions for High Current tDCS compared to Low Current tDCS. However, in contrast to the case of the left Broca's area as the seed, information still flowed into more spatially extended areas for the After High Current tDCS condition compared to Low Current tDCS. Table 4-2 lists the Brodmann areas with significantly increased outgoing information from the right Broca's area for the three stimulation sessions compared to the No tDCS condition.

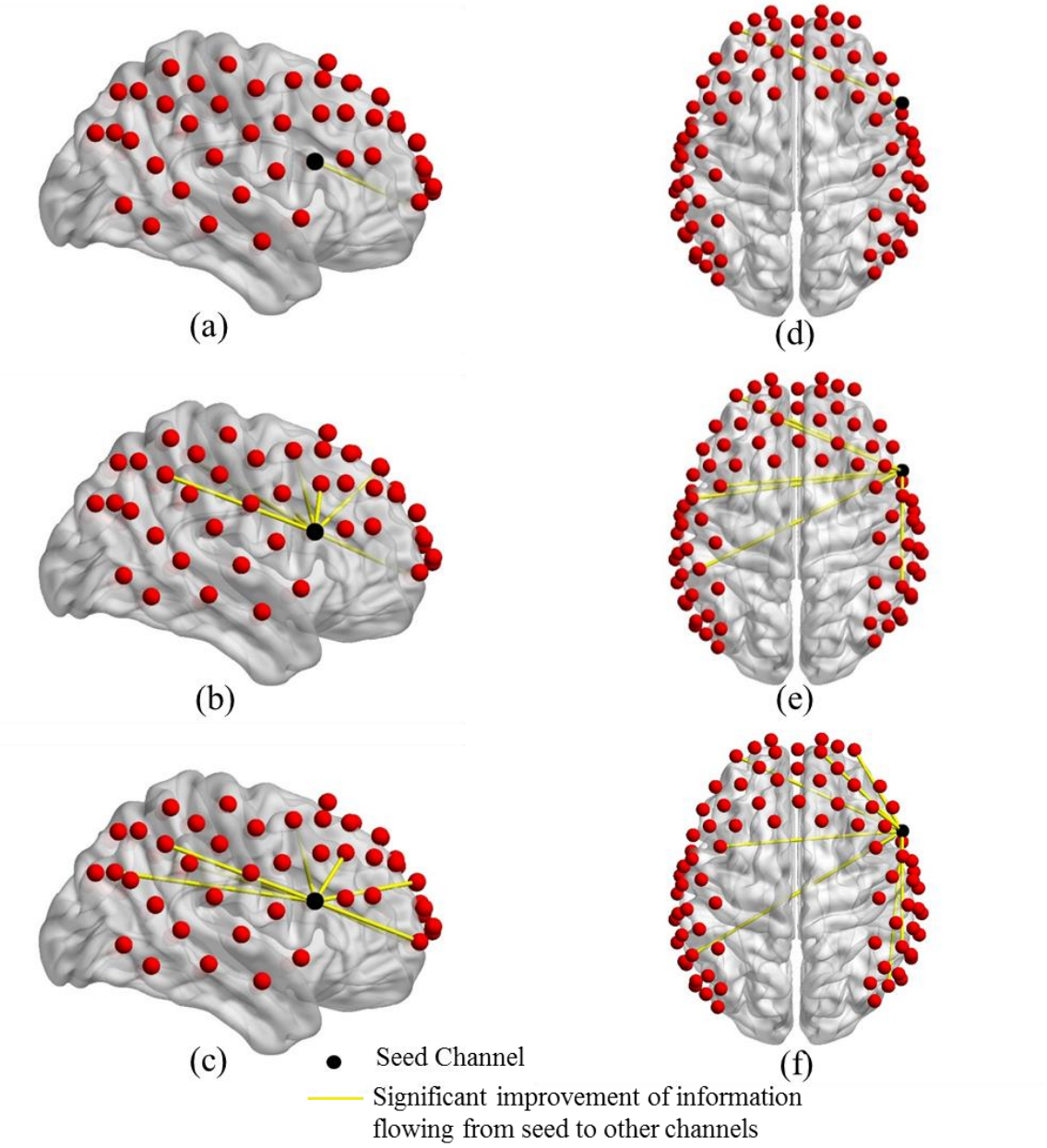

Figure 4-6 Changes in information flow direction between the right Broca's area (seed) and other cortical regions induced by different tDCS stimulation conditions. Group-level significant differences ($p<0.05$) in information flow direction between pairs of detector locations for the No tDCS condition versus Low Current tDCS [(a), (d)], versus High Current tDCS [(b), (e)], and versus After High Current tDCS [(c), (f)] stimulation conditions.

Table 4-2 Brodmann areas with significantly increased information influx originating from Channel 34 (right Broca's area)

Seed: Channel 34	Low Current tDCS	High Current tDCS	After High Current tDCS
Ipsilateral Hemisphere			
Brodmann Area 9		Yes	
Brodmann Area 10			Yes
Brodmann Area 22/39/40		Yes	Yes
Contralateral Hemisphere			
Brodmann Area 6		Yes	Yes
Brodmann Area 10	Yes	Yes	Yes
Brodmann Area 22/39/40		Yes	Yes

BA 6: Premotor Area; BA 9: Dorsolateral Prefrontal Cortex; BA 10: Frontopolar Area; BA 22/39/40: Wernicke's area.

4.3.2 Information Flow in the Endothelial Frequency Band (0.003 – 0.02 Hz)

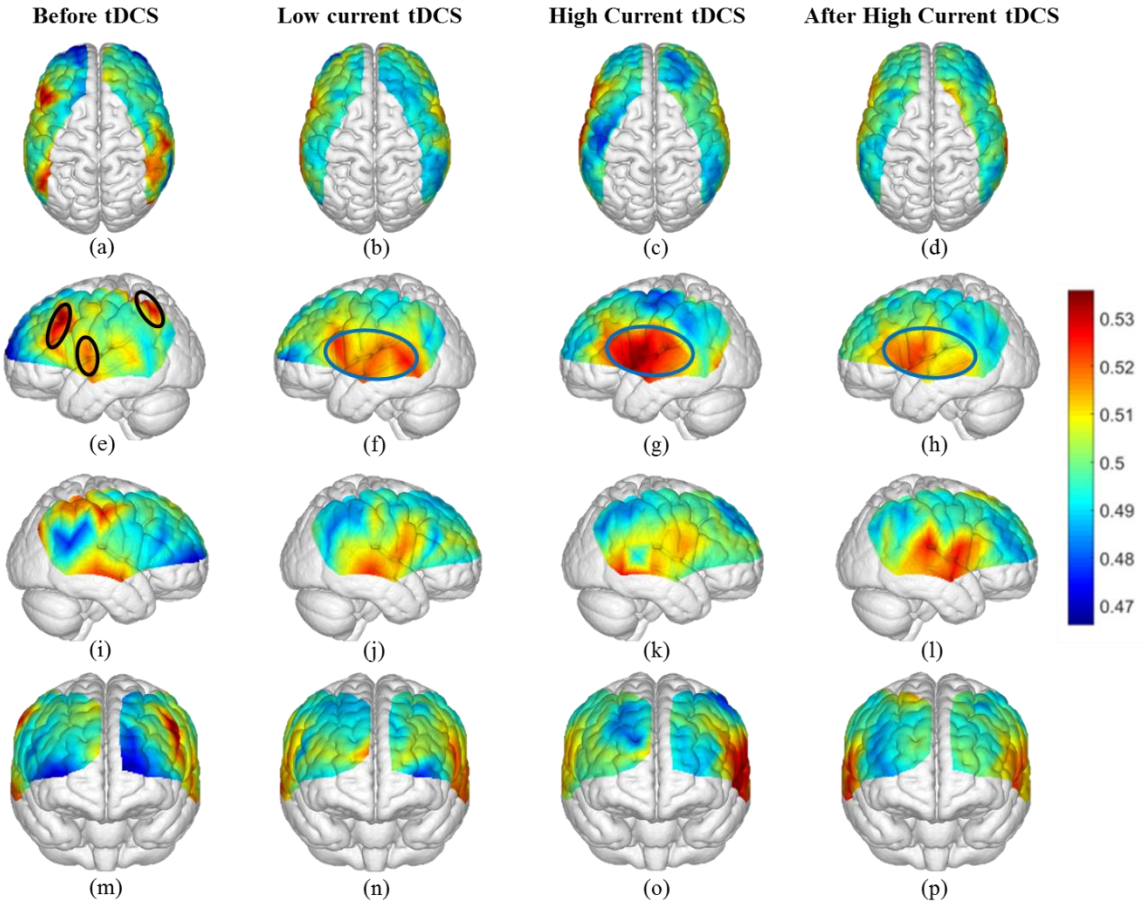

Figure 4-7 Mean dPTE in the endothelial frequency band for each channel displayed as a color-coded map viewed from top, left, right and front for four different sessions: No tDCS [(a), (e), (i) and (m)], Low Current tDCS [(b), (f), (j) and (n)], High Current tDCS [(c), (g), (k) and (o)] and After High Current tDCS [(d),(h), (l) and (p)]. Hot (yellow – red) and cold (blue – green) colors indicate information outflow and inflow, respectively.

Fig. 4-7 shows the average information flow in the endothelial frequency band between any channel location and all other cortical regions by using dPTE analysis for four different sessions (No tDCS, Low Current tDCS, High Current tDCS and After High Current tDCS). The color-coded map illustrates a single estimate of preferred direction of information flow (outgoing or incoming) for each channel. Fig. 4-7(e) shows that during the initial No tDCS session the outgoing

information was generated from the DLPFC (BA 9), MTG (BA 21) and Somatosensory Association Cortex (BA 7) regions indicated by black ovals, which are part of the default model network (DMN)[154]. In contrast, during and after stimulation the Broca's area (BA 44/45), MTG (BA21) and STG (BA 22), all circumscribed within a blue oval in Figs 4-7(f)-(h) became the hot spots for outgoing information. In addition, in the non-stimulated contralateral hemisphere, shown in Figs. 4-7(i)-(l), tDCS created lower level dPTE changes during Low and High Current tDCS for the endothelial frequency band.

Subsequently, the Broca's area, MTG and STG hot spots in the left hemisphere were chosen as the seeds for determining where the outgoing information was directed out of these regions on the cortex. Only Brodmann areas with significant increases in outgoing information from all the seeds, compared with the No tDCS condition, were illustrated in Table 4-3. For Low Current tDCS and After High Current tDCS, increased information flow was directed into the same Brodmann areas, while for High Current tDCS, increased information flow occurred into additional cortical regions, which are also part of the language-processing network[116-118].

Table 4-3 Brodmann areas with significantly increased information influx originating from hot spots in the left hemisphere

Hot spots on left hemisphere	Low Current tDCS	High Current tDCS	After High Current tDCS
Ipsilateral Hemisphere			
Brodmann Area 6		Yes	
Brodmann Area 9		Yes	
Brodmann Area 40	Yes	Yes	Yes
Contralateral Hemisphere			
Brodmann Area 40	Yes	Yes	Yes

Hot spots: Left Broca's area, MTG and STG. BA 6: Premotor Area; BA 9: Dorsolateral Prefrontal Cortex; BA 10: Frontopolar Area; BA 22/39/40: Wernicke's area.

4.3.3 Information Flow in the Neurogenic Frequency Band (0.02 – 0.04 Hz)

Fig. 4-8 shows information flow in the neurogenic frequency band between any channel location and all other cortical regions by using dPTE analysis for four different sessions (No tDCS, Low Current tDCS, High Current tDCS and After High Current tDCS). The color-coded map illustrates a single estimate of direction of information flow (outgoing or incoming) for each channel. Figs. 8(i) shows that during the initial No tDCS session the outgoing information hot spots were located over the DPFLC (BA 9), indicated by black ovals, which is part of the DMN[154]. In contrast, during and after stimulation the hot spots shifted to the Broca's area (BA 44/45), MTG (BA21) and STG (BA 22) of the left hemisphere, indicated by blue ovals in Figs. 4-8(j)-(l). It is noteworthy that when comparing to the left hemisphere, Figs. 4-8(e)-(h), where the anodal stimulation over Borca's area was applied, it appears that higher changes in dPTE occurred in the right hemisphere for the neurogenic frequency band. It is suspected that these information flow changes occurring in the hemisphere contralateral to the stimulation were facilitated by interhemispheric connections through the corpus callosum[155].

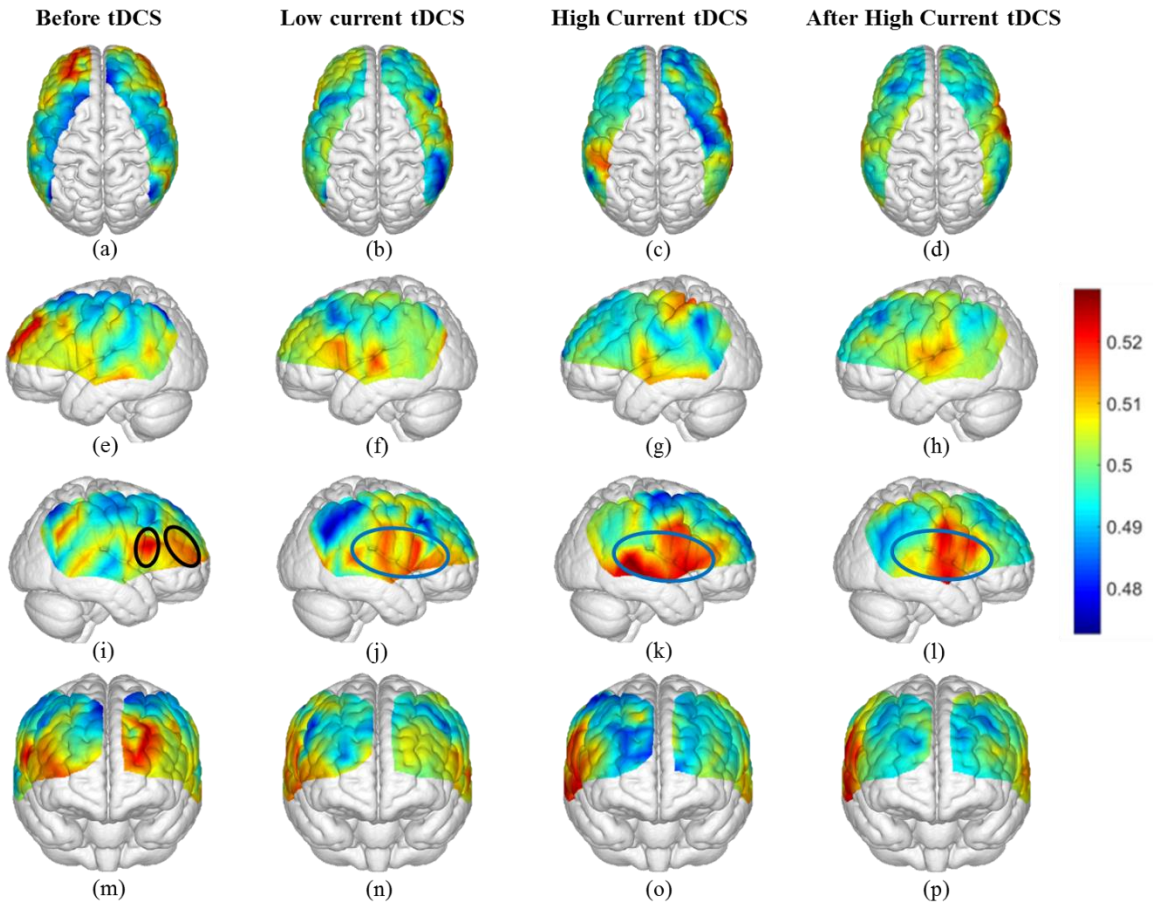

Figure 4-8 Mean dPTE in the neurogenic frequency band for each channel displayed as a color-coded map viewed from top, left, right and front for four different sessions: No tDCS [(a), (e), (i) and (m)], Low Current tDCS [(b), (f), (j) and (n)], High Current tDCS [(c), (g), (k) and (o)] and After High Current tDCS [(d),(h), (l) and (p)].)]. Hot (yellow – red) and cold (blue – green) colors indicate information outflow and inflow, respectively.

Subsequently, the Broca's area, MTG and STG hot spots in the right hemisphere were chosen as the seeds for determining where the outgoing information was directed from these regions to other cortical areas. Only Brodmann areas with significant increases in outgoing information from all these seed regions, compared to the No tDCS condition, were illustrated in Table 4-4. Interestingly, in contrast to the results for the endothelial frequency band shown in Table 4-3, enhanced information flow occurred towards a larger number of cortical regions,

corresponding to Brodmann areas listed in Table 4-4, during High Current tDCS. The higher information outflow effect over these Brodmann areas persisted during the After High Current tDCS session. The longevity of these information flow patterns beyond the current stimulation period hints at the possibility that these effects are tDCS-induced changes in neuronal activity, possibly mediated by long-term potentiation (LTP) [156-158].

Table 4-4 Brodmann areas with significantly increased information influx originating from hot spots in the right hemisphere

Hot spots on right hemisphere	Low Current tDCS	High Current tDCS	After High Current tDCS
Ipsilateral Hemisphere			
Brodmann Area 9		Yes	Yes
Brodmann Area 10		Yes	Yes
Brodmann Area 40	Yes	Yes	Yes
Contralateral Hemisphere			
Brodmann Area 6		Yes	Yes
Brodmann Area 40	Yes	Yes	Yes

Hot spots: Right Broca's area, MTG and STG. BA 6: Premotor Area; BA 9: Dorsolateral Prefrontal Cortex; BA 10: Frontopolar Area; BA 22/39/40: Wernicke's area.

4.3.3 Information Flow in the Myogenic Frequency Band (0.04 – 0.15 Hz)

Fig. 4-9 shows information flow in the myogenic frequency band between any channel location and all other cortical regions by using dPTE analysis for four different sessions (No tDCS, Low Current tDCS, High Current tDCS and After High Current tDCS), as was done above for the other frequency bands. Figs. 4-9(m)-(p) show that for all four stimulation sessions, the hot spots of outgoing information appeared in the frontopolar areas (BA 10) of both hemispheres, indicated by black ovals. No significant change was found in the PTE of hot spots of each hemisphere between stimulation sessions. Therefore, information outflow in these hot spots was not affected

by the stimulation. The dPTE in key language areas (Broca's area and Wernicke's area) were not affected by the stimulation either. Therefore, we did not pursue any further seed-based analysis for this frequency band as was done for the endothelial and neurogenic bands.

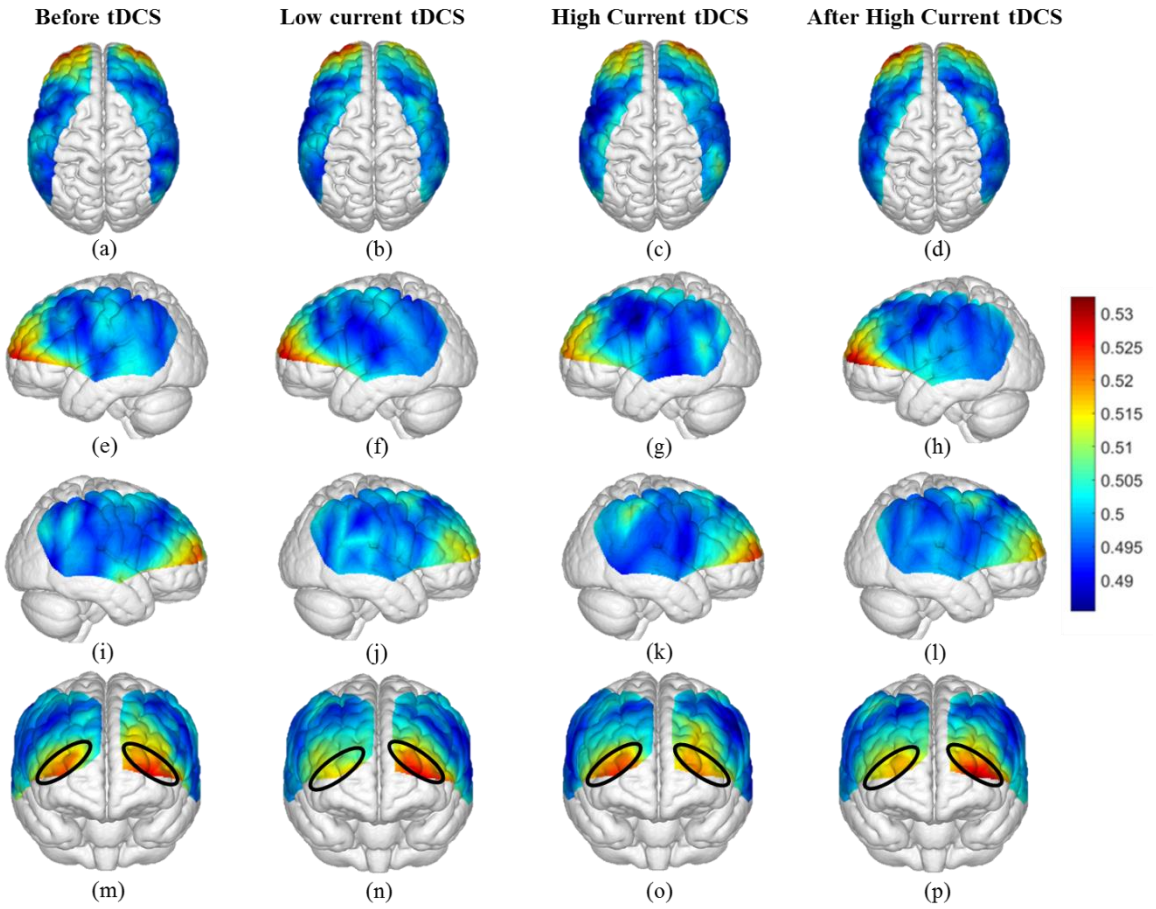

Figure 4-9 Mean dPTE in the myogenic frequency band for each channel displayed as a color-coded map viewed from top, left, right and front for four different sessions: No tDCS [(a), (e), (i) and (m)], Low Current tDCS [(b), (f), (j) and (n)], High Current tDCS [(c), (g), (k) and (o)] and After High Current tDCS [(d),(h), (l) and (p)]. Hot (yellow – red) and cold (blue – green) colors indicate information outflow and inflow, respectively.

4.4 Discussion

This study explored the impact of anodal tDCS applied over the left Broca's area on the direction of information flow deduced from hemodynamic fluctuations in the fNIRS signal as a whole and

in three distinct frequency sub-bands that are known to be attributed to endothelial, neurogenic and myogenic activity. Despite the lower spatial resolution and tissue depth probed compared to fMRI, the higher temporal resolution of fNIRS and its ability to easily collect data during electrical stimulation has enabled us to demonstrate different patterns of information flow induced by tDCS for different frequency bands.

4.4.1 DPTE Analysis of all fNIRS Frequencies (0.003-0.15 Hz) Shows that Anodal tDCS Over the Left Broca's Area Enhances Information Efflux to other Language-Processing Areas

Anodal stimulation over the left Broca's area made not only that region, but also its non-stimulated counterpart in the contralateral hemisphere strong emitters of information flow towards other language-processing areas. This is evident in the Fig. 4-4 hot spots for the three tDCS stimulation conditions, where the cold spots are the cortical areas of reception of information efflux from the hot spots. These results are consistent with a prior EEG study where TMS was applied alternately over the left and right anterior temporal lobes, and the left and right superior parietal lobes[159]. That study found that TMS applied on all four stimulation sites evoked a consistent increase of information flow around the stimulation site and its contralateral cortical region in the broad EEG frequency band of 3-45Hz. That study reported that the direction of stimulation affects cortical areas with established neuronal connections through two main commissural fibers[160].

The effect of stimulation on information flow across both hemispheres is shown in Tables 4-1 and 4-2 that identify the cortical areas receiving information from the left and right Broca's area respectively. For the ipsilateral hemisphere to the stimulation, those cortical areas are not only structurally connected with Broca's area through white matter tracts in the Arcuate Fasciculus (AF)[161, 162], but also are language-related regions[103, 115-118, 131, 163, 164]. The AF is thought to connect Broca's area to Wernicke's area (BA 22/39/40)[165, 166], but the temporal projections of the AF could also reach the STG (BA 22) and the MTG (BA 21). These latter regions have projections the reach premotor cortex (BA 6) and the middle frontal gyrus (BA 9 and BA

10)[161, 162]. For the contralateral hemisphere to the stimulation, communication with the stimulated area could be achieved through the corpus callosum and its projections to those areas[167]. Therefore, given those known structural connections it is not surprising that outgoing information from the Broca's area also flowed into ipsilateral and contralateral regions for BA 6, BA 9, BA 10, BA 21 and BA22/39/40. Wernicke's area (BA 39/40) plays role in language comprehension[163], STG (BA 22) is part of Wernicke's area and related with prosody comprehension[103], premotor cortex (BA 6) is related with maintenance and execution of speech[116, 117], DLPFC (BA 9) is related with speech planning[118] and frontopolar area (BA 10) is related with memory[131, 164].

Another noteworthy point is that the during High Current tDCS, MTG (BA 21) identified by the pink circle in Fig. 4-4 had significant changes in information influx, identified from pairwise t-tests in dPTE compared to the No tDCS condition in Table 4-1, from the left Broca's area while it also had information efflux towards other areas (Ipsilateral hemisphere: BA6, 9, 10, 22/39/40; Contralateral Hemisphere: BA 6, 9, 10, 22/39/40). Therefore the MTG became a secondary information transfer connector, which is known according to the previous literature[168].

Finally, Fig. 4-4 suggests that information flow patterns appearing during Low Current tDCS are qualitatively similar to those appearing during the High Current tDCS and After High Current tDCS sessions. However, when it comes to the question of whether Low Current tDCS is predictive of the information flow patterns created by higher currents, Tables 4-1 and 4-2 suggest that it is not. Nevertheless, some interesting frequency band specific resemblances in information flow patterns between stimulation sessions were noted and are discussed below.

4.4.2 TDCS Affected Information Flow Differently in Different Hemodynamic Frequency Bands

4.4.2.1 Endothelial Frequency Band (0.003-0.02 Hz)

TDCS created greater changes in outgoing information on the left hemisphere, over and around the stimulation area. As shown in Fig. 4-4, hot spots before tDCS in the left DLPFC and

Somatosensory Association Cortex, which are part of the DMN[154], disappeared after stimulation even for Low Current tDCS. At the same time with stimulation, outgoing information hot spots appeared over key language areas such as Broca's area, STG and MTG and persisted during the After tDCS session. The fact that information flowed out of these hotspots towards other cortical regions including Wernicke's area, DPFLC and premotor area is not surprising since these regions are known to be involved in pathways that activate for several speech-related tasks, such as picture naming[169] and overt speech production[170].

Hemodynamic fluctuation changes in the endothelial frequency band, reflect endothelial cell activity mediated by the release of nitric oxide (NO), a vasodilator[146, 171, 172]. It is possible that tDCS could increase NO production so as to increase brain perfusion[173]. However, the fact that there were significant increases in information efflux in the contralateral hemisphere also (Fig. 7), indicates that hemodynamic changes in this frequency band were at least in part related to changes in neuronal connectivity. Nevertheless, the largest increase in information efflux was observed locally, in the vicinity of the stimulation area. This local dependence is unlikely to be related to tDCS-induced heating at the current intensities used and were well below the known limits of current induced heating during tDCS[174, 175]. A NO-based mechanism of endothelial response to stimulation would be consistent with the findings summarized in Table 4-3, where the flow information patterns during Low Current tDCS were similar to the After High Current tDCS session, whereas a more intense and spatially extended response was observed during the High Current tDCS session. A positive relationship between the amount of NO release with the current density of tDCS has been previously reported[173].

In addition, in Table 4-3, Wernicke's area became an information receiver not only during High Current tDCS but also during Low Current tDCS and After High Current tDCS. Since Broca's area and Wernicke's area are the two main language areas[176], we hypothesize that the baseline connection between them is stronger compared to other cortical regions, which is why information flow between them was seen even during the Low Current tDCS condition.

Furthermore, in this frequency band the Low Current tDCS correctly predicted 2/2 Brodmann areas receiving increased information flow during the After High Current tDCS condition (Table 4-3).

4.4.2.2 Neurogenic Frequency Band (0.02-0.04 Hz)

Interestingly, tDCS created stronger changes in outgoing information on the non-stimulated right hemisphere, over and around the contralateral stimulation area. As shown in Fig. 4-8, the hot spots before stimulation occurred in right dorsolateral prefrontal cortex regions, which are part of the DMN[154]. After stimulation, these hot spots disappeared and new ones appeared over key language areas: Broca's area, STG and MTG, which became information efflux spots towards other cortical regions including Wernicke's area, DPFLC, the frontopolar and premotor areas. These latter cortical regions are known to activate in speech-related tasks, such as picture naming[169].

Hemodynamic oscillations in the neurogenic frequency band are attributed to intrinsic nervous activity[147]. Since tDCS could induce a sustainable response in the form of LTP-like plasticity within and across structurally connected brain regions[157, 158], it is possible that the right Broca's and related areas became information efflux hot spots due to the increased neuronal activity induced by the pre-existing connections with the left Broca's area. An LTP-like plasticity mechanism of neurogenic response to stimulation would be consistent with the findings summarized in Table 4-4, where the flow information patterns during How Current tDCS were similar to the After High Current tDCS session. These results are in contrast to those listed in Table 4-3 for the endothelial frequency band, where the Low Current tDCS sessions shared the same increased information influx regions as the After High Current tDCS session. An LTP-like plasticity hypothesis is also consistent with findings in the literature[88], indicating that the during 1 mA 5 min tDCS on motor cortex, there was a significant increase in motor-evoked potential

(MEP) amplitude representing the excitability of the motor system, and this effect still persisted after tDCS.

4.4.2.3 Myogenic Frequency Band (0.04-0.15 Hz)

TDCS appeared to have little effect on the information flow patterns of the myogenic frequency band, as there was no significant difference in dPTE for hot spots between stimulation sessions. As shown in Fig. 4-9, hot spots were located in the frontopolar areas (BA10) that are related to prospective memory. The left BA 10 is involved in verbal prospective memory, while right BA 10 is involved in visual-spatial prospective memory[131]. The non-dependence of information flow patterns on tDCS may be due to Mayer waves existing in the same frequency range (~0.1 Hz) from the supraorbital artery located on top of these Broadmann areas [157] and therefore may not be directly related to their function.

4.5 Conclusion

This study demonstrates the feasibility of using resting-state fNIRS to map changes in the direction of information flow induced by tDCS in the language-processing cortical networks of healthy subjects. While dPTE analysis showed that language-processing cortical regions in both hemispheres became sources of outgoing information flow after tDCS when the entire fNIRS signal was considered, specific differences in those patterns were seen when the detected hemodynamic fluctuations were studied in distinct frequency bands. We found that tDCS induced higher changes in outgoing information in the vicinity of the stimulated Broca's area for the endothelial frequency band, which we hypothesized to be due to a correlation between tDCS current density and NO release levels in brain tissues. On the other hand, for the neurogenic frequency band higher changes in outgoing information were induced in the vicinity of the right Broca's area, in the contralateral hemisphere to the stimulation location. We hypothesized that this increase in outgoing information was related to tDCS effects on LTP-like plasticity in

established neuronal connections for the language-processing network. Finally, no tDCS effects were seen in the myogenic frequency band, which likely relates to Mayer waves created by arterial blood vessels on the cortical surface. The methods described in this work for identifying changes in hemodynamic frequency-specific patterns of information flow induced by tDCS could be helpful in future studies on neurovascular coupling and possibly on the planning of stimulation-based therapeutic interventions.

Chapter 5 Conclusions and Future Work

The goal of this work was to study some of the altered cortical plasticity patterns induced by therapeutic interventions. The outcome of this research was the identification of fNIRS-derived brain activation patterns and functional connectivity as a means of planning, and possibly adapting, the course of interventions. The steps performed to achieve the goal of this work are outlined in the paragraphs below:

The first part of this study presented the utility of portable fNIRS technology as a means of mapping sensorimotor cortex plasticity in in children with CP to help explain changes seen in manual ability after a therapeutic intervention. Brain activation patterns indicated by laterality index and time-to-peak/duration of activation suggested that there were no children with CP in this study that significantly improved both their unimanual and bimanual abilities after CIMT while also normalizing their sensorimotor activation patterns, as measured by fNIRS. The global measures of hemodynamic responses indicated by laterality index and resting-state connectivity may be more useful for assessing longer-term treatment response.

The second part of this work demonstrated the feasibility of using resting-state fNIRS to study cortical network reorganization induced by tDCS in the language-processing cortical networks of healthy subjects. The steady-state functional connectivity indicated by seed-based functional connectivity and graph theory analyses revealed increased local and decreased remote

functional connectivity induced by tDCS. In addition, time-variant functional connectivity changes suggested that tDCS increased FCV of remote connections. Furthermore, Low Current tDCS could predicted qualitatively the increases in clustering coefficient and FCV, but not the increased local connectivity, created by High Current tDCS. This suggests the possibility of using Low Current tDCS in future work to test several different placements within one single session for predicting optimal electrode placement for High Current tDCS.

The third part of this work established a new methodology to reveal the altered directionality of functional connectivity between cortical regions induced by tDCS in three hemodynamic oscillation frequency bands (endothelial, neurogenic and myogenic frequency bands) mapped by fNIRS. Phase transfer entropy (PTE) was utilized to calculate the directionality of information flow. It was found that tDCS enhanced information outflow in the endothelial and neurogenic frequency bands flowing from the stimulated and contralateral Broca's area to other language-related processing areas. Also, tDCS affected information flow patterns differently in different frequency bands. The outgoing information flow was more intense in the left stimulated Broca's area for the endothelial frequency band, and the information flow during Low Current tDCS was similar with after High Current tDCS. On the other hand, outgoing information flow was more intense in the right homologous area to Broca's area for the neurogenic frequency band, and information outflow during High Current tDCS was similar with after High Current tDCS. In the myogenic frequency band, there was no significant change in key language areas (Broca's area and Wernicke's area). The findings of this work set the first step towards gaining insights for therapeutic intervention planning using information flow metrics in neuronal networks.

In the future, several things could be done to improve the understanding of cortical alterations induced by therapeutic interventions. First of all, whole head fNIRS imaging should be used whenever this technology is available. My research work only imaged sensorimotor cortex for CIMT on children with CP, and language-related cortical regions for tDCS on healthy adults. The CW-6 imaging system used for the CP study did not have whole head imaging capability, but

was portable enough to be transported to the clinic. The LABNIRS system used for the tDCS work was capable of whole head imaging, but it was impractical to set up all those sensors on one's head in a reasonable amount of time without help from at least one more person. Whole head imaging would provide a broader view on the effects of therapeutic interventions on cortical interactions and information flow as a whole. Secondly, only resting state studies were performed in the tDCS studies in this work. Activation tasks should be introduced in the protocol to enable study of functional compensation under different activation and stimulation conditions. In addition, the directionality of information flow may provide more insight into how language-processing circuits contribute to language performance when subjects perform related tasks. Thirdly, stroke patients should be involved in the study. In Chapter 3 and 4, only healthy subjects were investigated as the first step. More interesting and different patterns may be found when stroke patients are included due to their lesions on the brain affecting language area function. It is hoped that more research will be conducted in the future so that fNIRS-related biomarkers could be translated into treatment guidance.

Reference

[1] F. C. Alliance, "Incidence and prevalence of the major causes of brain impairment," ed: San Francisco, 2000.

[2] N. Paneth, T. Hong, and S. Korzeniewski, "The descriptive epidemiology of cerebral palsy," *Clinics in perinatology,* vol. 33, pp. 251-267, 2006.

[3] J. A. Langlois, W. Rutland-Brown, and K. E. Thomas, "Traumatic brain injury in the United States; emergency department visits, hospitalizations, and deaths," 2006.

[4] W. G. MEMBERS, A. S. Go, D. Mozaffarian, V. L. Roger, E. J. Benjamin, J. D. Berry*, et al.*, "Heart disease and stroke statistics—2014 update: a report from the American Heart Association," *circulation,* vol. 129, p. e28, 2014.

[5] J. Charles and A. M. Gordon, "A critical review of constraint-induced movement therapy and forced use in children with hemiplegia," *Neural plasticity,* vol. 12, pp. 245-261, 2005.

[6] A. McIntyre, R. Viana, S. Janzen, S. Mehta, S. Pereira, and R. Teasell, "Systematic review and meta-analysis of constraint-induced movement therapy in the hemiparetic upper extremity more than six months post stroke," *Topics in stroke rehabilitation,* vol. 19, pp. 499-513, 2012.

[7] K. Lowe, I. Novak, and A. Cusick, "Repeat injection of botulinum toxin A is safe and effective for upper limb movement and function in children with cerebral palsy," *Developmental Medicine & Child Neurology,* vol. 49, pp. 823-829, 2007.

[8] W. H. Jost, H. Hefter, A. Reissig, K. Kollewe, and J. Wissel, "Efficacy and safety of botulinum toxin type A (Dysport) for the treatment of post-stroke arm spasticity: Results of the German–Austrian open-label post-marketing surveillance prospective study," *Journal of the neurological sciences,* vol. 337, pp. 86-90, 2014.

[9] J. M. Baker, C. Rorden, and J. Fridriksson, "Using transcranial direct-current stimulation to treat stroke patients with aphasia," *Stroke,* vol. 41, pp. 1229-1236, 2010.

[10] A. J. Butler and S. L. Wolf, "Putting the brain on the map: use of transcranial magnetic stimulation to assess and induce cortical plasticity of upper-extremity movement," *Physical therapy,* vol. 87, pp. 719-736, 2007.

[11] R. Boyd, M. Morris, and H. Graham, "Management of upper limb dysfunction in children with cerebral palsy: a systematic review," *European Journal of Neurology,* vol. 8, pp. 150-166, 2001.

[12] J. Fridriksson, J. D. Richardson, J. M. Baker, and C. Rorden, "Transcranial direct current stimulation improves naming reaction time in fluent aphasia," *Stroke,* vol. 42, pp. 819-821, 2011.

[13] V. Fiori, M. Coccia, C. V. Marinelli, V. Vecchi, S. Bonifazi, M. G. Ceravolo*, et al.*, "Transcranial direct current stimulation improves word retrieval in healthy and nonfluent aphasic subjects," *Journal of Cognitive Neuroscience,* vol. 23, pp. 2309-2323, 2011.

[14] S. Rocha, E. Silva, Á. Foerster, C. Wiesiolek, A. P. Chagas, G. Machado*, et al.*, "The impact of transcranial direct current stimulation (tDCS) combined with modified constraint-induced movement therapy (mCIMT) on upper limb function in chronic stroke: a double-blind randomized controlled trial," *Disability and rehabilitation,* vol. 38, pp. 653-660, 2016.

[15] N. Bolognini, G. Vallar, C. Casati, L. A. Latif, R. El-Nazer, J. Williams*, et al.*, "Neurophysiological and behavioral effects of tDCS combined with constraint-induced movement therapy in poststroke patients," *Neurorehabilitation and neural repair,* vol. 25, pp. 819-829, 2011.

[16] T. L. Sutcliffe, W. C. Gaetz, W. J. Logan, D. O. Cheyne, and D. L. Fehlings, "Cortical reorganization after modified constraint-induced movement therapy in pediatric hemiplegic cerebral palsy," *Journal of child neurology,* vol. 22, pp. 1281-1287, 2007.

[17] T. L. Sutcliffe, W. J. Logan, and D. L. Fehlings, "Pediatric constraint-induced movement therapy is associated with increased contralateral cortical activity on functional magnetic resonance imaging," *Journal of child neurology,* vol. 24, pp. 1230-1235, 2009.

[18] M. Meinzer, D. Antonenko, R. Lindenberg, S. Hetzer, L. Ulm, K. Avirame*, et al.*, "Electrical brain stimulation improves cognitive performance by modulating functional connectivity and task-specific activation," *Journal of Neuroscience,* vol. 32, pp. 1859-1866, 2012.

[19] P. Marangolo, V. Fiori, U. Sabatini, G. De Pasquale, C. Razzano, C. Caltagirone*, et al.*, "Bilateral transcranial direct current stimulation language treatment enhances functional connectivity in the left hemisphere: preliminary data from aphasia," *Journal of cognitive neuroscience,* 2016.

[20] Z. Li, H. Liu, X. Liao, J. Xu, W. Liu, F. Tian*, et al.*, "Dynamic functional connectivity revealed by resting-state functional near-infrared spectroscopy," *Biomedical optics express,* vol. 6, pp. 2337-2352, 2015.

[21] R. M. Hutchison, T. Womelsdorf, E. A. Allen, P. A. Bandettini, V. D. Calhoun, M. Corbetta*, et al.*, "Dynamic functional connectivity: promise, issues, and interpretations," *Neuroimage,* vol. 80, pp. 360-378, 2013.

[22] E. Damaraju, J. Turner, A. Preda, T. Van Erp, D. Mathalon, J. Ford*, et al.*, "Static and dynamic functional network connectivity during resting state in schizophrenia," in *American College of Neuropsychopharmacology*, 2012.

[23] D. T. Jones, P. Vemuri, M. C. Murphy, J. L. Gunter, M. L. Senjem, M. M. Machulda*, et al.*, "Non-stationarity in the “resting brain’s” modular architecture," *PloS one,* vol. 7, p. e39731, 2012.

[24] M. A. Franceschini, S. Fantini, J. H. Thompson, J. P. Culver, and D. A. Boas, "Hemodynamic evoked response of the sensorimotor cortex measured noninvasively with near‐infrared optical imaging," *Psychophysiology,* vol. 40, pp. 548-560, 2003.

[25] F. Irani, S. M. Platek, S. Bunce, A. C. Ruocco, and D. Chute, "Functional near infrared spectroscopy (fNIRS): an emerging neuroimaging technology with important applications for the study of brain disorders," *The Clinical Neuropsychologist,* vol. 21, pp. 9-37, 2007.

[26] S. Cutini, S. B. Moro, and S. Bisconti, "Review: Functional near infrared optical imaging in cognitive neuroscience: an introductory review," *Journal of Near Infrared Spectroscopy,* vol. 20, pp. 75-92, 2012.

[27] A. Villringer, "Understanding functional neuroimaging methods based on neurovascular coupling," in *Optical Imaging of Brain Function and Metabolism 2*, ed: Springer, 1997, pp. 177-193.

[28] S. C. Bunce, M. Izzetoglu, K. Izzetoglu, B. Onaral, and K. Pourrezaei, "Functional near-infrared spectroscopy," *Engineering in Medicine and Biology Magazine, IEEE,* vol. 25, pp. 54-62, 2006.

[29] K. Takahashi, S. Ogata, R. Yamamoto, A. Maki, H. Hirasawa, M. Igawa*, et al.*, "Activation of the visual cortex imaged by 24-channel near-infrared spectroscopy," *Journal of biomedical optics,* vol. 5, pp. 93-96, 2000.

[30] M. Ferrari and V. Quaresima, "A brief review on the history of human functional near-infrared spectroscopy (fNIRS) development and fields of application," *Neuroimage,* vol. 63, pp. 921-935, 2012.

[31] B. Khan, T. Hodics, N. Hervey, G. Kondraske, A. M. Stowe, and G. Alexandrakis, "Functional near-infrared spectroscopy maps cortical plasticity underlying altered motor performance induced by transcranial direct current stimulation," *Journal of biomedical optics,* vol. 18, pp. 116003-116003, 2013.

[32] P. Rosenbaum, N. Paneth, A. Leviton, M. Goldstein, M. Bax, D. Damiano*, et al.*, "A report: the definition and classification of cerebral palsy April 2006," *Dev Med Child Neurol Suppl,* vol. 109, 2007.

[33] W. Kułak, W. Sobaniec, J.-Ś. Kuzia, and L. Boćkowski, "Neurophysiologic and neuroimaging studies of brain plasticity in children with spastic cerebral palsy," *Experimental neurology,* vol. 198, pp. 4-11, 2006.

[34] J. M. Keogh and N. Badawi, "The origins of cerebral palsy," *Current opinion in neurology,* vol. 19, pp. 129-134, 2006.

[35] A. Houwink, P. Aarts, A. C. Geurts, and B. Steenbergen, "A neurocognitive perspective on developmental disregard in children with hemiplegic cerebral palsy," *Research in developmental disabilities,* vol. 32, pp. 2157-2163, 2011.

[36] A. Van de Winckel, K. Klingels, F. Bruyninckx, N. Wenderoth, R. Peeters, S. Sunaert*, et al.*, "How does brain activation differ in children with unilateral cerebral palsy compared to typically developing children, during active and passive movements, and tactile stimulation? An fMRI study," *Research in developmental disabilities,* vol. 34, pp. 183-197, 2013.

[37] B. Hoare, J. Wasiak, C. Imms, and L. Carey, "Constraint-induced movement therapy in the treatment of the upper limb in children with hemiplegic cerebral palsy," *Cochrane Database Syst Rev,* vol. 2, 2007.

[38] A. C. Eliasson, L. Krumlinde‐Sundholm, B. Rösblad, E. Beckung, M. Arner, A. M. Öhrvall*, et al.*, "The Manual Ability Classification System (MACS) for children with cerebral palsy: scale development and evidence of validity and reliability," *Developmental Medicine & Child Neurology,* vol. 48, pp. 549-554, 2006.

[39] M. Law, S. Baptiste, M. McColl, A. Opzoomer, H. Polatajko, and N. Pollock, "The Canadian occupational performance measure: an outcome measure for occupational therapy," *Canadian Journal of Occupational Therapy,* vol. 57, pp. 82-87, 1990.

[40] S. Blundell, R. Shepherd, C. Dean, R. Adams, and B. Cahill, "Functional strength training in cerebral palsy: a pilot study of a group circuit training class for children aged 4–8 years," *Clinical Rehabilitation,* vol. 17, pp. 48-57, 2003.

[41] M. Randall, J. B. Carlin, P. Chondros, and D. Reddihough, "Reliability of the Melbourne assessment of unilateral upper limb function," *Developmental Medicine & Child Neurology,* vol. 43, pp. 761-767, 2001.

[42] L. Krumlinde-sundholm and A.-c. Eliasson, "Development of the Assisting Hand Assessment: a Rasch-built measure intended for children with unilateral upper limb impairments," *Scandinavian Journal of Occupational Therapy,* vol. 10, pp. 16-26, 2003.

[43] B. S. Russman and S. Ashwal, "Evaluation of the child with cerebral palsy," in *Seminars in pediatric Neurology*, 2004, pp. 47-57.

[44] K. Himmelmann and P. Uvebrant, "Function and neuroimaging in cerebral palsy: a population-based study," *Developmental Medicine & Child Neurology,* vol. 53, pp. 516-521, 2011.

[45] C. Sterling, E. Taub, D. Davis, T. Rickards, L. V. Gauthier, A. Griffin*, et al.*, "Structural neuroplastic change after constraint-induced movement therapy in children with cerebral palsy," *Pediatrics,* vol. 131, pp. e1664-e1669, 2013.

[46] M. Wilke, S. K. Holland, J. S. Myseros, V. J. Schmithorst, and W. S. Ball Jr, "Functional magnetic resonance imaging in pediatrics," *Neuropediatrics,* vol. 34, p. 225, 2003.

[47] H. Juenger, N. Kuhnke, C. Braun, F. Ummenhofer, M. Wilke, M. Walther*, et al.*, "Two types of exercise-induced neuroplasticity in congenital hemiparesis: a transcranial magnetic stimulation, functional MRI, and magnetoencephalography study," *Developmental Medicine & Child Neurology,* vol. 55, pp. 941-951, 2013.

[48] F. Orihuela-Espina, D. Leff, D. James, A. Darzi, and G. Yang, "Quality control and assurance in functional near infrared spectroscopy (fNIRS) experimentation," *Physics in medicine and biology,* vol. 55, p. 3701, 2010.

[49] V. Toronov, M. A. Franceschini, M. Filiaci, S. Fantini, M. Wolf, A. Michalos*, et al.*, "Near-infrared study of fluctuations in cerebral hemodynamics during rest and motor stimulation: temporal analysis and spatial mapping," *Medical physics,* vol. 27, pp. 801-815, 2000.

[50] U. Chaudhary, M. Hall, J. Gonzalez, L. Elbaum, M. Bloyer, and A. Godavarty, "Motor response investigation in individuals with cerebral palsy using near infrared spectroscopy: pilot study," *Applied optics,* vol. 53, pp. 503-510, 2014.

[51] M. J. Kurz, T. W. Wilson, and D. J. Arpin, "An fNIRS exploratory investigation of the cortical activity during gait in children with spastic diplegic cerebral palsy," *Brain and Development,* 2014.

[52] B. Khan, M. R. Delgado, H. Liu, G. Alexandrakis, N. J. Clegg, F. Tian*, et al.*, "Identification of abnormal motor cortex activation patterns in children with cerebral palsy by functional near-infrared spectroscopy," *Journal of biomedical optics,* vol. 15, pp. 036008-036008-14, 2010.

[53] T. Huppert, R. Hoge, S. Diamond, M. A. Franceschini, and D. A. Boas, "A temporal comparison of BOLD, ASL, and NIRS hemodynamic responses to motor stimuli in adult humans," *Neuroimage,* vol. 29, pp. 368-382, 2006.

[54] G. Strangman, M. A. Franceschini, and D. A. Boas, "Factors affecting the accuracy of near-infrared spectroscopy concentration calculations for focal changes in oxygenation parameters," *Neuroimage,* vol. 18, pp. 865-879, 2003.

[55] G. H. Klem, H. Lüders, H. Jasper, and C. Elger, "The ten-twenty electrode system of the International Federation. The International Federation of Clinical Neurophysiology," *Electroencephalography and clinical neurophysiology. Supplement,* vol. 52, p. 3, 1999.

[56] M. A. Franceschini, D. K. Joseph, T. J. Huppert, S. G. Diamond, and D. A. Boas, "Diffuse optical imaging of the whole head," *Journal of biomedical optics,* vol. 11, pp. 054007-054007-10, 2006.

[57] C. Julien, "The enigma of Mayer waves: facts and models," *Cardiovascular research,* vol. 70, pp. 12-21, 2006.

[58] Y. Zhang, M. A. Franceschini, D. A. Boas, and D. H. Brooks, "Eigenvector-based spatial filtering for reduction of physiological interference in diffuse optical imaging," *Journal of biomedical optics,* vol. 10, pp. 011014-01101411, 2005.

[59] G. Morren, M. Wolf, P. Lemmerling, U. Wolf, J. H. Choi, E. Gratton*, et al.*, "Detection of fast neuronal signals in the motor cortex from functional near infrared spectroscopy measurements using independent component analysis," *Medical and Biological Engineering and Computing,* vol. 42, pp. 92-99, 2004.

[60] S. Prince, V. Kolehmainen, J. P. Kaipio, M. A. Franceschini, D. Boas, and S. R. Arridge, "Time-series estimation of biological factors in optical diffusion tomography," *Physics in medicine and biology,* vol. 48, p. 1491, 2003.

[61] Q. Zhang, E. N. Brown, and G. E. Strangman, "Adaptive filtering for global interference cancellation and real-time recovery of evoked brain activity: a Monte Carlo simulation study," *Journal of biomedical optics,* vol. 12, pp. 044014-044014-12, 2007.

[62] N. M. Gregg, B. R. White, B. W. Zeff, A. J. Berger, and J. P. Culver, "Brain specificity of diffuse optical imaging: improvements from superficial signal regression and tomography," *Frontiers in neuroenergetics,* vol. 2, 2010.

[63] T. Funane, H. Atsumori, T. Katura, A. N. Obata, H. Sato, Y. Tanikawa*, et al.*, "Quantitative evaluation of deep and shallow tissue layers' contribution to fNIRS signal using multi-distance optodes and independent component analysis," *Neuroimage,* vol. 85, pp. 150-165, 2014.

[64] L. Gagnon, K. Perdue, D. N. Greve, D. Goldenholz, G. Kaskhedikar, and D. A. Boas, "Improved recovery of the hemodynamic response in diffuse optical imaging using short optode separations and state-space modeling," *Neuroimage,* vol. 56, pp. 1362-1371, 2011.

[65] T. J. Huppert, S. G. Diamond, M. A. Franceschini, and D. A. Boas, "HomER: a review of time-series analysis methods for near-infrared spectroscopy of the brain," *Applied optics,* vol. 48, pp. D280-D298, 2009.

[66] M. E. Kilmer, P. C. Hansen, and M. I. Espanol, "A projection-based approach to general-form Tikhonov regularization," *SIAM Journal on Scientific Computing,* vol. 29, pp. 315-330, 2007.

[67] J. Wang, "Recurrent neural networks for computing pseudoinverses of rank-deficient matrices," *SIAM Journal on Scientific Computing,* vol. 18, pp. 1479-1493, 1997.

[68] K. J. Friston, A. P. Holmes, K. J. Worsley, J. P. Poline, C. D. Frith, and R. S. Frackowiak, "Statistical parametric maps in functional imaging: a general linear approach," *Human brain mapping,* vol. 2, pp. 189-210, 1994.

[69] C. F. Beckmann, M. Jenkinson, and S. M. Smith, "General multilevel linear modeling for group analysis in FMRI," *Neuroimage,* vol. 20, pp. 1052-1063, 2003.

[70] A. F. Abdelnour and T. Huppert, "Real-time imaging of human brain function by near-infrared spectroscopy using an adaptive general linear model," *Neuroimage,* vol. 46, pp. 133-143, 2009.

[71] J. MacQueen, "Some methods for classification and analysis of multivariate observations," in *Proceedings of the fifth Berkeley symposium on mathematical statistics and probability*, 1967, pp. 281-297.

[72] M. A. Lindquist, J. Meng Loh, L. Y. Atlas, and T. D. Wager, "Modeling the hemodynamic response function in fMRI: efficiency, bias and mis-modeling," *Neuroimage,* vol. 45, pp. S187-98, Mar 2009.

[73] M. L. Seghier, "Laterality index in functional MRI: methodological issues," *Magnetic resonance imaging,* vol. 26, pp. 594-601, 2008.

[74] B. B. Biswal, "Resting state fMRI: a personal history," *Neuroimage,* vol. 62, pp. 938-944, 2012.

[75] D. Tomasi and N. D. Volkow, "Abnormal functional connectivity in children with attention-deficit/hyperactivity disorder," *Biological psychiatry,* vol. 71, pp. 443-450, 2012.

[76] E. J. Sanz-Arigita, M. M. Schoonheim, J. S. Damoiseaux, S. A. Rombouts, E. Maris, F. Barkhof*, et al.*, "Loss of 'small-world'networks in Alzheimer's disease: graph analysis of FMRI resting-state functional connectivity," *PloS one,* vol. 5, p. e13788, 2010.

[77] R. C. Mesquita, M. A. Franceschini, and D. A. Boas, "Resting state functional connectivity of the whole head with near-infrared spectroscopy," *Biomedical optics express,* vol. 1, pp. 324-336, 2010.

[78] D. A. Fair, A. L. Cohen, N. U. Dosenbach, J. A. Church, F. M. Miezin, D. M. Barch*, et al.*, "The maturing architecture of the brain's default network," *Proceedings of the National Academy of Sciences,* vol. 105, pp. 4028-4032, 2008.

[79] F. Faul, E. Erdfelder, A.-G. Lang, and A. Buchner, "G* Power 3: A flexible statistical power analysis program for the social, behavioral, and biomedical sciences," *Behavior research methods,* vol. 39, pp. 175-191, 2007.

[80] F. Tian, M. R. Delgado, S. C. Dhamne, B. Khan, G. Alexandrakis, M. I. Romero*, et al.*, "Quantification of functional near infrared spectroscopy to assess cortical reorganization in children with cerebral palsy," *Optics express,* vol. 18, pp. 25973-25986, 2010.

[81] H. Burton, S. Dixit, P. Litkowski, and J. R. Wingert, "Functional connectivity for somatosensory and motor cortex in spastic diplegia," *Somatosensory & motor research,* vol. 26, pp. 90-104, 2009.

[82] L. Sakzewski, J. Ziviani, and R. N. Boyd, "Best responders after intensive upper-limb training for children with unilateral cerebral palsy," *Archives of physical medicine and rehabilitation,* vol. 92, pp. 578-584, 2011.

[83] C. Papadelis, B. Ahtam, M. Nazarova, D. Nimec, B. Snyder, P. E. Grant*, et al.*, "Cortical somatosensory reorganization in children with spastic cerebral palsy: a multimodal neuroimaging study," *Front Hum Neurosci,* vol. 8, p. 725, 2014.

[84] F. Fregni, P. S. Boggio, M. Nitsche, F. Bermpohl, A. Antal, E. Feredoes*, et al.*, "Anodal transcranial direct current stimulation of prefrontal cortex enhances working memory," *Experimental brain research,* vol. 166, pp. 23-30, 2005.

[85] T. Z. Kincses, A. Antal, M. A. Nitsche, O. Bártfai, and W. Paulus, "Facilitation of probabilistic classification learning by transcranial direct current stimulation of the prefrontal cortex in the human," *Neuropsychologia,* vol. 42, pp. 113-117, 2004.

[86] R. Sparing, M. Dafotakis, I. G. Meister, N. Thirugnanasambandam, and G. R. Fink, "Enhancing language performance with non-invasive brain stimulation—a transcranial direct current stimulation study in healthy humans," *Neuropsychologia,* vol. 46, pp. 261-268, 2008.

[87] B. Elsner, J. Kugler, M. Pohl, and J. Mehrholz, "Transcranial direct current stimulation (tDCS) for improving function and activities of daily living in patients after stroke," *Cochrane Database Syst Rev,* vol. 11, 2013.

[88] M. A. Nitsche and W. Paulus, "Excitability changes induced in the human motor cortex by weak transcranial direct current stimulation," *The Journal of physiology,* vol. 527, pp. 633-639, 2000.

[89] L. J. Bindman, O. Lippold, and J. Redfearn, "The action of brief polarizing currents on the cerebral cortex of the rat (1) during current flow and (2) in the production of long-lasting after-effects," *The Journal of physiology,* vol. 172, pp. 369-382, 1964.

[90] D. P. Purpura and J. G. McMurtry, "Intracellular activities and evoked potential changes during polarization of motor cortex," *Journal of neurophysiology,* vol. 28, pp. 166-185, 1965.

[91] A. Flöel, N. Rösser, O. Michka, S. Knecht, and C. Breitenstein, "Noninvasive brain stimulation improves language learning," *Journal of Cognitive Neuroscience,* vol. 20, pp. 1415-1422, 2008.

[92] R. Holland, A. P. Leff, O. Josephs, J. M. Galea, M. Desikan, C. J. Price*, et al.*, "Speech facilitation by left inferior frontal cortex stimulation," *Current Biology,* vol. 21, pp. 1403-1407, 2011.

[93] A. Monti, F. Cogiamanian, S. Marceglia, R. Ferrucci, F. Mameli, S. Mrakic-Sposta*, et al.*, "Improved naming after transcranial direct current stimulation in aphasia," *Journal of Neurology, Neurosurgery & Psychiatry,* vol. 79, pp. 451-453, 2008.

[94] L. J. Bindman, O. Lippold, and J. Redfearn, "Long-lasting changes in the level of the electrical activity of the cerebral cortex produced by polarizing currents," *Nature,* vol. 196, pp. 584-585, 1962.

[95] B. Khan, T. Hodics, N. Hervey, G. Kondraske, A. Stowe, and G. Alexandrakis, "Enhancing motor performance improvement by personalizing non-invasive cortical stimulation with concurrent functional near-infrared spectroscopy and multi-modal motor measurements," in *SPIE BiOS*, 2015, pp. 93051A-93051A-13.

[96] A. C. Merzagora, G. Foffani, I. Panyavin, L. Mordillo-Mateos, J. Aguilar, B. Onaral*, et al.*, "Prefrontal hemodynamic changes produced by anodal direct current stimulation," *Neuroimage,* vol. 49, pp. 2304-2310, 2010.

[97] F. Tian, F. A. Kozel, A. Yennu, P. E. Croarkin, S. M. McClintock, K. S. Mapes*, et al.*, "Test-retest assessment of cortical activation induced by repetitive transcranial magnetic stimulation with brain atlas-guided optical topography," *Journal of biomedical optics,* vol. 17, pp. 116020-116020, 2012.

[98] J. C. Ye, S. Tak, K. E. Jang, J. Jung, and J. Jang, "NIRS-SPM: statistical parametric mapping for near-infrared spectroscopy," *Neuroimage,* vol. 44, pp. 428-447, 2009.

[99] A. Antal, R. Polania, C. Schmidt-Samoa, P. Dechent, and W. Paulus, "Transcranial direct current stimulation over the primary motor cortex during fMRI," *Neuroimage,* vol. 55, pp. 590-596, 2011.

[100] B. R. White, A. Z. Snyder, A. L. Cohen, S. E. Petersen, M. E. Raichle, B. L. Schlaggar*, et al.*, "Resting-state functional connectivity in the human brain revealed with diffuse optical tomography," *Neuroimage,* vol. 47, pp. 148-156, 2009.

[101] B. Biswal, F. Zerrin Yetkin, V. M. Haughton, and J. S. Hyde, "Functional connectivity in the motor cortex of resting human brain using echo‐planar mri," *Magnetic resonance in medicine,* vol. 34, pp. 537-541, 1995.

[102] X. Cui, S. Bray, and A. L. Reiss, "Functional near infrared spectroscopy (NIRS) signal improvement based on negative correlation between oxygenated and deoxygenated hemoglobin dynamics," *Neuroimage,* vol. 49, pp. 3039-3046, 2010.

[103] D. Wildgruber, A. Riecker, I. Hertrich, M. Erb, W. Grodd, T. Ethofer*, et al.*, "Identification of emotional intonation evaluated by fMRI," *Neuroimage,* vol. 24, pp. 1233-1241, 2005.

[104] H. Niu, S. Khadka, F. Tian, Z.-J. Lin, C. Lu, C. Zhu*, et al.*, "Resting-state functional connectivity assessed with two diffuse optical tomographic systems," *Journal of biomedical optics,* vol. 16, pp. 046006-046006-5, 2011.

[105] R. Polanía, M. A. Nitsche, and W. Paulus, "Modulating functional connectivity patterns and topological functional organization of the human brain with transcranial direct current stimulation," *Human brain mapping,* vol. 32, pp. 1236-1249, 2011.

[106] M. Xia, J. Wang, and Y. He, "BrainNet Viewer: a network visualization tool for human brain connectomics," *PloS one,* vol. 8, p. e68910, 2013.

[107] R. M. Hutchison, T. Womelsdorf, J. S. Gati, S. Everling, and R. S. Menon, "Resting-state networks show dynamic functional connectivity in awake humans and anesthetized macaques," *Human brain mapping,* vol. 34, pp. 2154-2177, 2013.

[108] A. Kucyi, T. V. Salomons, and K. D. Davis, "Mind wandering away from pain dynamically engages antinociceptive and default mode brain networks," *Proceedings of the National Academy of Sciences,* vol. 110, pp. 18692-18697, 2013.

[109] H. Niu, J. Wang, T. Zhao, N. Shu, and Y. He, "Revealing topological organization of human brain functional networks with resting-state functional near infrared spectroscopy," *PLoS One,* vol. 7, p. e45771, 2012.

[110] J.-R. Ding, W. Liao, Z. Zhang, D. Mantini, Q. Xu, G.-R. Wu*, et al.*, "Topological fractionation of resting-state networks," *Plos one,* vol. 6, p. e26596, 2011.

[111] W. Liao, Z. Zhang, Z. Pan, D. Mantini, J. Ding, X. Duan*, et al.*, "Altered functional connectivity and small-world in mesial temporal lobe epilepsy," *PloS one,* vol. 5, p. e8525, 2010.

[112] M. D. Humphries, K. Gurney, and T. J. Prescott, "The brainstem reticular formation is a small-world, not scale-free, network," *Proceedings of the Royal Society of London B: Biological Sciences,* vol. 273, pp. 503-511, 2006.

[113] M. Kaiser and C. C. Hilgetag, "Nonoptimal component placement, but short processing paths, due to long-distance projections in neural systems," *PLoS computational biology,* vol. 2, p. e95, 2006.

[114] S. Achard and E. Bullmore, "Efficiency and cost of economical brain functional networks," *PLoS computational biology,* vol. 3, p. e17, 2007.

[115] A. S. Dick, S. Goldin-Meadow, U. Hasson, J. I. Skipper, and S. L. Small, "Co-speech gestures influence neural activity in brain regions associated with processing semantic information," *Human brain mapping,* vol. 30, pp. 3509-3526, 2009.

[116] M. Meinzer, C. Breitenstein, U. Westerhoff, J. Sommer, N. Rösser, A. D. Rodriguez*, et al.*, "Motor cortex preactivation by standing facilitates word retrieval in aphasia," *Neurorehabilitation and neural repair,* vol. 25, pp. 178-187, 2011.

[117] M. Meinzer, R. Lindenberg, M. M. Sieg, L. Nachtigall, L. Ulm, and A. Flöel, "Transcranial direct current stimulation of the primary motor cortex improves word-retrieval in older adults," *Frontiers in aging neuroscience,* vol. 6, 2014.

[118] A. Fertonani, S. Rosini, M. Cotelli, P. M. Rossini, and C. Miniussi, "Naming facilitation induced by transcranial direct current stimulation," *Behavioural brain research,* vol. 208, pp. 311-318, 2010.

[119] K. Herholz, U. Pietrzyk, H. Karbe, M. Würker, K. Wienhard, and W.-D. Heiss, "Individual metabolic anatomy of repeating words demonstrated by MRI-guided positron emission tomography," *Neuroscience letters,* vol. 182, pp. 47-50, 1994.

[120] M. Daianu, N. Jahanshad, E. L. Dennis, A. W. Toga, K. L. McMahon, G. I. De Zubicaray*, et al.*, "Left versus right hemisphere differences in brain connectivity: 4-Tesla HARDI tractography in 569 twins," in *Biomedical Imaging (ISBI), 2012 9th IEEE International Symposium on*, 2012, pp. 526-529.

[121] D. E. Stark, D. S. Margulies, Z. E. Shehzad, P. Reiss, A. C. Kelly, L. Q. Uddin*, et al.*, "Regional variation in interhemispheric coordination of intrinsic hemodynamic fluctuations," *Journal of Neuroscience,* vol. 28, pp. 13754-13764, 2008.

[122] N. Ramnani and A. M. Owen, "Anterior prefrontal cortex: insights into function from anatomy and neuroimaging," *Nature reviews. Neuroscience,* vol. 5, p. 184, 2004.

[123] F. D. V. Fallani, L. Astolfi, F. Cincotti, D. Mattia, M. G. Marciani, S. Salinari*, et al.*, "Cortical functional connectivity networks in normal and spinal cord injured patients: evaluation by graph analysis," *Human brain mapping,* vol. 28, pp. 1334-1346, 2007.

[124] E. Sivan, H. Parnas, and D. Dolev, "Fault tolerance in the cardiac ganglion of the lobster," *Biological cybernetics,* vol. 81, pp. 11-23, 1999.

[125] H. L. Filmer, P. E. Dux, and J. B. Mattingley, "Applications of transcranial direct current stimulation for understanding brain function," *Trends in neurosciences,* vol. 37, pp. 742-753, 2014.

[126] M. A. Nitsche, L. G. Cohen, E. M. Wassermann, A. Priori, N. Lang, A. Antal*, et al.*, "Transcranial direct current stimulation: state of the art 2008," *Brain stimulation,* vol. 1, pp. 206-223, 2008.

[127] R. Polanía, W. Paulus, A. Antal, and M. A. Nitsche, "Introducing graph theory to track for neuroplastic alterations in the resting human brain: a transcranial direct current stimulation study," *Neuroimage,* vol. 54, pp. 2287-2296, 2011.

[128] P. Marangolo, V. Fiori, M. A. Calpagnano, S. Campana, C. Razzano, C. Caltagirone*, et al.*, "tDCS over the left inferior frontal cortex improves speech production in aphasia," *Frontiers in Human Neuroscience,* vol. 7, 2013.

[129] P. Marangolo, C. Marinelli, S. Bonifazi, V. Fiori, M. Ceravolo, L. Provinciali*, et al.*, "Electrical stimulation over the left inferior frontal gyrus (IFG) determines long-term effects in the recovery of speech apraxia in three chronic aphasics," *Behavioural brain research,* vol. 225, pp. 498-504, 2011.

[130] Y. Harpaz, Y. Levkovitz, and M. Lavidor, "Lexical ambiguity resolution in Wernicke's area and its right homologue," *Cortex,* vol. 45, pp. 1097-1103, 2009.

[131] A. Costa, M. Oliveri, F. Barban, S. Bonnì, G. Koch, C. Caltagirone*, et al.*, "The right frontopolar cortex is involved in visual-spatial prospective memory," *PLoS One,* vol. 8, p. e56039, 2013.

[132] J. Gonzalez-Castillo, P. Wu, M. Robinson, D. Handwerker, S. Inati, and P. Bandettini, "Detection of task transitions on 45 mins long continuous multi-task runs using whole brain connectivity," *Organization for Human Brain Mapping. Beijing, China,* 2012.

[133] A. M. Hermundstad, D. S. Bassett, K. S. Brown, E. M. Aminoff, D. Clewett, S. Freeman*, et al.*, "Structural foundations of resting-state and task-based functional connectivity in

the human brain," *Proceedings of the National Academy of Sciences,* vol. 110, pp. 6169-6174, 2013.

[134] M. Rubinov and O. Sporns, "Complex network measures of brain connectivity: uses and interpretations," *Neuroimage,* vol. 52, pp. 1059-1069, 2010.

[135] V. Latora and M. Marchiori, "Efficient behavior of small-world networks," *Physical review letters,* vol. 87, p. 198701, 2001.

[136] D. J. Smit, C. J. Stam, D. Posthuma, D. I. Boomsma, and E. J. De Geus, "Heritability of "small-world" networks in the brain: A graph theoretical analysis of resting-state EEG functional connectivity," *Human brain mapping,* vol. 29, pp. 1368-1378, 2008.

[137] M. A. Nitsche and W. Paulus, "Sustained excitability elevations induced by transcranial DC motor cortex stimulation in humans," *Neurology,* vol. 57, pp. 1899-1901, 2001.

[138] R. Holland, A. P. Leff, W. D. Penny, J. C. Rothwell, and J. Crinion, "Modulation of frontal effective connectivity during speech," *NeuroImage,* vol. 140, pp. 126-133, 2016.

[139] M. Lobier, F. Siebenhühner, S. Palva, and J. M. Palva, "Phase transfer entropy: a novel phase-based measure for directed connectivity in networks coupled by oscillatory interactions," *Neuroimage,* vol. 85, pp. 853-872, 2014.

[140] M. Wibral, B. Rahm, M. Rieder, M. Lindner, R. Vicente, and J. Kaiser, "Transfer entropy in magnetoencephalographic data: quantifying information flow in cortical and cerebellar networks," *Progress in biophysics and molecular biology,* vol. 105, pp. 80-97, 2011.

[141] A. Hillebrand, P. Tewarie, E. Van Dellen, M. Yu, E. W. Carbo, L. Douw*, et al.*, "Direction of information flow in large-scale resting-state networks is frequency-dependent," *Proceedings of the National Academy of Sciences,* vol. 113, pp. 3867-3872, 2016.

[142] B. M. Bosch, A. Bringard, G. Ferretti, S. Schwartz, and K. Iglói, "Effect of cerebral vasomotion during physical exercise on associative memory, a near-infrared spectroscopy study," *Neurophotonics,* vol. 4, p. 041404, 2017.

[143] C. Aalkjær, D. Boedtkjer, and V. Matchkov, "Vasomotion–what is currently thought?," *Acta Physiologica,* vol. 202, pp. 253-269, 2011.

[144] T. Sakurai and N. Terui, "Effects of sympathetically induced vasomotion on tissue-capillary fluid exchange," *American Journal of Physiology-Heart and Circulatory Physiology,* vol. 291, pp. H1761-H1767, 2006.

[145] H. Nilsson and C. Aalkjær, "Vasomotion: mechanisms and physiological importance," *Molecular interventions,* vol. 3, p. 79, 2003.

[146] A. Stefanovska, "Coupled oscillatros: complex but not complicated cardiovascular and brain interactions," *IEEE Engineering in medicine and biology magazine,* vol. 26, 2007.

[147] R. Zhang, J. H. Zuckerman, K. Iwasaki, T. E. Wilson, C. G. Crandall, and B. D. Levine, "Autonomic neural control of dynamic cerebral autoregulation in humans," *Circulation,* vol. 106, pp. 1814-1820, 2002.

[148] G. H. Klem, H. O. Lüders, H. Jasper, and C. Elger, "The ten-twenty electrode system of the International Federation," *Electroencephalogr Clin Neurophysiol,* vol. 52, pp. 3-6, 1999.

[149] Z. Zhang and R. Khatami, "Predominant endothelial vasomotor activity during human sleep: a near‐infrared spectroscopy study," *European Journal of Neuroscience,* vol. 40, pp. 3396-3404, 2014.

[150] Y. Zhang, D. H. Brooks, M. A. Franceschini, and D. A. Boas, "Eigenvector-based spatial filtering for reduction of physiological interference in diffuse optical imaging," *Journal of biomedical optics,* vol. 10, pp. 011014-01101411, 2005.

[151] M. Rosenblum, A. Pikovsky, J. Kurths, C. Schäfer, and P. A. Tass, "Phase synchronization: from theory to data analysis," *Handbook of biological physics,* vol. 4, pp. 279-321, 2001.

[152] M. Staniek and K. Lehnertz, "Symbolic transfer entropy: inferring directionality in biosignals," *Biomedizinische Technik/Biomedical Engineering,* vol. 54, pp. 323-328, 2009.

[153] F. Tian, Z.-J. Lin, and H. Liu, "EasyTopo: A toolbox for rapid diffuse optical topography based on a standard template of brain atlas," in *Proc. of SPIE Vol*, 2013, pp. 85782J-1.

[154] M. D. Greicius, B. Krasnow, A. L. Reiss, and V. Menon, "Functional connectivity in the resting brain: a network analysis of the default mode hypothesis," *Proceedings of the National Academy of Sciences,* vol. 100, pp. 253-258, 2003.

[155] M. Quigley, D. Cordes, P. Turski, C. Moritz, V. Haughton, R. Seth*, et al.*, "Role of the corpus callosum in functional connectivity," *American journal of neuroradiology,* vol. 24, pp. 208-212, 2003.

[156] T. J. Teyler and P. DiScenna, "Long-term potentiation," *Annual review of neuroscience,* vol. 10, pp. 131-161, 1987.

[157] S. J. Pelletier and F. Cicchetti, "Cellular and molecular mechanisms of action of transcranial direct current stimulation: evidence from in vitro and in vivo models," *International Journal of Neuropsychopharmacology,* vol. 18, p. pyu047, 2015.

[158] J. P. Brasil-Neto, "Learning, memory, and transcranial direct current stimulation," *Frontiers in psychiatry,* vol. 3, 2012.

[159] C. Repper-Day, "Mapping dynamic brain connectivity using EEG, TMS, and Transfer Entropy," University of Manchester, 2017.

[160] C. J. Bajada, H. A. Haroon, H. Azadbakht, G. J. Parker, M. A. L. Ralph, and L. L. Cloutman, "The tract terminations in the temporal lobe: Their location and associated functions," *Cortex,* 2016.

[161] A. D. Friederici, "Pathways to language: fiber tracts in the human brain," *Trends in cognitive sciences,* vol. 13, pp. 175-181, 2009.

[162] J. K. Rilling, M. F. Glasser, T. M. Preuss, X. Ma, T. Zhao, X. Hu*, et al.*, "The evolution of the arcuate fasciculus revealed with comparative DTI," *Nature neuroscience,* vol. 11, 2008.

[163] N. F. Dronkers, D. P. Wilkins, R. D. Van Valin, B. B. Redfern, and J. J. Jaeger, "Lesion analysis of the brain areas involved in language comprehension," *Cognition,* vol. 92, pp. 145-177, 2004.

[164] E. Tulving, S. Kapur, H. J. Markowitsch, F. Craik, R. Habib, and S. Houle, "Neuroanatomical correlates of retrieval in episodic memory: auditory sentence recognition," *Proceedings of the National Academy of Sciences,* vol. 91, pp. 2012-2015, 1994.

[165] M. Catani and D. K. Jones, "Perisylvian language networks of the human brain," *Annals of neurology,* vol. 57, pp. 8-16, 2005.

[166] M. Catani and M. T. de Schotten, *Atlas of human brain connections*: Oxford University Press, 2012.

[167] A. Benedictis, L. Petit, M. Descoteaux, C. E. Marras, M. Barbareschi, F. Corsini*, et al.*, "New insights in the homotopic and heterotopic connectivity of the frontal portion of the human corpus callosum revealed by microdissection and diffusion tractography," *Human brain mapping,* vol. 37, pp. 4718-4735, 2016.

[168] E. Bullmore and O. Sporns, "The economy of brain network organization," *Nature Reviews Neuroscience,* vol. 13, pp. 336-349, 2012.

[169] S. Kiran, E. L. Meier, K. J. Kapse, and P. A. Glynn, "Changes in task-based effective connectivity in language networks following rehabilitation in post-stroke patients with aphasia," *Frontiers in human neuroscience,* vol. 9, 2015.

[170] S. B. Eickhoff, S. Heim, K. Zilles, and K. Amunts, "A systems perspective on the effective connectivity of overt speech production," *Philosophical Transactions of the*

Royal Society of London A: Mathematical, Physical and Engineering Sciences, vol. 367, pp. 2399-2421, 2009.

[171] U. Förstermann and W. C. Sessa, "Nitric oxide synthases: regulation and function," *European heart journal,* vol. 33, pp. 829-837, 2011.

[172] H. D. Kvernmo, A. Stefanovska, K. A. Kirkebøen, and K. Kvernebo, "Oscillations in the human cutaneous blood perfusion signal modified by endothelium-dependent and endothelium-independent vasodilators," *Microvascular research,* vol. 57, pp. 298-309, 1999.

[173] D. P. Trivedi, K. J. Hallock, and P. R. Bergethon, "Electric fields caused by blood flow modulate vascular endothelial electrophysiology and nitric oxide production," *Bioelectromagnetics,* vol. 34, pp. 22-30, 2013.

[174] M. Bikson, A. Datta, and M. Elwassif, "Establishing safety limits for transcranial direct current stimulation," *Clinical neurophysiology: official journal of the International Federation of Clinical Neurophysiology,* vol. 120, p. 1033, 2009.

[175] M. A. Nitsche, D. Liebetanz, N. Lang, A. Antal, F. Tergau, and W. Paulus, "Safety criteria for transcranial direct current stimulation (tDCS) in humans," *Clinical Neurophysiology,* vol. 114, pp. 2220-2222, 2003.

[176] J. R. Binder, J. A. Frost, T. A. Hammeke, R. W. Cox, S. M. Rao, and T. Prieto, "Human brain language areas identified by functional magnetic resonance imaging," *Journal of Neuroscience,* vol. 17, pp. 353-362, 1997.